


To my kids
Jaikishan & Lakshmi

C E R T I F I C A T E

I hereby declare that the work presented in
this thesis is original and has not formed the basis
for award of any degree by any university or institution.

T.N. Rajaraman
(T.N. RAJARAMAN)
Author

Certified

(J.N. DESAI)
Professor in charge

STATEMENT

The work presented in the thesis was carried out by the author at the Physical Research Laboratory, Ahmedabad, under the expert guidance of Dr. J.N. Desai.

The work reports the first, direct spectroscopic measurements of upper atmospheric temperatures in India.

Systematic spectroscopic observations of thermospheric temperatures from low latitude stations are very few. Our understanding of the thermal structure of the upper atmosphere has evolved largely from the vast amount of satellite drag data obtained over the past several years. The exospheric temperature derived with this technique is a convenient index of total density. Its usefulness as a representation of neutral temperature is however, questionable. It is because that the basic difficulty in deriving exospheric temperature from satellite drag data lies in the fact that in the altitude region where most of the drag data are available, the total density corresponds mostly to the density of atomic oxygen. The assumption that atomic oxygen is invariant at a specific reference level (usually 120 km) in the lower thermosphere is one of the weakest assumptions in the derivation of temperature from the total density measurements. In comparison with the temperatures measured from radar backscatter and airglow

technique, it gives a completely different picture of diurnal, seasonal and latitudinal variations. On the other hand the Doppler temperatures from 6300 Å night airglow line width measurements (250 km level) are already within 5% of the exospheric temperature (JACCHIA, 1977), the O(I) 6300 Å line width temperatures can be used quite accurately to infer exospheric temperatures. The present study reports exospheric temperatures inferred from Doppler line width measurements of O(I), 6300 Å night airglow line, using a Pressure scanned Fabry-Perot spectrometer, over Mt Abu (24.6°N , 72.7°E geographic, 15.0° geomagnetic latitude), India.

The author gives a brief summary of the temperature structure of the earth's upper atmosphere in Chapter I and outlines the different methods (satellite drag method, backscatter technique, insitu measurements by rockets etc) of determining upper atmospheric temperature. Also a review is given of the temperature measurements so far done and the present state of knowledge in the measurements by Fabry-Perot spectrometer.

The line widths which are typically of the order of about 0.04 Å were measured by scanning over the line profile by means of a Pressure-scanned Fabry-Perot spectrometer. The Fabry-Perot plates were of $\lambda/25$ surface quality and 70 mm

aperture. These were coated with multilayer dielectric high reflection coating of 72% reflectivity. Free spectral range of the spectrometer was 0.125 Å. The Fabry-Perot chamber pressure was varied in steps. Detection was by a photon counting system. For each pressure step photon counts for 1 sec. were accumulated and registered on a line printer. A 2.5 Å half band width interference filter, temperature controlled to $\pm 0.5^{\circ}\text{C}$ was used to isolate the 6300 Å line. The S/N ratio is optimized by the proper selection of photomultiplier high tension and the pulse height discrimination level setting. The photomultiplier was cooled to -5°C using freon cooled glycol water circulation. The entire instrumentation was indigenously developed by the author and described in detail in Chapter II.

The observations extended from evening twilight to midnight. The observed line profile is a convolution of the actual line profile and the instrument function. Determination of the true Doppler width of the airglow line therefore requires a deconvolution procedure. Instrument profile was determined each night either once or twice using He-Ne ($\lambda 6328 \text{ Å}$) laser. Two different methods i) Half width method ii) Synthetic profile method, were employed for deconvolution. The author describes the data acquisition

sequence and data reduction procedure in Chapter III. A laser mode analysis for studying the assymetry of the laser profile is also presented in this chapter.

About 32 nights temperature results are presented in Chapter IV. More than 125 temperature values are given. The experimental temperatures are compared with JACCHIA (1970) model exospheric temperatures. 60% of the temperatures compare very well with an accuracy of $\pm 50^{\circ}\text{K}$ with model temperatures. The average night time F region temperatures are found to lie between 800°K to 1000°K .

One of the significant results obtained was the observation of temperature enhancements of the order of $100 - 300^{\circ}\text{K}$ over JACCHIA (1970) model temperatures. The temperature enhancements are found to correlate very well with the occurrence of spread-F over equator. Later satellite observations have also shown temperature increases of similar magnitude. These results are dealt with in detail in Chapter IV.

Two complete fringes are scanned in one travel of the piston and the distance between the peaks which is the free spectral range of the instrument in pressure scale equals 5.5 cm. It was found on many occasions that the values obtained were much different from 5.5 cm. Since no

nonuniform pressure variation is possible, this is attributed to the change in wind vector during the scan and corresponding shift of the fringe centre wavelength, thereby producing a spacing other than 5.5 cm. Fringe profiles were studied for 12 nights and wind accelerations from 50 mts to 400 mts were seen. A correlation between the level of $h'F$ (virtual height of F_2 layer) and the onset of wind acceleration is established. It was also seen that the 6300 A intensities do not correlate with wind accelerations. A study of line width fluctuations in the individual profiles was made and this also yielded wind accelerations of the same order. The results of these two studies are presented in chapter V.

The summary, discussion and conclusions of the above study are presented in chapter VI, identifying also areas for future work in this subject. Finally, a list of original papers published in different parts of the world, to which references have been made by the author in the presentation, has been included at the end.



(J.N. DESAI)



(T.N. RAJARAMAN)

ACKNOWLEDGEMENTS

I take this opportunity to express my deep gratitude to my thesis guide Prof. J. N. Desai for his invaluable guidance, advice, encouragement, affection and friendship in the execution of this study and in the preparation of the thesis. I am indebted to him in a large extent.

I express my sincere thanks to Prof. K. D. COLE, La Trobe University, Bundoora, Australia and Dr. S.S. Degaonker, PRL for many useful discussions and suggestions.

I owe a great deal to Dr. K. S. Rao for the help rendered in numerical analysis and computer programming.

I am indebted to Prof. M.V.R.K. Murthy of Bhabha Atomic Research Centre, Bombay who introduced me to the field of optical fabrication techniques and optical testing of components and for the facilities he provided me at BARC in making the Fabry-Perot plates.

Fruitful discussions with Prof. Ragavarao, Prof. P. V. Kulkarni, Prof. R. P. Kane, Prof. R. Pratap, Dr. P.D. Angreji and Dr. G. Subramaniam are gratefully acknowledged.

Thanks are also due to Dr. V. V. Somayajulu, Vikram Sarabhai Space Centre, Trivandrum and Dr. J. H. Sastri, Indian Institute of Astrophysics, Kodaikanal for the ionospheric information.

I express my gratitude to Mr. N. S. Jog and Mr. P. K. Kikani who developed the electronic circuits and to Mr. S. D. Rawat who helped in multilayer coatings of Fabry-Perot plates.

Help rendered by Shri P. S. Shah, Airconditioning Engineer and his colleagues in making the refrigeration system for the photomultiplier and by all the workshop personnel in making the complete spectrometer system are gratefully acknowledged.

I thank M/s R. K. Mahadkar, N. C. Shah and A. R. Gupta who have given valuable help at Mt Abu during observations.

It is a pleasure to thank Mr. H. I. Pandya and Mrs. Saroj Jani for giving uninterrupted computational assistance and plotting of graphs.

The inspiration and encouragement provided by my friends particularly by Mr. T. Chandrasekhar, Mr. N.M. Ashok Mr. Kaish Sahu, Mr. P. N. Guzdar and Mr. Sridharan R., is gratefully acknowledged.

I thank Mr. G. S. Panchal of New India Industries Ltd., Baroda who helped in making excellent drawings and in the preparation of figures.

I profusely thank Mr. D. R. Bhavsar of M.S. University of Baroda, Baroda who typed this thesis neatly and efficiently.

I thank the Director, Physical Research Laboratory for giving me this opportunity to carry out this investigation.

The financial support for this study was provided by Department of Space, Government of India, which is gratefully acknowledged.

Finally I am happy to acknowledge here the moral and editorial support of my wife which was essential to carry me through month's of work on the thesis.

- : C O N T E N T S : -

	<u>Page</u>
Certificate 	i
Statement 	ii
Acknowledgements 	vii
Contents 	x
 CHAPTER I <u>INTRODUCTION</u>	 1
1.1 Temperature Profile of the earth's atmosphere	 2
1.2 Atmospheric models	5
1.3 Determination of Upper atmospheric Temperaturex	 8
1.3.1 Satellite Drag Method	8
1.3.2 In Situ measurements	9
1.3.3 Diffusion method	10
1.3.4 Incoherent Scatter Technique	10
1.4 Spectroscopic Temperatures	12
1.5 Review of Earlier Fabry-Perot measurements	 16
1.5.1 Photographic work with Fabry-Perot	 16
1.5.2 Photoelectric Fabry-Perot measurements	 18
 CHAPTER II <u>INSTRUMENTATION</u>	 26
2.1 Basic Considerations	27
2.2 Spectroscopic Devices	28
2.3 Fabry-Perot Spectrometer	30
2.4 Basic Design of FPS for Airglow linewidth measurements	 32

2.5	Parameters of FPS and their optimization	32
2.6	Transmittance of Etalon	37
2.7	Choice of Parameters in the Present Experiment	39
2.8	Detection, Counting and Printing Systems	42
2.9	Scanning System	43
CHAPTER III	<u>DATA ACQUISITION REDUCTION, CALIBRATION AND ERROR ANALYSIS</u>	45
3.1	Data Acquisition	45
3.2	Laser Calibration	47
3.3	Data Analysis, Deconvolution Scheme	49
3.4	Methods of finding true Doppler width, Method of Synthetic Profiles	51
3.5	Half width method	53
3.6	Errors in Temperature Measurements	55
3.6.1	Error due to uncertainty in Finesse	55
3.6.2	Error due to unevenness in Pressure variation	55
3.6.3	Error due to scatter in the experimental data	56
3.6.4	Error due to smoothing procedure adopted	57
3.6.5	Dark level fluctuation	57
3.6.6	Stray light level fluctuation	58
3.7	Contamination Problem	58
3.8	Effect of change in 6300 Å intensity	60
3.9	Error due to light leakage	61

CHAPTER IV	<u>RESULTS</u>	62
4.1	Temperature Plots and Analysis method	62
4.2	Neutral Temperatures	64
4.3	Temperature Enhancements and Spread-F connection	65
4.4	Low and Very High Temperatures, Relation with Intensities	71
CHAPTER V	<u>NEUTRAL-WIND ACCELERATIONS AND CORRELATION STUDIES</u>	74
5.1	Technique for measuring winds	75
5.2	Present Method	77
5.3	Results and Correlation Studies	79
5.4	Study of linewidth fluctuations	82
CHAPTER VI	<u>DISCUSSION OF RESULTS AND SCOPE FOR FURTHER WORK</u>	85
6.1	Neutral Temperatures	85
6.2	Temperature Enhancements and Spread-F	87
6.3	Neutral Wind Accelerations and Linewidth fluctuations	91
REFERENCES	R1

CHAPTER - I

INTRODUCTION

Although atmospheric phenomena like meteor trails, aurora, noctilucent clouds have been observed by man for a long period of time, it is only relatively recently that the understanding of the upper atmosphere has been accomplished through their detailed study and observations. The advent of rockets and satellites have now opened up the subject matter to the province of "in situ" measurements, and one can now definitely say that our basic understanding of the upper atmosphere of earth is fairly complete. Still however, there are many detailed features that remain to be well understood - particularly those associated with the dynamical behaviour of the atmosphere. One may also distinguish here between the "global dynamical effects" associated with the driving impulse originating outside the earth's atmosphere, best studied only through satellites by virtue of their global coverage, and the local dynamical effects like effects associated with internal gravity waves, spread F, counter electrojet etc, which are best likely to be understood through a long series of observations from a site (or sites) of relevant atmospheric parameters. Present work can be placed in this category. In this work the author has given a report of

the F region night time temperatures inferred by observing the Doppler width of 6300 Å O(I) night airglow line by a pressure Scanned Fabry-Perot Spectrometer over Mount Abu (24°N), India, over a period of a little over two years.

1.1 TEMPERATURE PROFILE OF EARTH'S ATMOSPHERE

The neutral atmosphere of earth is conveniently divided into zones based on its thermal structure. The lowest region of atmosphere in which the familiar meteorological phenomena are encountered, is a region characterized by a positive lapse rate of temperature (i.e. the temperature decreasing with increasing height) and is called the troposphere. Depending upon the latitude, the troposphere extends from 10 to 17 kms. Above the troposphere we have the stratosphere with a negative lapse rate and hence stable against convection. Source of heat in this region is absorption by ozone of the solar ultraviolet radiation. Stratosphere extends to about 50 kms. Above stratosphere, we have the mesosphere which extends upto 85 kms and has again a positive lapse rate of temperature. Top of the mesosphere is mesopause which is the coolest region of earth's atmosphere. Heat flows towards this region by conduction from above and is removed by radiation in infrared and visible airglow, and by downward eddy diffusion in the mesosphere. Above the mesopause, solar EUV radiation is

the major energy input source, although charged particles and photochemical reactions also do contribute. In this region which is known as the thermosphere, the temperature increases steadily from a low value at its base to a very high value ($\approx 1500^{\circ}$ K) at F region heights (≈ 250 km) above which it essentially attains a constant value by virtue of the large thermal conductivity. Hence F region temperatures can be used as an index of the exospheric temperatures - the constant asymptotic value attained in the upper thermosphere.

Typical temperature structure of the earth's atmosphere is shown in Fig. 1. For a quick summary of the temperature structure reference may be made to SIEGFRIED J. BAUER (1973).

The atmospheric structure in general, and the temperature structure in particular shows variations both on short and long time scales (few hours to year or years). Some of these are coupled with flux variation from the sun. Some are of origin internal to the atmosphere. The large heat capacity of the atmosphere below 150 kms keep the magnitude of the temperature variations small, but above 150 km, the heat capacity of the atmosphere is low and the range of temperature fluctuation is much larger.

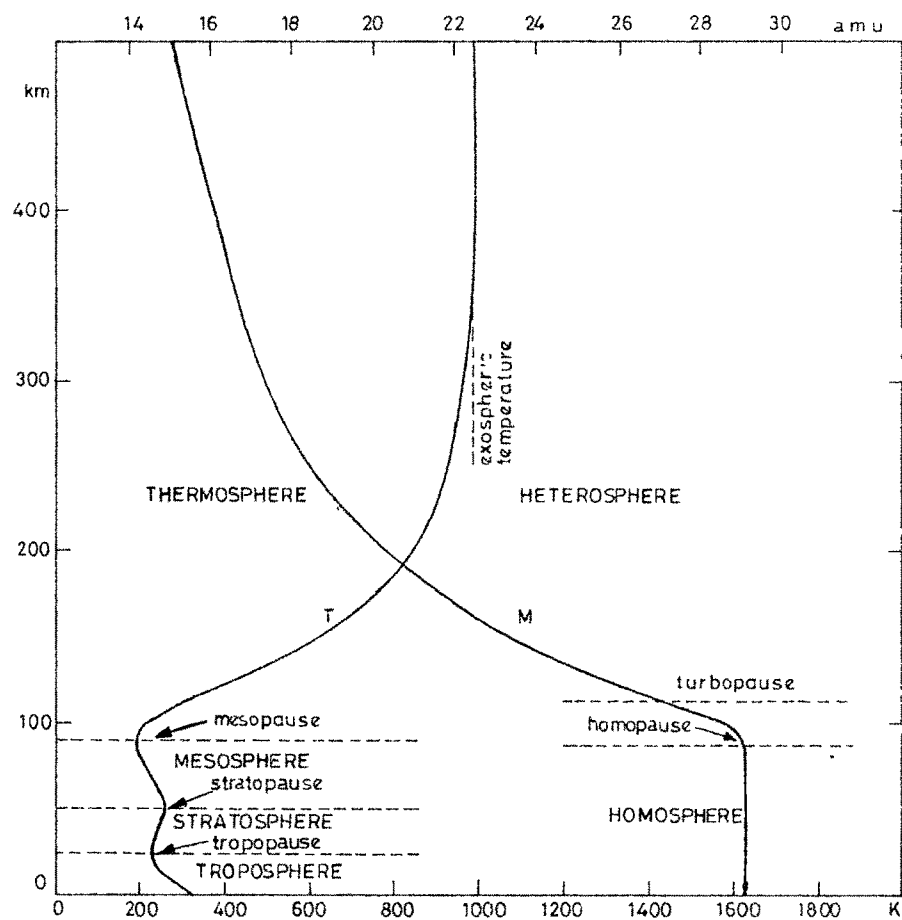


FIG.1 The current terminology for the description of the upper atmospheric layers is based either on the temperature (T in deg K) or the mean molecular mass (M in atomic mass units) vertical profiles

(TAKEN FROM "IONOSPHERIC TECHNIQUES AND PHENOMENA"
ALAIN GIRAUD AND MICHEL PETIT, D. REIDEL PUBLI 1973)

Below the height of 110 - 120 kms the eddy diffusion coefficient of atmospheric constituents are larger than their molecular diffusion coefficient. Above this height the molecular diffusion takes over so that different constituents are distributed according to their individual scale heights viz. following the equation

$$N_i(Z) = N_i(Z_0) \frac{T(Z_0)}{T(Z)} \exp \left[- \int_{Z_0}^Z \frac{dz}{H} \right] \dots (1)$$

$$H = \frac{RT}{M_i g}$$

where

N_i = Number concentration of constituent 'i' of molecular weight M_i

Z = height

R = gas constant

T = Temperature

Region of the atmosphere above 120 kms where equation (1) applies is known as 'Heterosphere'. In static diffusive equilibrium model the number density distribution and the temperature profile are coupled through equation (1).

However one can still have a dynamical perturbation of a

short period (like internal gravity wave [HINES, (1965)] causing significant departures from the above equation similar effect could perhaps account for the wave like modulation of temperatures inferred from diffusion of vapour trails by DESAI AND NARAYANAN (1970).

Rocket released vapour trails have clearly shown the sharp turbopause level presumably separating 'heterosphere' from the lower homosphere' at a height between 100 to 110 kms. DESAI ET AL, (1975). BLAMONT AND BARAT (1969)

1.2 ATMOSPHERIC MODELS

Several models of earth's atmosphere, which present temperature, pressure, density and other properties as a function of time, altitude and latitude have been constructed in recent years. The semi empirical model of HARRIS AND PRIESTER (1962 A,B) was the major attempt, after NICOLET (1961) made a beginning, to put the available observational data in a quantitative form to construct a comprehensive model from 120 to 2000 km altitude for various levels of solar activity, with fixed boundary conditions at the 120 km level and diffusive equilibrium above. JACCHIA (1965) and COSPAR International Reference Atmosphere CIRA (1965) models are only modified versions of the same. With the accumulation of more data, new models have now been

constructed. The low latitude model of CIRA for the 25 to 120 km region has been developed by GROVES (1971). The high altitude model for atmosphere above 90 km has been developed by JACCHIA (1970 B, 1971). It is primarily based on satellite drag results, and the values have been matched at lower heights with mass-spectrometer and other in-situ measurements. In JACCHIA'S model, considerable changes over the models of CIRA (1965) and United States Standard Atmosphere (USSA) supplement (1966), have been incorporated, particularly in respect of the fixed lower boundary condition (which has been brought down from 120 km to 90 km) and the O/O_2 ratio at 120 km (which has been considerably increased). Mixing is assumed to prevail to a height of 100 km and diffusive equilibrium thereafter. All the recognised variations connected with temporal, solar, geomagnetic and latitudinal parameters are represented by empirical relations. However the maximum of temperature, at 1400 hr, as from this model and at 1600 hr (or later), as derived from incoherent scatter observations, poses a serious problem for this model.

The mean CIRA has been developed for an altitude range 25 to 500 km by CHAMPION AND SCHWEINFURTH (1971) for mean conditions near 30° latitude and for a solar flux of 145×10^{-22} watts m^{-2} Hz^{-1} , based on the models of GROVES (1971) and JACCHIA (1971). JACCHIA'S model has been

modified for polar region by BLUM AND HARRIS (1973).

The reliability of the upper atmospheric models are mainly based, on the turbopause level (assumed constant at 100 mkm) and the fixed lower boundary conditions. Changes of composition at the base of the thermosphere can have important consequences in several ionospheric phenomena (CHANDRA AND STUBBE, 1970 ; MAYR AND MAHAJAN, 1971 ; TAUBENHEIM, 1971 ; RUSTER AND KING, 1973). The variation of atomic oxygen concentration and the O/N_2 ratio have large influence on the vertical structure of composition in the thermosphere. STUBBE (1972) has shown that because of horizontal transport of air, the O/N_2 ratio in the lower thermosphere is affected and that there are departures from barometric law.

From incoherent scatter observations, WALDTEUFEL AND Mc CLURE (1969, 1971) and WALDTEUFEL AND COGGER (1971) have presented global exospheric temperature models. JACCHIA (1977) model is the updated version of his previous models in light of more recent data. Relevant features of this model are described later in this work as the temperatures measured here are compared with those calculated by that model.

1.3 DETERMINATION OF UPPER ATMOSPHERIC TEMPERATURES

There are many different methods for the determination of upper atmosphere temperatures. Some of them are direct and others give results which can be interpreted in terms of temperature. Satellite drag measurements, in-situ measurements of density and temperature by rockets and satellite borne instruments, incoherent scatter technique diffusion techniques and the spectroscopic method are some of the methods that are outlined in the following paragraphs. Since the subject of the present work falls on the last category the author has reviewed the status of the work done so far under the subtitle spectroscopic determination of upper atmospheric temperatures.

1.3.1 SATELLITE DRAG METHOD

Upper atmospheric temperatures can be inferred from the density measurements, provided composition is known. Satellite drag measurements of the atmospheric neutral gas density have provided most of our present day knowledge of the thermal structure of the atmosphere [(e.g. JACCHIA 1965) P.B. HAYS ET AL, (1969)]. Density determinations in the thermosphere have, mainly been made by means of satellite drag measurements. A body of effective cross section A ,

moving with a velocity V , through a gas of density ρ experiences an aero-dynamic drag D , given by

$$D = \frac{1}{2} C_D A \rho V^2$$

where C_D is the drag coefficient. Knowing the satellite velocity, density is obtained by observing the change in the orbital inclination of the satellite from the ground. The methods and results of these determinations have been discussed by JACCHIA (1963), KING-HELE (1966), PRIESTER ET AL, (1967), and ROEMER (1971).

In the altitude range of 300 to 500 km the principal constituent is atomic oxygen and other constituents may justifiably be neglected. Use of diffusive equilibrium (eqn. 1) then permits determination of temperatures.

1.3.2 IN-SITU MEASUREMENTS

In-situ measurements of the density and temperature of molecular nitrogen from altitude of about 140 to 300 km have been made employing a series of thermosphere probe launchings. The probe consists of an omegatron mass spectrometer (fixed tuned to N_2) and an optical aspect instrument. These measurements rely on the interpretation of the vertical gradient of the neutral species to derive temperature. SPENCER ET AL, (1970) have reviewed in detail

these probe measurements. SPENCER AND CARIGNAN (1972) report thermospheric molecular nitrogen temperature variations made on San Macro III satellite in the attitude range 210 to 300 km over the equator. O'NEILL (1972) has reported N_2 vibrational temperatures and N_2 , O_2 molecular density measurements by rocket borne electron induced luminescence between 100 to 150 km altitude.

1.3.3 DIFFUSION METHOD

In the lower thermosphere in the height range 120 to 200 km upper atmospheric densities can be obtained from the measurement of diffusion of rocket released trails of luminescent material. GOLOMB AND MCLEOD (1966) ; REES (1971) LLOYD AND SHEPARD (1966), and DESAI AND NARAYANAN (1970) have inferred upper atmospheric temperatures from measured diffusion coefficients of artificial vapour releases. In deducing the temperature from diffusion of vapour clouds, primarily the temperature gradients are measured assuming diffusive equilibrium. Precision in height measurements is very good, but to infer temperatures some additional assumptions are needed like e.g. known temperature at some height.

1.3.4 INCOHERENT SCATTER TECHNIQUE

One of the most powerful ground based methods of studying thermospheric properties is by incoherent radar

scatter observations. This method is currently in use only at three locations, viz., Jicamarca (12°S), Puerto Rico (19°N), and St Nancy (45°N). Thermal fluctuations of the ionospheric plasma gives rise to the incoherent scattering of radio waves GORDON (1958), BOWLES (1961). A detailed study of the technique important results obtained and limitations of this method have been presented by WALDTEUFEL (1971). The power spectra of the back scattered echoes can be interpreted in terms of electron and ion temperatures. The properties of the neutral atmosphere are deduced, using a nonlinear profile of the exospheric temperature, the shape factor in the temperature profile and the atomic oxygen density at a reference altitude in the diffusive equilibrium region. Because of the small magnitude of scattering cross-section of electrons (viz. Thomson scatter cross-section) very powerful transmitters, large antennas and sophisticated data processing are involved. However for all its cost and complicated ness the incoherent scatter has emerged as a very powerful tool in studying earth's atmosphere GIRARD AND PETIT (1978)

Typical vertical profiles of temperature of neutrals (T_n), ions (T_i) and electrons (T_e) of the daytime mid latitude ionosphere is given in Fig. 2.

The incoherent scatter measurements brought out for the first time that the observed temperature maximum is not

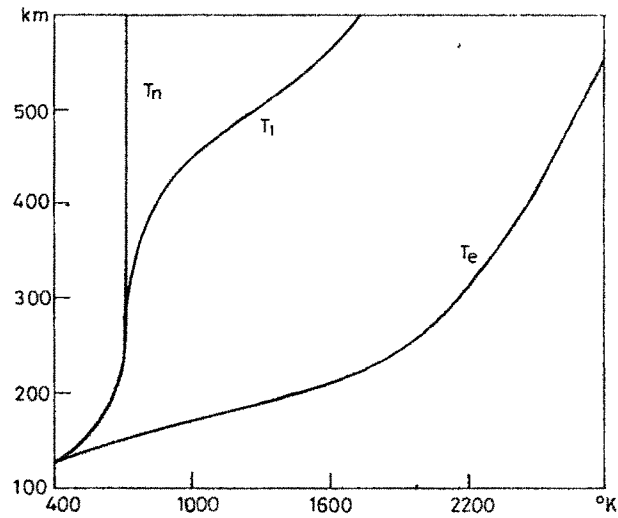


FIG 2 Typical vertical profiles of the temperatures of neutrals (T_n) of ions (T_i) and of electrons (T_e), in the daytime middle latitude ionosphere. At night, when photoionization stops, thermal equilibrium is restored, and T_e and T_i become equal to T_n .

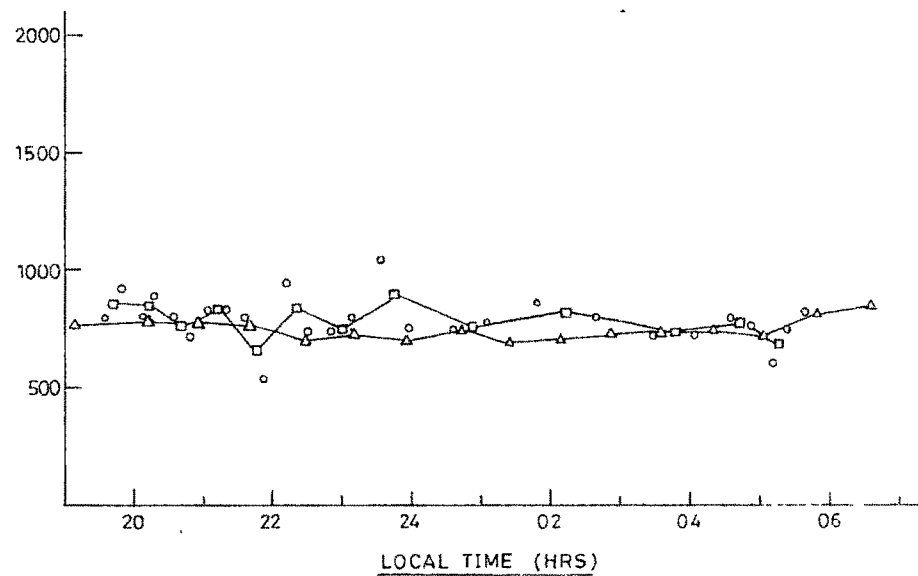


FIG. 3 Doppler and backscatter temperatures measured during the night of October 14-15, 1969. The triangles indicate the ion temperatures measured at an altitude of 300 km above Millstone Hill. The circles denote temperatures deduced from individual Doppler profiles; the squares correspond to temperatures obtained when two consecutive Doppler profiles are combined.

(P. B. HAYS ETAL, J. GEOPHYS. RES. 75, 25, 1970 - PAGE 4882)

in phase with that derived from satellite drag method (NISBET 1967 ; CARRU ET AL, 1967).

WALDTEUFEL (1971) has compared the temperature results from incoherent scatter measurements, rocket probe measurements and satellite drag measurements and concludes that all these results are converging. CHAMPION (1970) and REES (1971A) have shown that during the geomagnetic storm of November 1968 temperature derived by satellite drag method, chemical release technique and from 6300 Å (OI) emission line showed good agreement to one another. HERNANDEZ ET AL, (1975), HAYS ET AL, (1970) have clearly shown the close agreement between the night time exospheric neutral temperature from the Doppler width of the 6300 Å night glow line and the ion and electron temperatures from incoherent scatter measurements. Fig. 3 gives (HAYS ET AL, 1970) the Doppler and backscatter temperatures measured simultaneously from Millstone Hill.

1.4 SPECTROSCOPIC TEMPERATURES

Spectroscopic measurements on optical emissions from upper atmosphere offers a means of directly measuring neutral temperatures. The measurements may be made on artificial luminiscent vapour clouds released by means of rockets or on natural airglow emissions. Measurements may either involve intensity distribution in the molecular

rotation vibration spectra or the line width of an emission line such as night airglow 6300 Å (OI).

The concept of rotational temperature rests upon the assumption that the population of the upper rotational levels J' for the species follows a Boltzmann distribution taking into account the statistical weight factor $2J' + 1$

$$N(J') = N(0) (2J' + 1) \left\{ \exp \left[- \frac{B_{v'}}{K} J'(J' + 1) \right] \right\}$$

where we are considering a simple diatomic molecule with rotational constant

$$B_{v'} = \frac{h}{8\pi^2 CI} \text{ and } I \text{ is the moment of inertia}$$

The intensity of a given line is proportional to the product of the line strength $S(J')$ and the population so that,

$$I(J') = S(J') N(J')$$

and if we take logarithm on both sides,

$$\log \left[\frac{I(J')}{(2J'+1) (S(J'))} \right] = - \frac{hc B_{v'}}{KT} J' (J' + 1)$$

Plots of the left side versus $J'(J'+1)$ are commonly used to obtain rotational temperatures [SHEPHERD (1971)]. The reduction of the data in this way is entirely unambiguous and thoroughly straight forward. The validity of the result,

as a temperature, depends first on the initial assumption, and it is not always obvious that this is true for the upper atmosphere. HUNTEN ET AL, (1963) constructed a filter wheel photometer, with three interference filters which viewed different parts of the N_2^+ band. The three signals were combined in analog fashion to give an output which was a measure of the rotational temperature. MILLER AND SHEPHERD (1968) developed an interference filter photometer for rocket use. Rotational temperatures have also been successfully obtained from the OH radical in the night airglow. One of the most impressive of these is that obtained by CONNES AND GUSH (1960) using a Michelson interferometer.

Similarly, a vibrational temperature can be defined on the basis of the populations of vibrational levels. But, in most cases, it turns out that the populations are determined primarily by the excitation processes, and are insensitive to the atmospheric temperature. Hence vibrational temperatures have been little used in obtaining temperatures for the upper atmosphere SHEPHERD (1971) .

Finally, one can measure a Doppler temperature from line widths of atomic emissions. Here the interpretation is particularly straight forward. Along the line of sight of the observing instrument, the emitting molecules have a

velocity component which follows a Maxwellian distribution

$$N(v) dv = N(0) \exp(-\alpha v^2) dv$$

This transforms into wave number space through the Doppler shift equation as

$$I(\sigma) d\sigma = I(0) \exp - \left[\frac{4 \log 2 (\sigma - \sigma_0)^2}{w^2} \right]$$

where σ_0 is the wave number ($1/\lambda$) for the line center and 'w' the full width at half intensity is given by

$$w = 7.16 \times 10^{-7} \times \sigma \times \sqrt{\frac{T}{M}}$$

where M is the atomic weight of the species.

A measurement of the line width, therefore leads to temperature, but the Doppler method has an important advantage over the others so far discussed. That is, one can see directly whether or not a thermal equilibrium exists as any departures from a Gaussian line shape indicate a non thermal process. Thus, useful and valid information is obtained, even if it does not lead to temperature. Large scale motions in the atmosphere can also lead to observable effects such as winds, which shift the line but do not distort it. Turbulence is capable of changing the shape of the line and preventing a valid measurement. Even here, information which assists in the interpretation is being gained.

Most of the Doppler line width measurements are made on night airglow emissions and aurora with Fabry Perot spectrometers (FPS). The requirement of small spectral range scanning with large angular acceptance and high resolving power make Fabry Perot Spectrometers highly suitable for this type of work. These points will be emphasised in the chapter on instrumentation. The status of the type of work so far done with Fabry Perot Spectrometers for temperature measurements is reviewed here.

1.5 REVIEW OF EARLIER FABRY-PEROT MEASUREMENTS

Airglow emissions provide a means of obtaining upper atmospheric temperatures at the height of emitting layers. Thus OH emissions provide a method of obtaining temperatures at 80-90 km region through the analysis of intensity distribution in the rotation vibration spectra [KVIFTE (1967); NOXON (1964)]. Similarly Doppler width measurements on 5577\AA (OI) atomic oxygen lines have also been extensively used to obtain temperatures at their respective heights of emission. In this respect, 6300\AA has been particularly important as it monitors the exospheric temperature [ROBLE ET AL, (1968)].

1.5.1 PHOTOGRAPHIC WORK WITH FABRY-PEROT

First line width temperature measurements on 6300\AA (OI)

night airglow line were made using photographic recording of Fabry-Perot interferometer fringes. BABCOCK (1923) made observations to determine the wavelength of the unidentified green line. VEGARD (1937) tried to estimate the difference in temperatures of regions near the top and bottom of auroral features from the photographs of the fringe systems; but the use of low reflecting power and a low order (5400) excluded any possibility of either an absolute temperature determination or the detection of any change in the line width corresponding to even 1000°K difference in temperature.

In recent observations WARK AND STONE (1955) have obtained fringes due to both $\lambda 5577 \text{ \AA}$ line from the night airglow and $\lambda 5461 \text{ \AA}$ from an Hg^{198} source on the same photograph. The true width of the mercury line is determined from separate experiments and the width of the $\lambda 5577 \text{ \AA}$ line is deduced from the ratio of the widths of the lines observed in the night glow experiment.

Photographic temperature determinations reported for the airglow $\lambda 5577 \text{ \AA}$ line range from the upper limit deduced by ARMSTRONG (1953) from BABCOCK'S data (1923) and MULYARCHIK (1959) reported limits both of about 450°K to the temperature determinations of WARK. Later WARK (1960) gave a

complete description of the instrument and experiment and arrived at a temperature average of 184°K from four measurements.

The photographic technique suffers from the serious drawback of poor time resolution, namely one exposure per night. Somehow not much was done on 6300 Å (OI) line photographically. The introduction of photoelectric techniques at the beginning of IGY period enabled measurements with a better time resolution to be made.

1.5.2 PHOTOELECTRIC FABRY-PEROT MEASUREMENTS

The basic " Etendue " advantage of the Fabry-Perot (and in general an interference spectrometer) was first recognised by JACQUINOT (1948). The development of low loss multilayer high reflection dielectric coatings and the photoelectric recording techniques have made airpressure scanned Fabry-Perot Spectrometer a versatile equipment in high resolution study of weak extended emissions.

The method was first applied to the $\lambda 5577\text{Å}$ airglow line by ARMSTRONG (1956). A number of photoelectric measurements were made in this paper with an approximate time resolution of 20 min/profile, temperatures range from 180° to 220°K with a median of 190°K derived from 15 measurements.

HERNANDEZ AND TURTLE (1965) used a pressure scanned $5\frac{1}{2}$ inches effective aperture Fabry-Perot interferometer from Bedford Mass. The 5577 Å line kinetic temperatures from these measurements range from 150 to 260°K with a mean of 210°K. All the measurements were taken at Zenith.

KARANDIKAR (1968) made observations of the 5577 Å line profile in aurora with a pressure scanning Fabry-Perot interferometer at Fort Churchill, Canada, located near the auroral zone maximum. The deduced Doppler temperatures for faint diffused glows yielded values in the range 170 - 690°K with about 80% values lying in the range 200 - 400°K.

JARRETT AND HOEY (1966) used a 7 cm clear aperture Fabry-Perot interferometer to monitor 6300 Å O(I) line from night airglow with a spacing of 8.635 mm and a reflectivity of 0.78. The incoming photons were focused on the cathode of an EMI type 9558 photomultiplier tube cooled by solid carbon dioxide. The output of the multiplier was fed to a pre amplifier, amplifier and a rate meter. The output of the rate meters was given to a Honeywell strip chart recorder. The interferometer was operated from Saint Michel observatory in Haute Provence (lat 43°55'N, long 5°43'E). They concluded that the experimental temperature are some

what higher than the expected values so derived from the satellite drag data of HARRIS AND PRIESTER (1964). Moreover their variation with local time is more marked than one would expect. They have given an explanation that this may be due to the patchiness of the 6300 Å emission layer. They argue that arising from this patchy nature of night glow their interferometer would effectively examine different heights of the F layer at successive time intervals.

BIONDI AND FEIBELMAN (1968) used a pressure Tuned Fabry-Perot Spectrometer from Airglow observatory, Laurel Mountain, Pennsylvania and determined the line shapes of oxygen $\lambda 6300$ Å and $\lambda 5577$ Å radiation. The spacing of the plates is 7 mm and the photomultiplier is cooled to -80°C by means of dry ice. The apparatus was operated in current as well as pulse counting mode. Their findings are : 1. In no case is any evidence found for a dissociative line shape in 6300 Å. II. Most of the $\lambda 6300$ Å profiles have thermal Doppler shapes from which temperature of $\text{OI}('D)$ atoms are deduced. III. In some cases the line shape exhibits skewness. There is a possibility in one set of observations that wind shear effects have been detected.

HAYS ET AL, (1969) measured 6300 Å Doppler broadened emission line of atomic oxygen $\text{O } 'D \text{ ---- } \text{O } ^3P$ with "6" inch high resolution Fabry-Perot interferometer during a magnetic

storm from Ann Arbor, Michigan. Two major instrumental improvements are the flatness figure of the plates are $\lambda/180$ and incorporation of a cooled ITT/FW130 photomultiplier with an effective 0.1 inch diameter photocathode thereby reducing the dark current to approximately 1c/sec. The Doppler temperatures obtained gave a realistic indication of the storm time variation of the exospheric temperature. The measured temperature variation is in general agreement with model predictions. P.B. HAYS ET AL, (1970) made comparative studies of the radar and optical temperature measurements in the F region. Temperature measurements were made by the Millstone Hill Incoherent Scatter radar facility ($42^{\circ}30'N$, $71^{\circ}36'W$) and the Michigan Airglow observatory ($42^{\circ}17'N$, $83^{\circ}45'W$) during Oct. 1969. The basic idea behind such study is that during the night midlatitude ion and neutral gas temperatures do not differ to any significant degree near 300 km. The Fabry-Perot instrument used is the same as that used in the previous paragraph and the results appear to be very good. Averaging the temperature values over the night leads to a mean Doppler temperature of $790^{\circ}K$ whereas the mean back scatter temperature is $745^{\circ}K$. This corresponds to a systematic difference of about 5.7% which is well within the accuracy limits. The results presented here gave added confidence in the ion temperature values obtained with the radar back scatter technique and

showed that the 6300 Å Doppler temperature measurements can be used as a monitor of the exospheric neutral gas temperature.

Temperature measurements made by BLAMONT AND LUTON (1972) fromOGO VI satellite provide the most interesting direct observations to date. A spherical Fabry-Perot interferometer whose principle is due to CONNES (1958) was used for this purpose. The results obtained by the authors are : The analysis of OGO VI neutral temperature measurements for September 1969 storm has confirmed the dependence of the geomagnetic perturbation on latitude and has shown several important new features. Neutral temperatures present unexpected maximums in the polar regions and appears to depend on the local time. The observed effect is strongerⁱⁿ night time than in day time. The temperature of the neutral components deduced from these measurements has an accuracy of $\pm 65^{\circ}\text{K}$.

FEIBELMAN ET AL, (1972) employed two Fabry-Perot interferometers of aperture 45 and 100 mm of substantially high resolution and measured ionospheric temperatures from oxygen $\lambda 6300 \text{ Å}$ and $\lambda 5577 \text{ Å}$ spectral line profiles. They have concluded that the exospheric temperatures $T_n(\infty)$ determined from $\lambda 6300 \text{ Å}$ profiles are usually somewhat higher than the temperature calculated from JACCHIA's model &

differences as large as 300°K are noted when $T_n(\infty)$ equals $1500 - 1600^{\circ}\text{K}$. The post sunset and predawn rate of change of $T_n(\infty)$ is often substantially higher than JACCHIA'S prediction. The 5577A (E region) measured temperatures range from 200 to 220°K on quiet nights and $500 - 600^{\circ}\text{K}$ during geomagnetic storms.

By measuring the Doppler shift of the two $\lambda 6300\text{\AA}$ Fabry-Perot fringe profiles direct measurement of thermospheric winds were done by HAYS AND ROBLE (1971) during geomagnetic storms. The results showed a large northerly wind component of the order of 250 to 300 mt/sec. in the altitude region of the maximum of $\lambda 6300\text{\AA}$ emission near 400 km.

DESAI AND RAJARAMAN (1976) measured Doppler line width of $\lambda 6300\text{\AA}$ over MtAbu, India. Neutral temperatures obtained agreed well with JACCHIA model temperatures.

HERNANDEZ ET AL, (1975) made simultaneous measurements of Doppler temperature with a Fabry-Perot spectrometer and electron temperatures from incoherent scatter from JICAMARCA Radio observatory. The mean difference between the incoherent scatter and optical measurements was 26°K for simultaneous measurements and 31°K for all measurements (compared using JACCHIA 1971 model). Since the height of

the incoherent scatter measurement was 400 km and the mean height of the 6300 Å emission was 270 km, this difference is consistent with the $\approx 28^{\circ}\text{K}$ temperature difference in the appropriate JACCHIA models.

HERNANDEZ AND ROBLE (1974, 1976) made direct measurements of thermospheric winds and temperatures during geomagnetic quiet and storm periods. The thermospheric temperature and winds at a height near the F2 peak are determined from the Doppler broadening and shift respectively of the atomic oxygen line emission at 6300.308 Å. The experimentally derived temperatures and winds are compared with a three dimensional semiempirical model of the neutral thermosphere. The large scale details of measured and calculated night time meridional wind components are in general agreement, showing maximum equatoward winds during the summer months. Measured and calculated zonal winds agree for the equinoctical and winter months ; however the measured night time zonal winds are westward during summer months in contrast to model calculations that indicate a midnight eastward to westward transition.

During geomagnetic storm periods the night time equatoward winds are generally enhanced from their

quiet time values with a maximum measured velocity of 640 mts/sec. during a $K_p = 9$ (storm). The zonal winds generally develop a westward component relative to the geomagnetic quiet zonal winds. During intense geomagnetic activity the zonal winds are westward at 100 - 200 mts/sec in the early evening hours, flowing in the direction of magnetospheric convection and opposite of model predictions. The night time neutral gas temperatures are observed to increase from their geomagnetic quiet values during the storm and are in general concurrence with OGO VI model predictions.

CHAPTER - II

INSTRUMENTATION

The aim of recent interferometric studies (ARMSTRONG 1969) of the airglow and aurora has been that of temperature determination from measurements of the fringe, profiles. Experimentally the problem reduces to a determination of the fringe half width in terms of order separation of successive fringes. For a line of wave length ' λ ' influenced solely by thermal broadening the half intensity width ' h ' is related to the absolute temperature ' T ' and atomic weight ' M ' of the emitting atoms by the simple relation

$$h = 7.16 \times 10^{-7} \times \lambda \times \sqrt{T/M} \dots\dots (2)$$

due to BUISSON AND FABRY (1912). Rapid progress in multilayer coating techniques since 1949 and improvements in the sensitivity of the photomultiplier tubes during 1950s have made interferometric photoelectric instrumentation quite handy. In recent years Fabry-Perot interferometers have gained wider application in studied of the profiles of spectral lines emitted by excited atoms in various regions of the earth's ionosphere. (HERNANDEZ AND TURTLE 1965 ; HILLIARD AND SHEPHERD 1966 ; JARRETT AND HOEY 1966 ; BIONDI AND FEIBELMAN 1968 ; ARMSTRONG 1968 ; HAYS ET AL, 1969).

2.1 BASIC CONSIDERATIONS

Obtaining temperatures from the measurements of line profiles required highly accurate measurement of line width, because of the fact that the width is proportional to square root of temperature. Secondly the airglow is faint with the emission rate in the visible region varying from a few Rayleighs (R) to a kilo Rayleigh (KR) or little more. The Rayleigh is a unit (HUNTEN ET AL, 1956) giving the number of photons emitted per second from a column of 1 cm^2 in diameter extending along the line of sight through the emitting region, and corresponds to an emission rate E , of 10^6 photons per second from this column. The surface brightness of a uniform layer of emission rate E is simply,

$B = 10^6 E / 4\pi \text{ photons cm}^{-2} \text{ s}^{-1} \text{ sterad}^{-1}$ Hence with the airglow we are concerned with B from 10^5 to $10^8 \text{ photons cm}^{-2} \text{ s}^{-1} \text{ sterad}^{-1}$ which demands spectrometers of large angular acceptance. The spectrometer device to be used for the measurements of the Doppler width from airglow emissions must therefore satisfy the following requirements.

- (i) Should have adequately high resolution. Instrumental halfwidth should be preferably somewhat less than the halfwidth to be measured. For $\lambda 6300 \text{ \AA}$ night airglow emission line the width is typically 0.035 \AA .

- (ii) Instrumental function must be accurately known.
This is because the instrument width cannot be made arbitrarily small (or else the flux collecting power becomes too low). So, in general the true airglow line width has to be obtained by deconvoluting the observed line width with the known instrument function.
- (iii) The spectrometer must have a large flux gathering power. Flux gathering power can be increased by
 - i) using large aperture dispersing element and
 - ii) choosing a spectrometer system with large throughput (luminosity resolving power product) (MEABURN 1976).

2.2 SPECTROSCOPIC DEVICES

Consider a spectrometer that accepts flux to be analysed from an extended source of surface brightness B (measured in terms of photons $\text{cm}^{-2} \text{s}^{-1} \text{Sterad}^{-1}$). If the device has an entrance aperture A and accepts flux over a solid angle Ω the flux received will be

$$F = \tau \times A \times \Omega \times B \text{ photon/sec}$$

where τ being system transmissivity. ' Ω ' depends, however, inversely upon the resolving power of the spectrometer and

the product $\lambda \times R$ becomes a constant as shown by JAQUINOT (1954). Different spectrometer systems such as prism, grating, Fabry-Perot and Michelson differ with respect to their value of λR . JAQUINOT (1954, 1960) further compared the different systems in this respect and showed that interference spectrometers like Fabry-Perot and Michelson have a large advantage 100 over the grating spectrometers and even larger over prism spectrometers. This advantage is essentially by virtue of the circular symmetry of dispersion in interferometers. Further in case of interferometers the value of λR can be increased further by a large factor by adopting special design (field widening). Field widening is achieved in Fabry-Perot systems by using spherical plates (CONNES 1958) or in Michelson interferometer by introducing a dispersive element in the path of the one of the interfering beams (HILLIARD AND SHEPHERD 1966). Spherical Fabry-Perot interferometer has been used by BLAMONT AND LUTON (1972) in OGo6 satellite for measuring Doppler temperatures of $\lambda 6300\text{\AA}$ airglow line.

Figure 4 (SHEPHERD 1971) compares the offaxis angles at different spectral widths for Diffraction Grating Spectrometer (DGS) Fabry-Perot Spectrometer (FPS) and Wide Angle Michelson Interferometer (WAMI). For the spectral

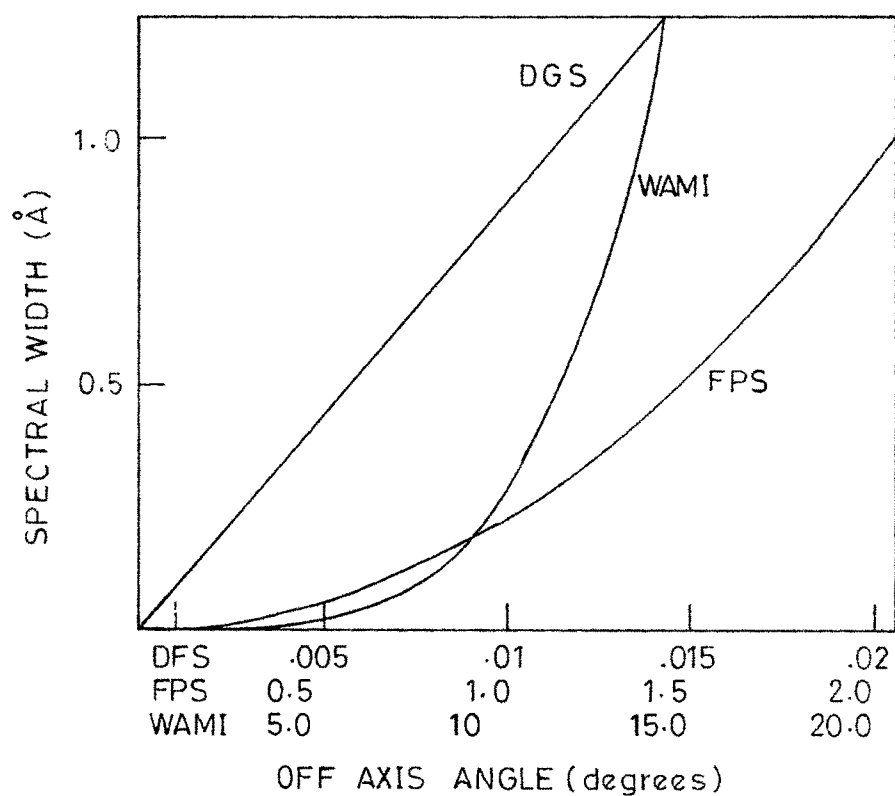


FIG 4 Dispersion curves for various spectroscopic devices. The off-axis angle or slit width is plotted against the associated spectral width for a diffraction grating spectrometer, Fabry-Perot spectrometer, and wide-angle Michelson interferometer. For a given spectral width axis angle increases rapidly for those devices in just that order. Note that a separate degrees scale is required for each device.

widths needed ($< 0.035\text{\AA}$) large advantage of WAMI AND FPS over DGS is quite apparent. WAMI however, has one disadvantage that the line width is to be recovered indirectly from the fringe visibility. (which is a parameter experimentally observed). FPS on the other hand directly observes the fringe profile and hence much better control on experiment is possible and interfering effects if any present, during a particular observation set, can readily be seen. Also now the airglow features have been well identified and their characteristics known, attention has turned to the dynamical behaviour of specific emissions as a function of the many variables that characterize geophysical phenomena. Hence for many problems only a limited spectral range is required, limited often to a single band or line. Hence the conditions of well separated emission spectra and narrow spectral ranges, together with demands of large angular acceptance with high resolving power make Fabry-Perot Spectrometers well suited for this type of experiment.

2.3 FABRY-PEROT SPECTROMETER

Even after the large throughput advantage of Fabry-Perot Spectrometer over Grating spectrometers was realized, it took sometime before Fabry-Perot spectrometers became

widely accepted spectroscopic devices in Atmospheric and Astronomical Studies. A major factor that contributed to the wide acceptance of FPS systems was the development of low light loss multilayer dielectric coatings having high reflectivity, (BANNING 1947) . The transmittance of Fabry-Perot Spectrometer at the fringe peak is given by

$$\tau = \left[\frac{T}{1-R} \right]^2 = \left[1 - \frac{A}{1-R} \right]^2$$

where

- T = Transmissivity of each FP plate
- R = Reflectivity of each FP plate
- A = 1 - (R + T) = Absorption of each FP plate

At high values of R needed in Fabry-Perot etalons (R \gg 75%) metallic coatings like aluminium and silver show significant absorption which results in drastic reduction of τ . Multilayer dielectric coatings can on the other hand give very high values of 'R' with 'A' remaining practically zero. Hence etalons with dielectric high reflection coatings can have $\tau = 1$. Effect of A on τ is shown in figure 5 (TITLE 1970). Typically for fresh silver at R = 85% A = 5%. Hence $\tau_A = 43\%$ This clearly shows the necessity of using multilayer dielectric coatings for etalons intended for use in Airglow spectroscopy.

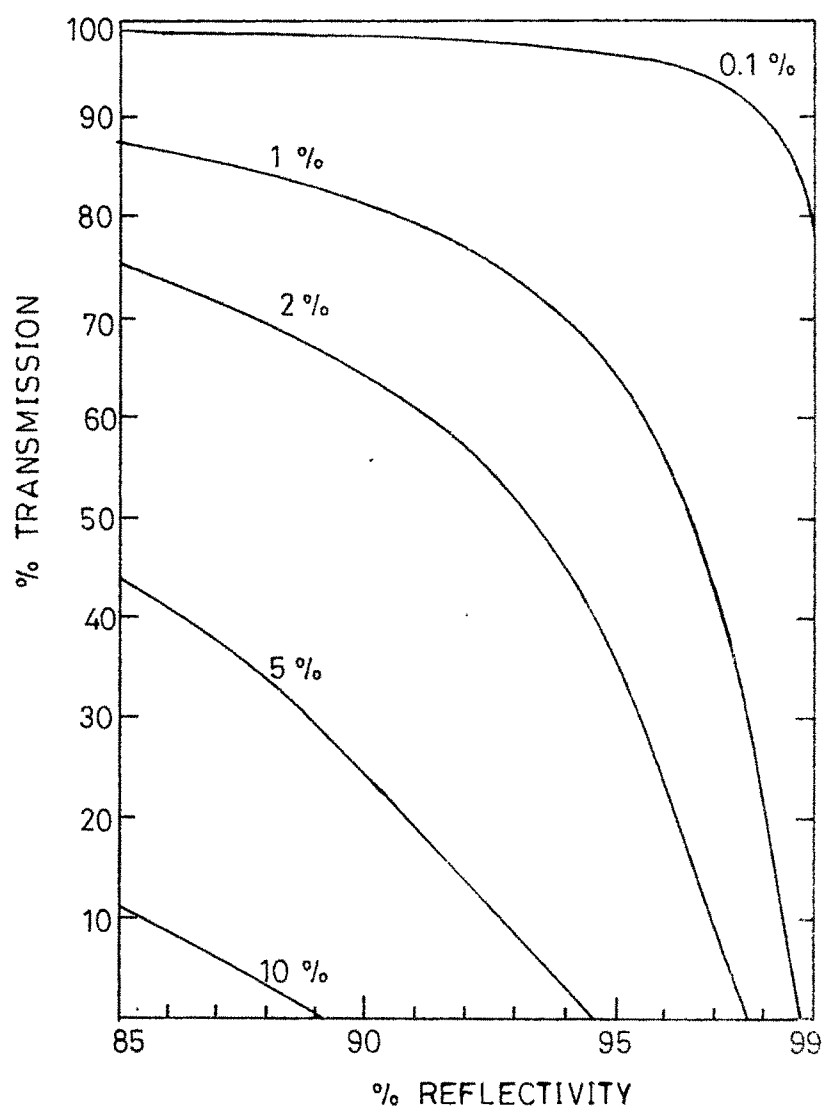


Fig. 5 The maximum transmission, A_{max} , versus reflectivity R_e for several values of mirror light loss L_l . (after Title, 1970).

2.4 BASIC DESIGN OF FPS FOR AIRGLOW LINE WIDTH STUDIES

Air pressure scanned (KARANDIKAR 1968) FPS systems are most widely used in airglow spectroscopy, although piezo electrically scanned devices (BLAMONT AND LUTON 1972, HERNANDEZ 1970) have also been used at times. For basic design of air pressure scanned Fabry-Perot spectrometer One may refer to MEABURN (1976). Essentially one has a pressure tight chamber housing of Fabry-Perot etalon, collimating lens, analysing diaphragm and photomultiplier detector. Line to be analysed is scanned by varying the air pressure in the chamber by some device. Schematic representation of the system is given in Fig. 6.

2.5 PARAMETERS OF FPS AND THEIR OPTIMIZATION

If the separation between the Fabry-Perot plates is 't' then the free spectral range is

$$\Delta \lambda = \frac{\lambda^2}{2\mu t}$$

' μ ' being the refractive index of the medium between the plates (usually air). If we analyze an ideally monochromatic incident flux, using Fabry-Perot Spectrometer with an analysing diaphragm of infinitely narrow angular size, the output function will be what is called the etalon

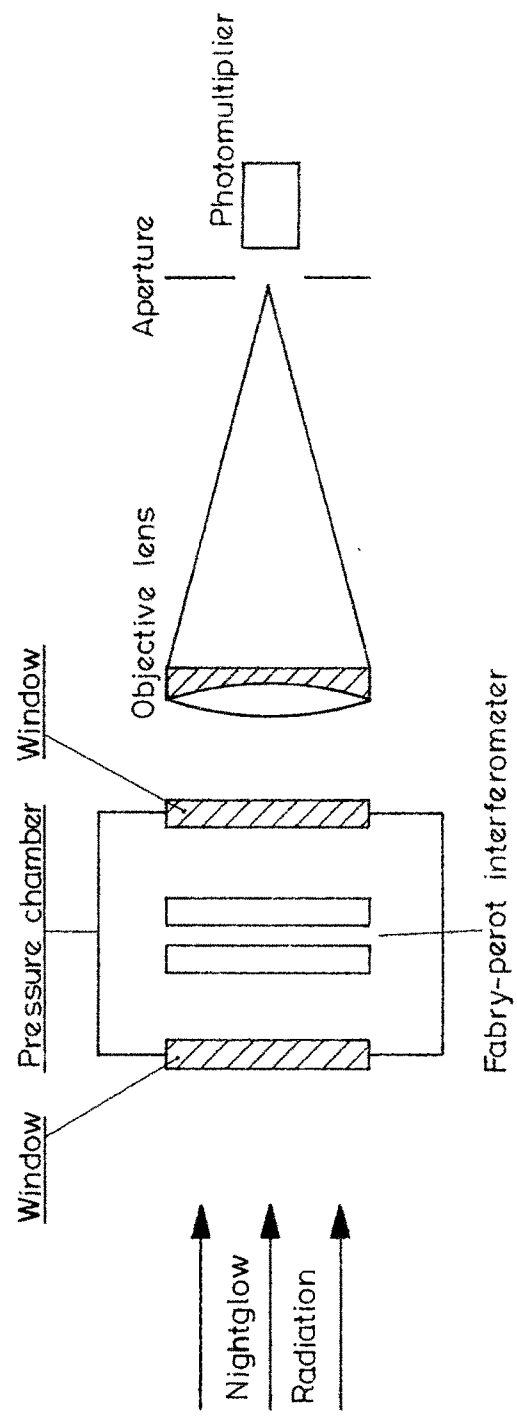


Fig 6 Pressure scanning Fabry Perot interferometer. Basic design

function E. If the width of the etalon function E is "e" (in wavelength units) then the ratio $\Delta\lambda/e$ is the effective finesse of the Fabry-Perot spectrometer. The basic parameters of the Fabry-Perot spectrometer are

- (i) Form of the instrument function
- (ii) Overall transmission of the FPS.

Property of FPS in this respect and conditions for its best use have been studied in great detail by CHABBAL (1958). Here only the essential results are summarized.

The form of the instrument function is jointly determined by

- (i) plate reflectivity and
- (ii) plate figure

Plate reflectivity contribution is expressed in terms of well known Airy function. (BORN AND WOLF 1959 ; CANDLER 1951 ; WILLIAMS 1950). Ratio of the width of free spectral range to that of Airy function is termed as the " Reflective Finesse N_A ".

$$N_A = \frac{\pi \sqrt{R}}{(1 - R)}$$

where R = Reflectivity of FP plates. The etalon function E is also broadened by imperfections of the flatness

of FP plates (and also due to misalignment i.e. lack of perfect parallelism between the plates). Plate imperfectness may be

- (i) microtopographical errors, essentially randomly distributed
- (ii) plate curvature

Analytical forms of the broadening functions associated with plate figure imperfections have been discussed by DUFOUR AND PICA (1945) and HILL (1963). We only note here the following important points.

Microtopographical errors are expressed in terms of the root mean square fluctuations from an ideal plane. Let this (expressed as a fraction of wavelength - normally Hg 5461A) be λ/n . The broadening due to this type of plate figure imperfection is Gaussian in its analytical form and has a width given by $1/N_D$ where $N_D = n/4.7$. So typically if the plates are qualified as say $\lambda/50$, limiting finesse due to plate figure will be $N_D = 50/4.7 = 10.6$.

Other major type of plate figure error is its curvature. Here the Sagitta $[(1 - \cos\theta)r]$ is expressed as $\delta x = \lambda/n$; The broadening function can now shown to be rectangular in shape with full width in terms of

fraction of free spectral range, given by $2/n$; so that the associated coefficient of finesse is $n/2$ overall performance of the etalon will now be described by a broadening function E which itself is a convolution of three independent broadening functions viz.

- (i) Airy function (A)
- (ii) Broadening due to microtopographical errors (D_G)
- (iii) Broadening due to plate curvature errors (D_R)

The two latter functions convolved together are usually written as $D = D_G * D_R$. Form of D can vary from Gaussian to rectangular in extreme cases. Overall etalon function is $E = A * D$ and width of E will be larger than individual widths of D_G , D_R and A . As a guideline one can always recall when two Gaussian functions G_1 and G_2 are convolved, the resulting function G is also a Gaussian and if g_1 , g_2 and g are the respective widths then

$$g = \sqrt{g_1^2 + g_2^2}$$

Finally there is broadening associated with scanning aperture, scanning aperture being of finite radius, allows a finite wavelength interval to fall on the detector. Let us restrict the consideration to situation where aperture is

placed exactly on the axis of Fabry-Perot Spectrometer. (is concentric with the fringe system). Off axis aperture will in general cause assymmetric scanning function and is therefore undesirable. The value of wavelength interval ' $\delta\lambda$ ' passed by the scanning aperture is readily obtained using the basic Fabry-Perot etalon equation

where t = Seperation of FP plates
 n = order of interference and
 λ = wavelength of light

Let ' r ' be the radius of the aperture and ' f ' be the focal length of the collimating lens. Semiangle made by the aperture at the lens is $\phi = r/f$. Hence since all the wavelengths within $\delta\lambda$ are transmitted with equal efficiency ($\simeq 1$), form of broadening function associated with the scanning aperture is also rectangular of width

$\delta\lambda = \frac{\lambda\theta^2}{2}$. One can associate coefficient of finesses with this given by

$$(N_F)^{-1} = \frac{\delta\lambda}{\Delta\lambda}$$

$\Delta\lambda$ being the free spectral range. Unless the source brightness is very large $\delta\lambda$ cannot be made very small.

2.6 TRANSMITTANCE OF ETALON

It was seen earlier that the transmission of ideal F.P. etalon is

$$\tau = \left[1 - \frac{A}{1 - R} \right]^2$$

A being the absorption coefficient of FP plates. For properly made dielectric high reflection coatings $A \simeq 0$ and $\tau = 1$; For non ideal FP etalon (with plate imperfections, finite scanning aperture) there is further reduction in transmission. Let

$$\tau_A = \left[1 - \frac{A}{(1 - R)} \right]^2$$

Depending upon the relative widths of functions A (Airy), D and F (the function associated with scanning aperture) there is further loss of transmittance which will be described now. Here a brief summary of results which find immediate application is presented. For details reference should be made to CHABBAL (1958, 1953).

Quite often the primary constraint on the experimenter will be the quality of available Fabry-Perot plates, which means that one starts with a predetermined value of N_D . Values of N_A and N_F have now to be optimized with respect to resolution and transmittance.

Figure 7b gives the variation of transmittance with the ratio N_A / N_D for the two cases where D could either be D_G (plate figure limited by microtopographical errors) or D_F (curvature of plates). It is seen that substantial reduction in \mathcal{C}_E could happen particularly if D is D_G , when

$$N_A / N_D > 1$$

on the other hand choice of too low a value of N_A could cause large reduction in effective overall finesse, and hence the resolution without corresponding gain in transmittance. When resolution and transmittance are equally important as in the case of night airglow line width study, $N_A \simeq N_D$ is a good choice.

It is also necessary to match the size of the scanning aperture with the etalon finesse as determined by the width of the function

$$E = A * D$$

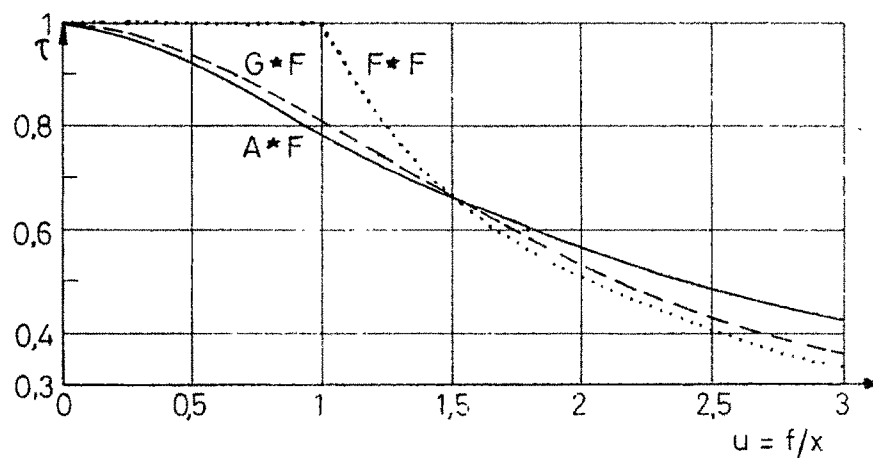


Fig. 7a. Above set shows effect on Transmission T_E of the width due to scanning aperture to that of the etalon function (i.e. ratio N_E/N_F ; in fig. f/x). Etalon function could be: rectangular F
Gaussian G
or Airy A

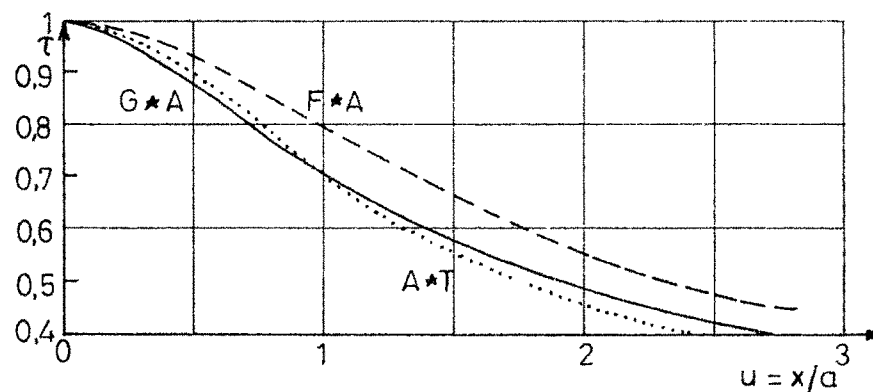


Fig. 7b. Above set shows effect of the ratio of width of plate function to the width of Airy function on the transmission (i.e. N_A/N_D ; in fig. x/a) D could be rectangular F
Gaussian G
or Triangular T

This is seen from the curves given in Fig. 7a which shows the dependence of τ_F on the ratio of width of etalon function to that of scanning function. Scanning function is always rectangular, defined by finesse N_F . Etalon function could have any form extreme cases being Airy, Gaussian or rectangular. Hence τ_F is shown as a function of N_E / N_F when E could be either R, G or F. Here again it is observed that to have a combined optimization for transmittance and resolution

$$N_E \simeq N_F$$

seems to be a good choice. Overall Fabry-Perot Spectrometer transmission is then given by

$$\tau = \tau_A \times \tau_E \times \tau_F$$

2.7 CHOICE OF PARAMETERS IN PRESENT EXPERIMENT

The Fabry-Perot plates used in the present experiment were 70 mm aperture and $\lambda/30$ flatness ; plate figure being basically curvature limited. Since 70 mm is not quite large enough aperture for night airglow observations, it was necessary to have τ as large as possible without unduly sacrificing resolution. In accordance with the thumb rule

$$N_A = N_D$$

Plates were coated with alternate layers of Zns and MgF_2 (5 layers) to give a reflectivity of 75% and $N_A = 10.9$. Because parallelism was not servocontrolled, some misalignment was expected which would further reduce N_D . Preliminary tests indicated that $N_D > 10$ was not likely to be achieved. With N_A and N_D both about 10, N_E was expected to be around 7. With collimating lens of focal length 500 mms, scanning aperture of diameter 2.7 mm was used which gives

$$\frac{\delta\lambda}{\lambda} = 3.6 \times 10^{-6} ; \text{ or } \delta\lambda = 2.27 \times 10^{-2} \text{ \AA}$$

Etalon spacer chosen was approximately 1.5 cm which gives a free spectral range of 0.13Å. This choice was based on the requirement that maximum resolution be attained without order overlap occurring. About three times the line width expected (0.04 Å) was considered a good choice. N_F was therefore

$$\frac{0.13}{2.27} \times 10^2 \simeq 6$$

overall spectrometer finesse expected was approximately

$$\left[\left(\frac{1}{6} \right)^2 + \left(\frac{1}{7} \right)^2 \right]^{-\frac{1}{2}} \simeq 4.5$$

Laser calibrations showed in general an average finesse of little less than 3 ($\simeq 2.9$). Significantly lower value of observed finesse is mostly due to contribution of misalignment. Optically contacted Fabry-Perot etalons which have now become available in recent years permit working with very high degree of parallelism and would ofcourse be now a better choice. Other alternative, which is active or dynamic stability has been obtained by means of servocontrol using white light fringes (RAMSAY 1966 ; 1962), a reference wedge etalon etc. In the dynamic case a feedback stabilisation method described by HERNANDEZ AND MILLS (1973) in which creating correction signals proportional to the displacement of the fringe maxima of three auxiliary spectral sources with respect to a fixed reference point and feeding these signals back to the interferometer piezo electric drive so that the correcting signals become time invariant, and the interferometer is stabilised in parallelism up to $\lambda/1000$, is remarkable.

General schematic arrangement of the entire system is shown in Fig. 8. The Fabry-Perot plates are accommodated on a step in a brass chamber and rests on the full area and not on three ball supports as described by NILSON AND SHEPHERD (1961). The plates were fabricated by the author at the optical workshop of Bhabha Atomic Research Centre,

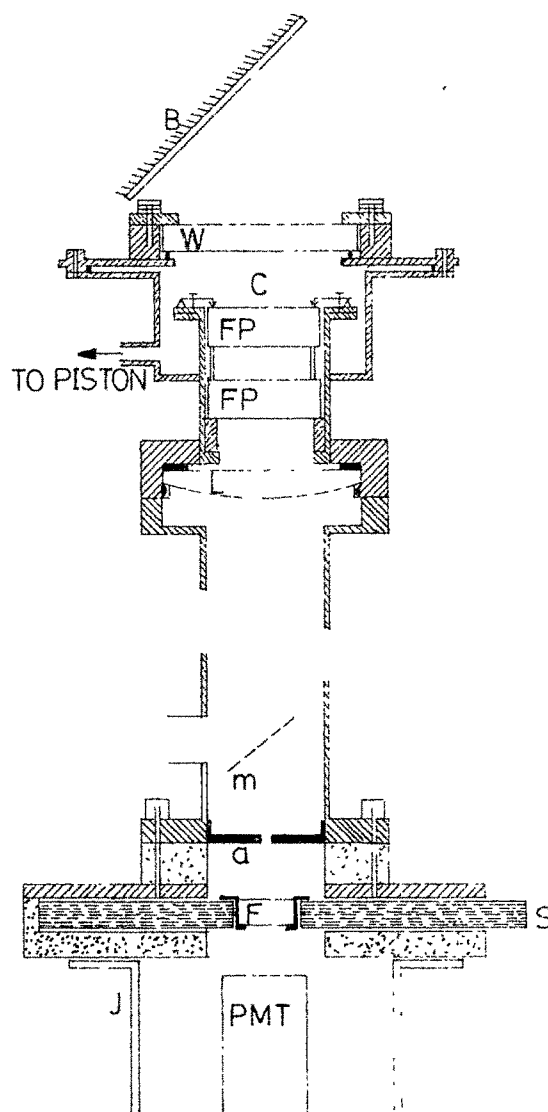


Fig. 8 Experimental set-up of the Fabry-Perot interferometer (Pressure variation section is not shown)

- | | |
|--------------------------|-----------------------------------|
| W - Window | a - Scanning aperture |
| C - Pressure chamber | F - Interference filter |
| FP - Fabry perot plates | S - Blanking shutter |
| L - Collimating lens | PMT - Photomultiplier |
| m - Viewing mirror | J - Jacket (cooling) for PMT |
| B - Mirror for admitting | airglow radiation to spectrometer |

Bombay, India. There is a mirror 'm' which can be introduced from a side window to view the fringes for checking the alignment with a spectral lamp (cd) and is taken out during observations. Below the scanning aperture 'a' is an interference filter 'F' and a photomultiplier P.M.T. The interference filter has a halfwidth of 2.5\AA with a central pass band wavelength of 6301\AA and a transmission of about 40%. The temperature of the filter is maintained at 15°C by a servocontrolled circuit and the filter is tuned to 6300\AA exact. The accuracy of this temperature control is $\pm 0.3^{\circ}\text{C}$. A plane mirror is kept over the front window W of the spectrometer set up which can be moved in azimuth and elevation to direct radiation in to the spectrometer from any portion of the sky.

2.8 DETECTION COUNTING AND PRINTING SYSTEMS

The detector was a 14 stage PHILIPS photomultiplier, type TVP 56 with a trialkali S20 cathode having a quantum efficiency of 0.1. The photomultiplier housing is a double walled brass chamber where cooled glycol is circulated by means of a water pump thus keeping the photomultiplier around -10°C . The glycol is cooled by means of an immersion type cooler refrigeration system made in Physical Research Laboratory. The photomultiplier was operated at 2500V.

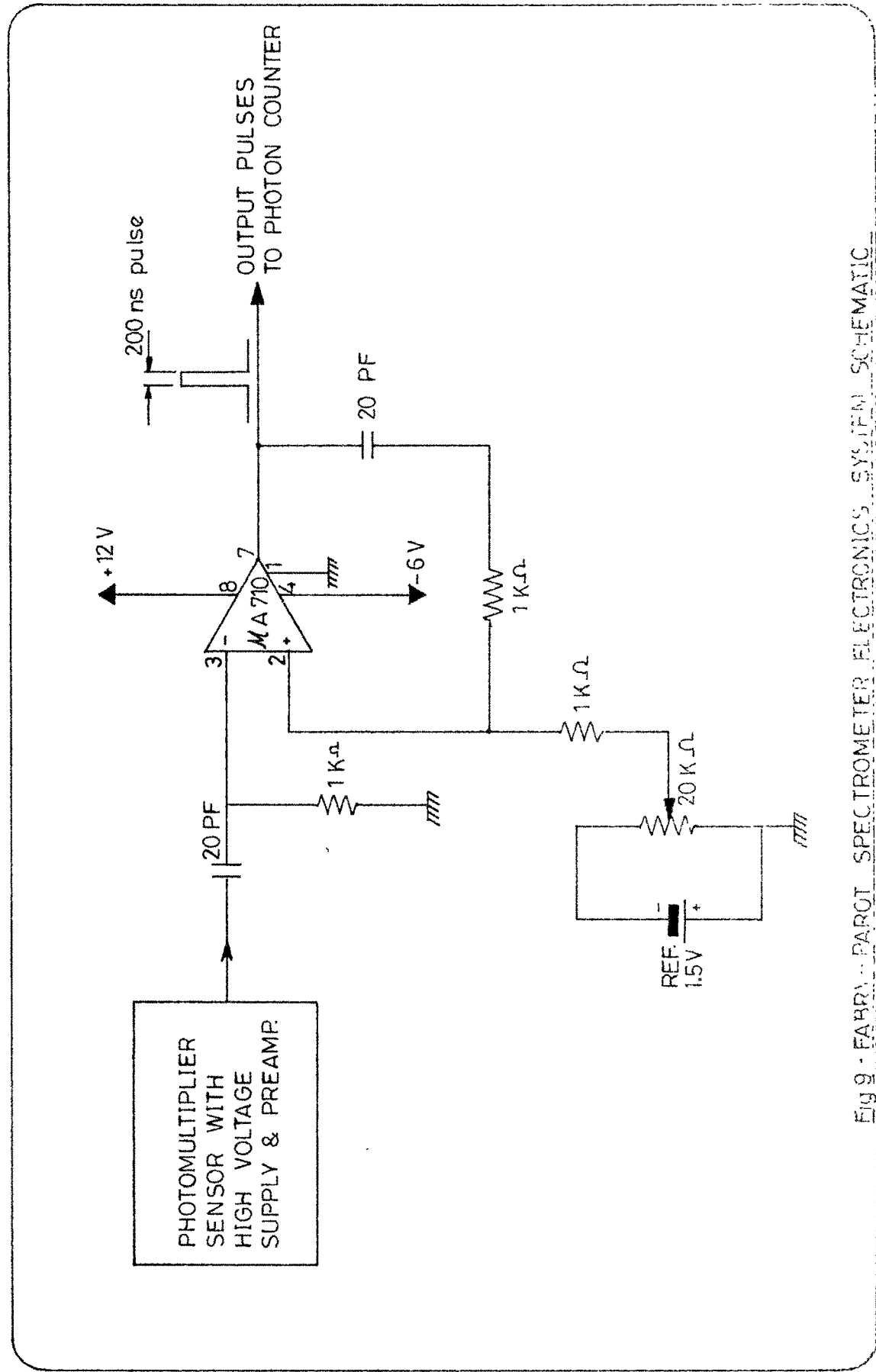


Fig 9 - FARBY - PAROT SPECTROMETER ELECTRONICS SYSTEM SCHEMATIC

The output of the photomultiplier is operated in a pulse counting mode. Its output passing through a discriminator and pulse shaping circuit. This type of pulse counting was employed by many workers (FEIBELMAN ET AL, 1972, HAYS ET AL, 1969). The single electron pulses were discriminated at a suitable voltage level and monoshot pulses were generated for counter using Fairchild IC μ A 710 (MILLER 1968). Detailed circuit diagram is shown in Fig. 9. These pulses were displayed in a frequency counter and simultaneously printed in a digital printer.

2.9 SCANNING SYSTEM

As it was shown earlier that the Fabry-Perot plates are contained in a pressure tight housing and the concentric ring interference pattern is imaged by a lens on a plate containing a small aperture centered on the pattern. Thus a portion of the radiation constituting the central spot of the pattern passes through the aperture to the detecting photomultiplier. The wavelength corresponding to constructive interference at the central spot is made to change with time or in other words the fringe system is scanned with time by pressurising the medium, thereby producing a consequent change in the refractive index of the medium in the chamber. This type of index of refraction

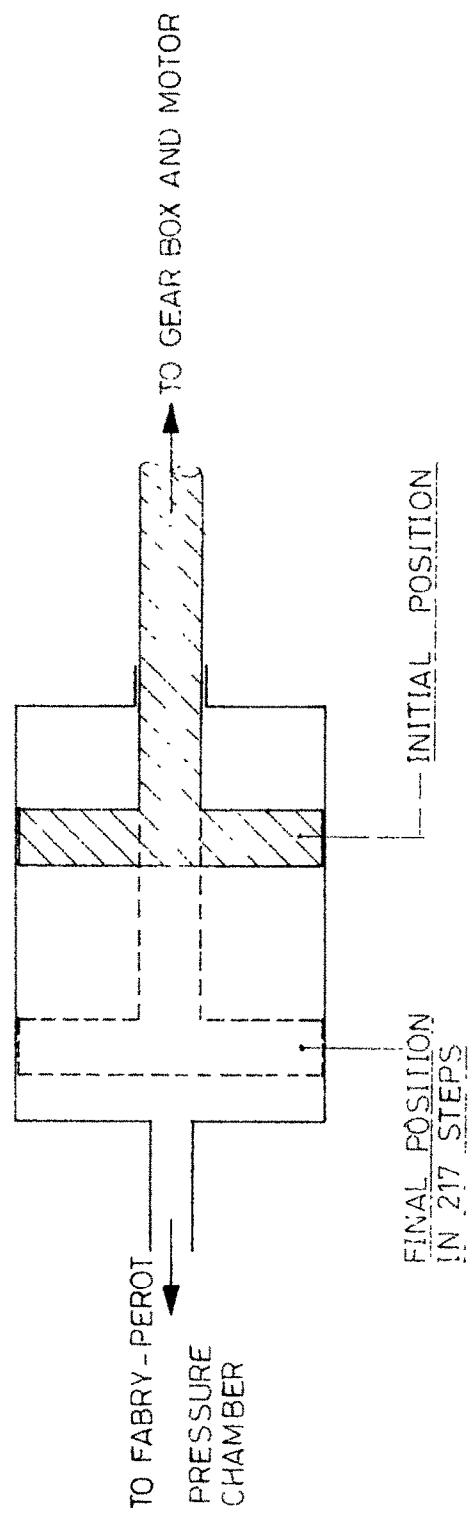


Fig 10 Schematic diagram of scanning piston device

scanning was described by CHANTREL (1958), KUAN ET AL, (1968) and COOK (1960). This refractive index variation is effected by means of a Cam and Piston arrangement. The Piston system is shown in fig. 10. It contains a cylindrical Cam with the piston connected to a screw and gear system to the main shaft of a continuous Ac motor of 1/10 HP. The continuous motion of motor is converted to step motion by using a geneva gear system. Steppings are repeated at ≈ 3 seconds interval. As the motor operates the screw advances and pushes the piston forward. Total travel of the piston is 26 mms which is effected in 217 equal steps by means of a geneva gear drive. Since it is a reversible motor and hence the direction of travel of the piston can be reversed and scanning is effected during forward as well as in the reverse motion of the piston. Since the volume that is changed in equal steps the pressure steppings (ΔP) are nonlinear. Since the exact value of pressure at each step is known, fringe profile is plotted after linearising pressure values.

CHAPTER - III

DATA ACQUISITION, REDUCTION, CALIBRATION AND ERROR ANALYSIS :

The Fabry-Perot spectrometer used for the present work was a digitally pressure scanned instrument with photon counting detection synchronised with pressure steps. The description of the instrument along with the subsystems is given in the previous chapter. The instrument was operated from Mt Abu (24°N) India, during 1976-78. Data were acquired during the months of December to April only, these being clear sky months.

3.1 DATA ACQUISITION

As stated earlier the scanning of the fringe profile was achieved by means of the piston device. Piston movement was in steps at intervals of ≈ 2.5 sec. Disadvantage of the simple piston device for effecting pressure variation was the nonlinear stepping in pressure (steps being in equal volume). However this is not a serious problem as each step was calibrated in terms of pressure absolutely and the starting pressure was always atmospheric. The data acquisition sequence was as follows. In between the steps of the piston a microswitch gave a pulse which sequentially actuated the following events :

- (i) Transfer and print of the previously registered counts on the printer.

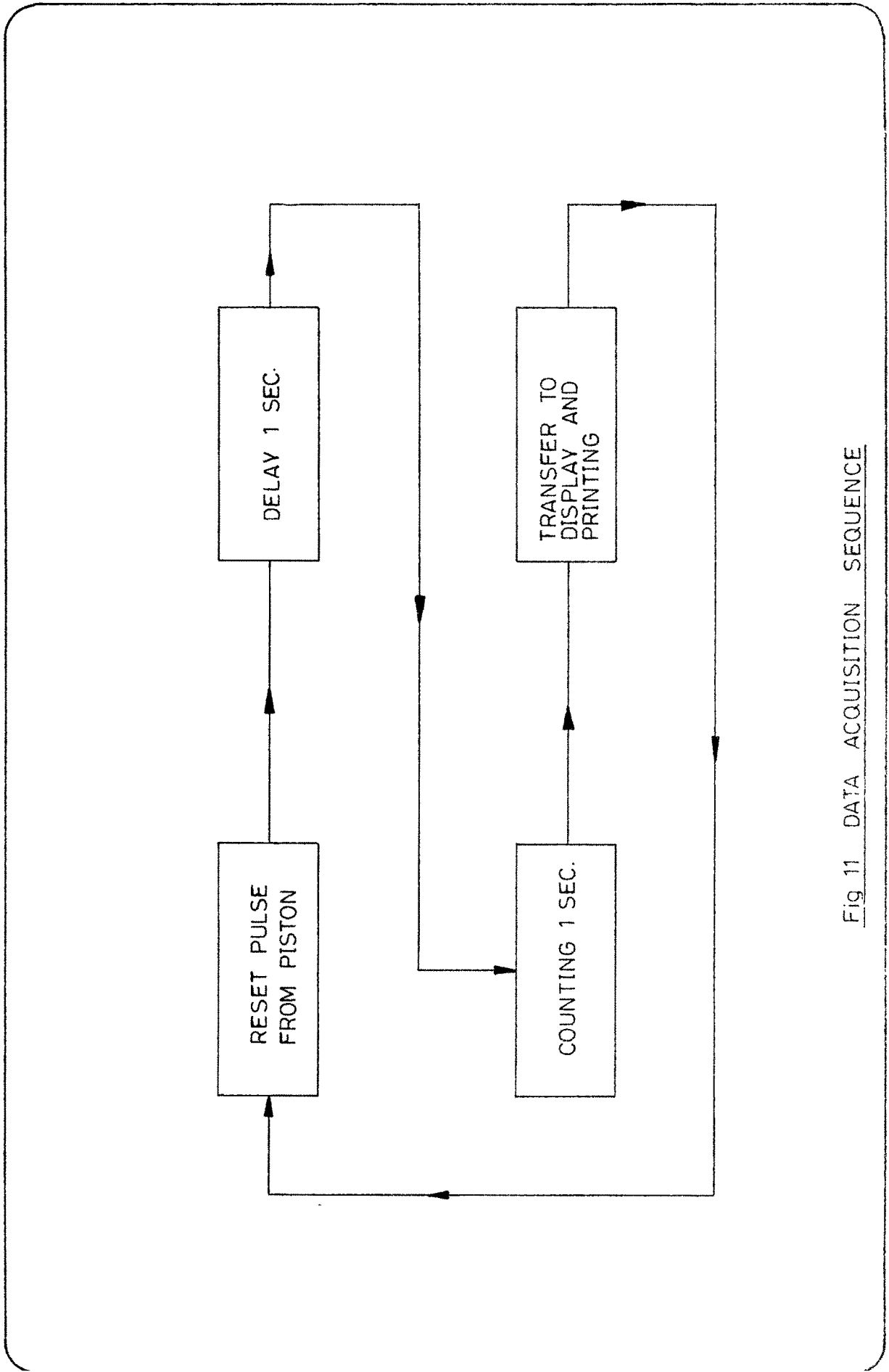


Fig 11 DATA ACQUISITION SEQUENCE

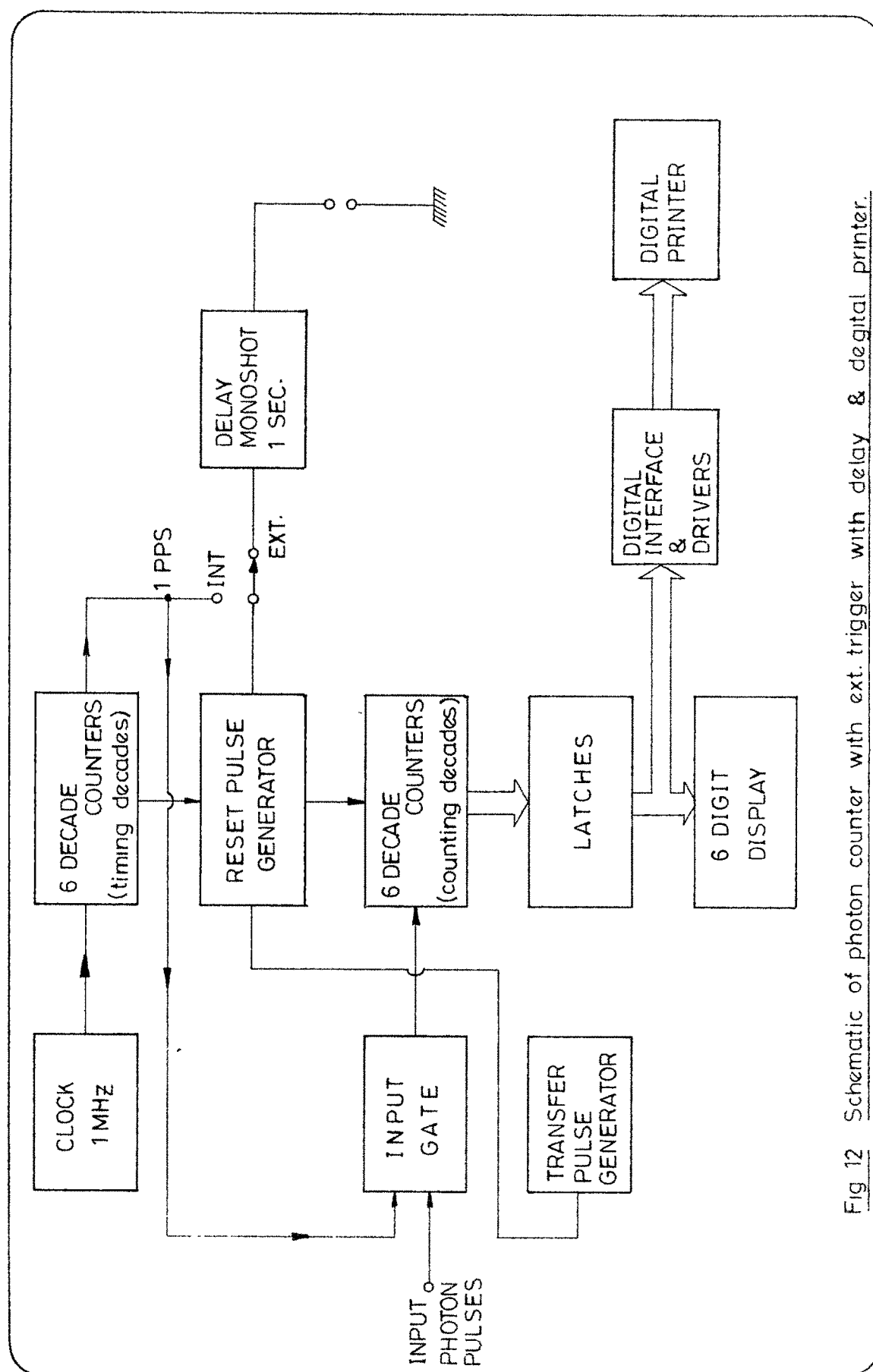


Fig 12 Schematic of photon counter with ext. trigger with delay & digital printer.

- (ii) Reset counter to zero.
- (iii) After a delay of 1 sec. open the gate to allow the photomultiplier counts to the counter.
- (iv) Shut the gate after 1 sec.

Fig. 11 gives the block diagram of data acquisition sequence. The delay of 1 sec. is arranged in between two data points for pressure relaxation and equilibrium in the chamber.

Fig. 12 gives the block diagram of the photon counter with external trigger and delay. The counter and the circuits were developed in the physical Research Laboratory.

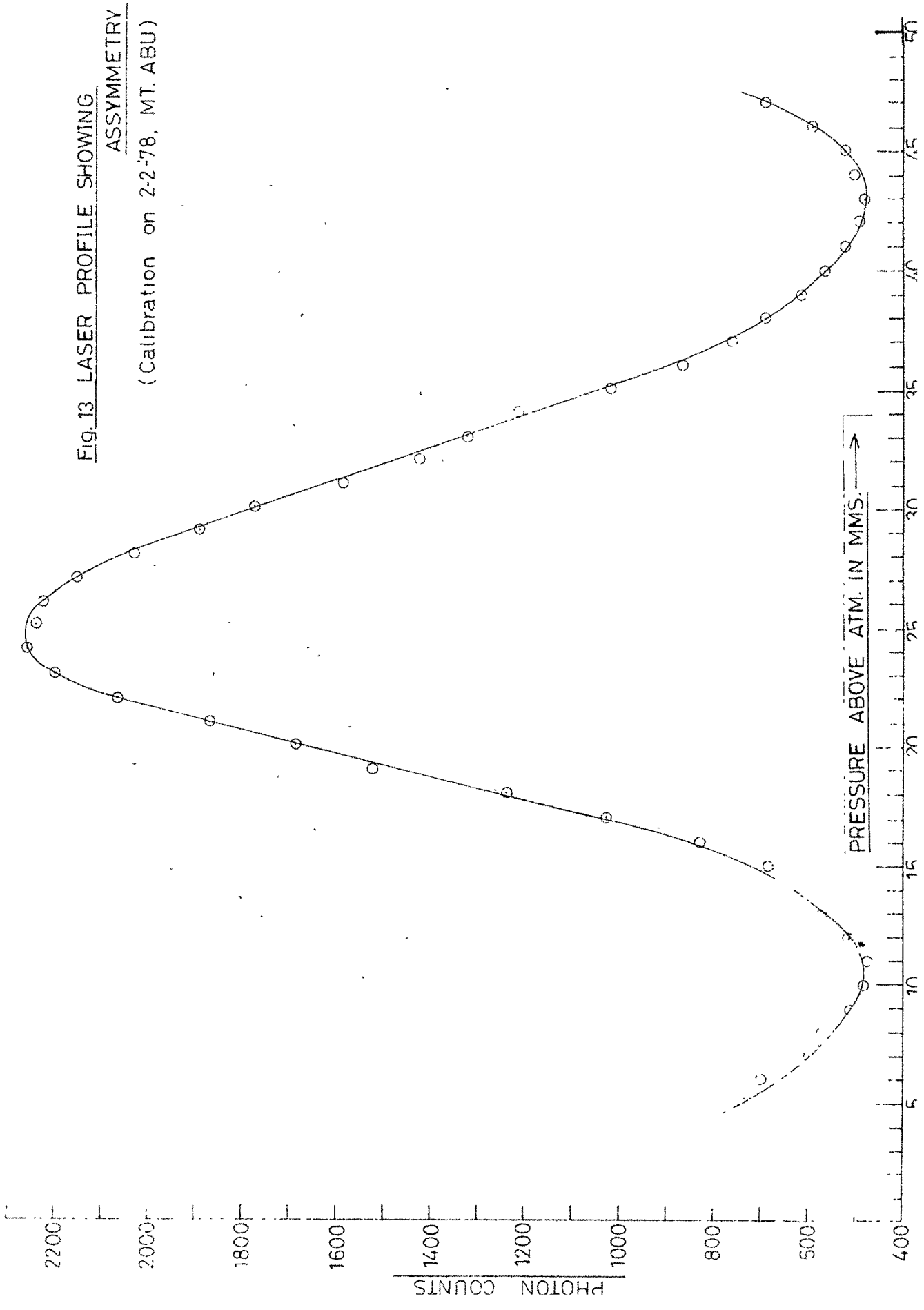
Data was acquired both during forward as well as reversed travel of the piston. The piston travel was in 217 sees giving a total pressure change of about 16 cms of Mercury, thus producing a wavelength scan of about 0.32 Å. Since the free spectral range of the Fabry-Perot interferometer was 0.1296 Å, approximately two and a half orders were scanned over a single travel of the piston. At the end positions of the piston microswitches were provided to cut off the power supply to the motor. A switch was also kept to reverse the direction of travel of the piston.

In situations where intensity of airglow radiation was rather low at 6300 Å, four scans were added in phase in order to improve the signal to noise ratio.

3.2 LASER CALIBRATION

The instrumental profile of the Fabry-Perot spectrometer was acquired using a commercially available He-Ne laser (λ 6328 Å). Since tuning of the interferometer was done manually identical degree of parallelism of interferometer plates could not be ensured every time and hence after tuning the interferometer laser calibration of the instrument was done either before airglow line scan or after. Upto December 1977 end, calibrations were performed with ORIEL laser with polarised, 1 mw output. End of the working life of that laser required it to be substituted by COHERENT OPTICS 2 mw laser, with unpolarised output. In the unpolarised output with the plasma tube length $L \approx 30$ cms, there are two orthogonally polarised beams separated in frequency by an amount $C/2L \approx 650 \text{ MHz}$ or 0.008 Å. Hence one can not consider this beam as ideally monochromatic. Effect of this double frequency output was carefully calculated and found to be equivalent to broadening of observed instrument function by an amount ≈ 0.0012 Å, in mean observed instrument width of 0.047 Å. Observed instrument widths were reduced by this amount to get the true instrument width.

At times an additional problem was encountered with this laser in that, the observed instrument function showed asymmetry. Since airglow profiles never showed such asymmetry, it was concluded that the asymmetry was caused by the laser. Fig. 13 and 14 show the typical laser profiles recorded on two occasions. The profile in Fig. 13 is clearly asymmetric. In order to understand the cause of asymmetry we carried out a high resolution spectroscopic study of the laser beam using a variable airgap Fabry-Perot interferometer with ≈ 15 cm path length and Fabry-Perot plates of surface quality $\lambda/100$. Photographs of the fringe systems obtained at different times are shown in fig. 15. Essentially it was found that at times the output from this laser contained 3 modes with intermode frequency separation of 650 MHz . In that situation intensity distribution amongst the modes is quite uneven and one of the three modes is very weak. Hence the overall profile seen by the Fabry-Perot interferometer shows asymmetry. This effect occurs probably when insufficient time is allowed for laser to stabilise. Otherwise only two modes are observed with more or less equal intensity. Output from SPECRA-PHYSICS, 1 mw, laser with unpolarized output was also examined for the sake of comparison. This always showed only two modes. Presumably, the higher power output of 2 mw in coherent optics laser allows it to sustain at times 3 modes.



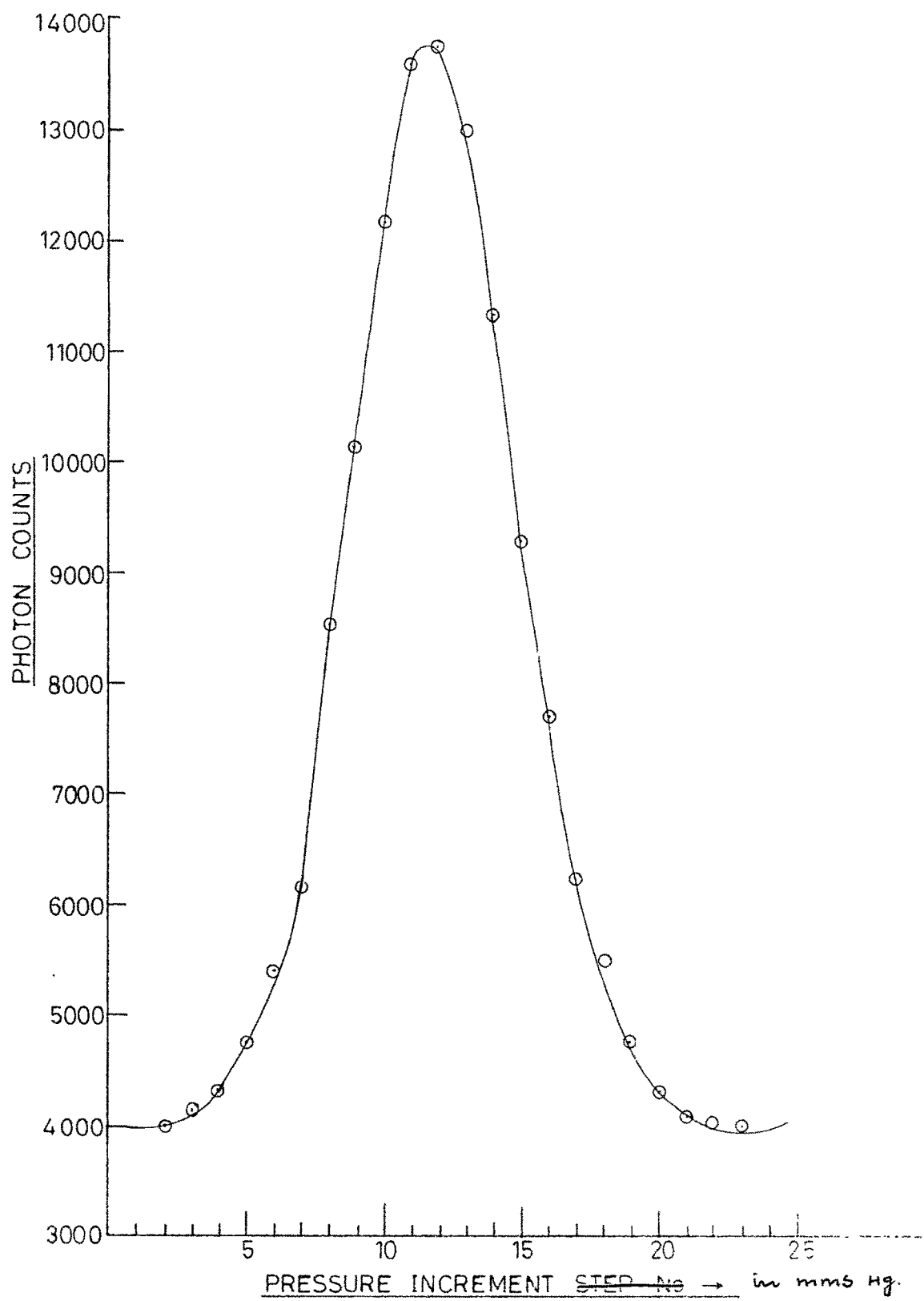


Fig. 14 LASER PROFILE SHOWING SYMMETRY
(Calibration on 7-2-78, Mt. Abu)

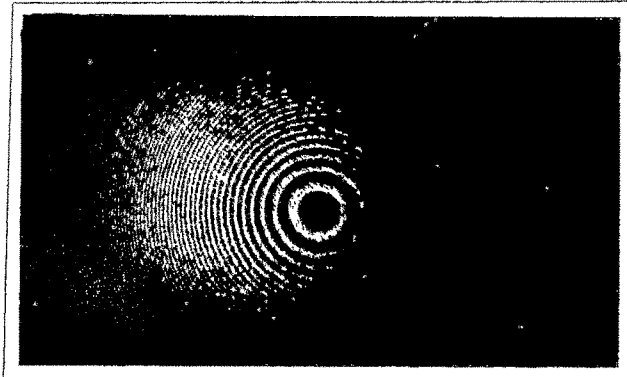
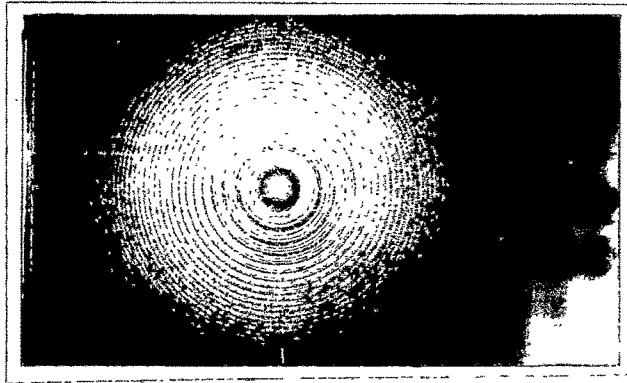


Fig. 15 : Laser fringes photographed at different times

- a) showing three distinct modes
- b) showing two modes
- c) showing single mode, one mode suppressed by a polarizer

3.3 DATA ANALYSIS, DECONVOLUTION SCHEME

The observed profile obtained using a Fabry-Perot spectrometer is a convolution of true emission line profile and the instrument function. One of the difficulties in determining the temperature of the emitting oxygen atoms from the Doppler broadening of fringes was that the Doppler width of the fringe was masked by an instrumental width of the same order of magnitude. When the two functions are of comparable width, careful monitoring of the instrumental profile and subsequent deconvolution procedure to isolate the emission line profile from the observed profile is very important.

The output profile obtained with a Fabry-Perot spectrometer is the recorded profile " Y " is in general a convolution of profile ' B ' of the source spectrum and the profile ' I ' of the instrument function [RAUTION (1958) ; JACQUINOT AND DUFOUR (1948)] . This is mathematically expressed as

$$Y = B * I \quad (* \text{ denotes convolution})$$

which means

$$Y(\lambda_0) = \int_{-\infty}^{+\infty} B(\lambda) I(\lambda - \lambda_0) d\lambda$$

Taking fourier transforms

$$Y = B \times I$$

The Fourier transform of " Y " is equal to the product of the Fourier transforms of B and I. B can be obtained by dividing the Fourier transform of Y by that of I, followed by an inverse transformation. This is the general deconvolution scheme.

The form of the function ' I ' is again a convolution of several independent functions.

- i) Airy function given by the reflectivity of the plates
- ii) Plate finesse function limited by microtopographical errors in plate flatness. Form of this function is Gaussian.
- iii) Plate finesse function determined by the curvature of plates. Form of this function is rectangular.
- iv) Finesse function is limited by the errors in parallelism of the plates.
- v) Instrument resolution as limited by the angular width of the acceptance aperture at the focal length of the collimating lens. For a circular scanning diaphragm centered on the fringe system the form of the function is rectangular.

Of these functions excepting (iv), all functions remain constant. Since aligning the interferometer cavity

to get identical degree of parallelism of different days of observations is not possible, it is imperative to acquire laser instrumental profile on each night along with the recording of airglow line. Frequently the instrumental profile was recorded twice. After adjusting for parallelism by visually seeing the fringes from a Cd lamp using a red filter, either the airglow line is recorded followed by a calibration scan or viceversa.

Use of laser line at $\lambda 6328 \text{ \AA}$ (close to the emission line at $\lambda 6300 \text{ \AA}$) permits one to use the profile recorded as the true instrument function which is the convolution of individual functions related to different broadening factors (viz. i to v listed above). Hence the analytical form of the individual broadening functions were not considered. HERNANDEZ (1966) discussed in detail these broadening functions and had given analytical expressions. Since the difference in the wavelength of the airglow line ($\lambda 6300 \text{ \AA}$) and the laser line ($\lambda 6328 \text{ \AA}$) is small, the form of $I(\lambda - \lambda_0)$ at both wavelengths was assumed to be same. It was assumed that the laser line is a ' δ ' function.

3.4 METHODS OF FINDING TRUE DOPPLER WIDTH, METHOD OF SYNTHETIC PROFILES :

For determining the true Doppler width and hence

the temperature the method of synthetic profiles was mostly employed in the present experiment. This method is well discussed by many authors. HAYS AND ROBLE (1971) ; FEIBELMAN ETAL (1972) ; RAJARAMAN ETAL (1979) . This is summarised as follows :

Doppler broadened atomic oxygen line profiles at 6300 Å for different temperature ranges between 700°K - 1200°K at 100°K interval were computer generated. The observed instrumental profile is then convolved with these Doppler profiles, pertaining to different temperatures, using computer and a series of synthetic profiles were obtained for each set of data. (Since for every set the instrumental profile was different). The observed airglow profile was plotted and then matched with this series of synthetic profiles and the closest fitting curve was selected as that representing the true temperature. Arbitrary shift of the base line in general was accepted as to be due to contribution of continuum which was not separately determined. One particular set of synthetic profiles with an airglow profile (λ 6300 Å) on 8th Dec 1977 is shown in figure 16. The matching is evident from the figure and the temperature estimated was 930°K with a probable error of $\pm 40^\circ\text{K}$.

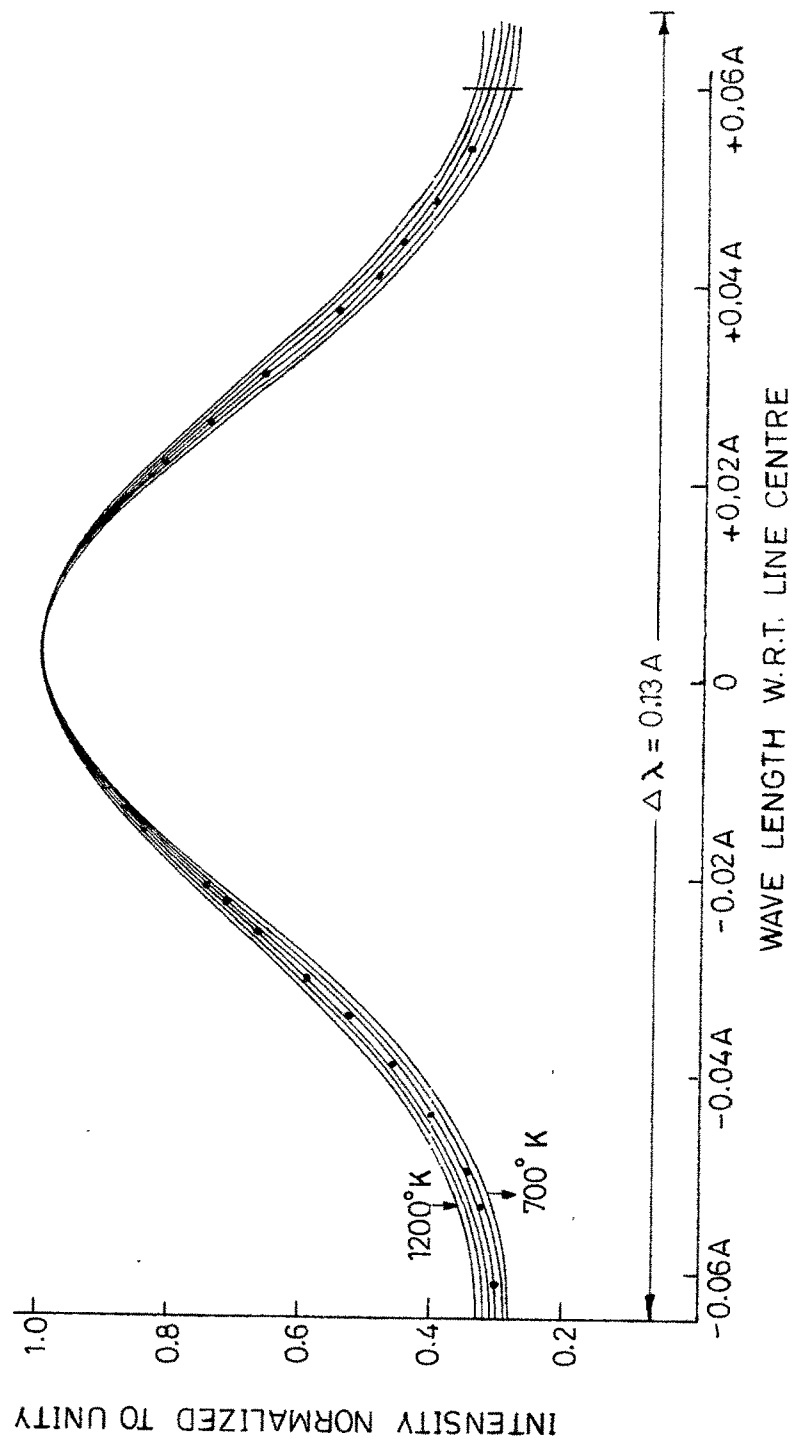


Fig 16 A comparison of the observed 6300 Å night airglow profiles with a set of synthetic profiles. (8 Dec. 1977.)

3.5 HALF WIDTH METHOD

For a large amount of data, frequently a quicker modified method was employed which made use of only observed half widths. The method was as follows :

From the synthetic profiles generated by convoluting Doppler profiles of different widths, for discrete sets of instrument profiles, a convolution was constructed with

$\frac{i}{i * d}$ and $\frac{d}{i * d}$ as variables. Here

i = width of instrument function I

d = Doppler width of Gaussian function for range of temperatures selected.

This curve is shown in figure 17, and compared with theoretically calculated curves assuming

- i) I is Gaussian in form
- ii) I is rectangular in form
- iii) I is Airy in form

It is observed that the curve computed from the actually observed instrument functions is between Airy and Gaussian. In computing this curve width of instrument function ranged from 0.051 Å to 0.044 Å. These were the actual extreme values obtained for the width of instrument function. In 70% of the cases the width of instrument function ranged from 0.049 Å to 0.045 Å. It is seen that the convolution graph for the actually observed instrument functions shows

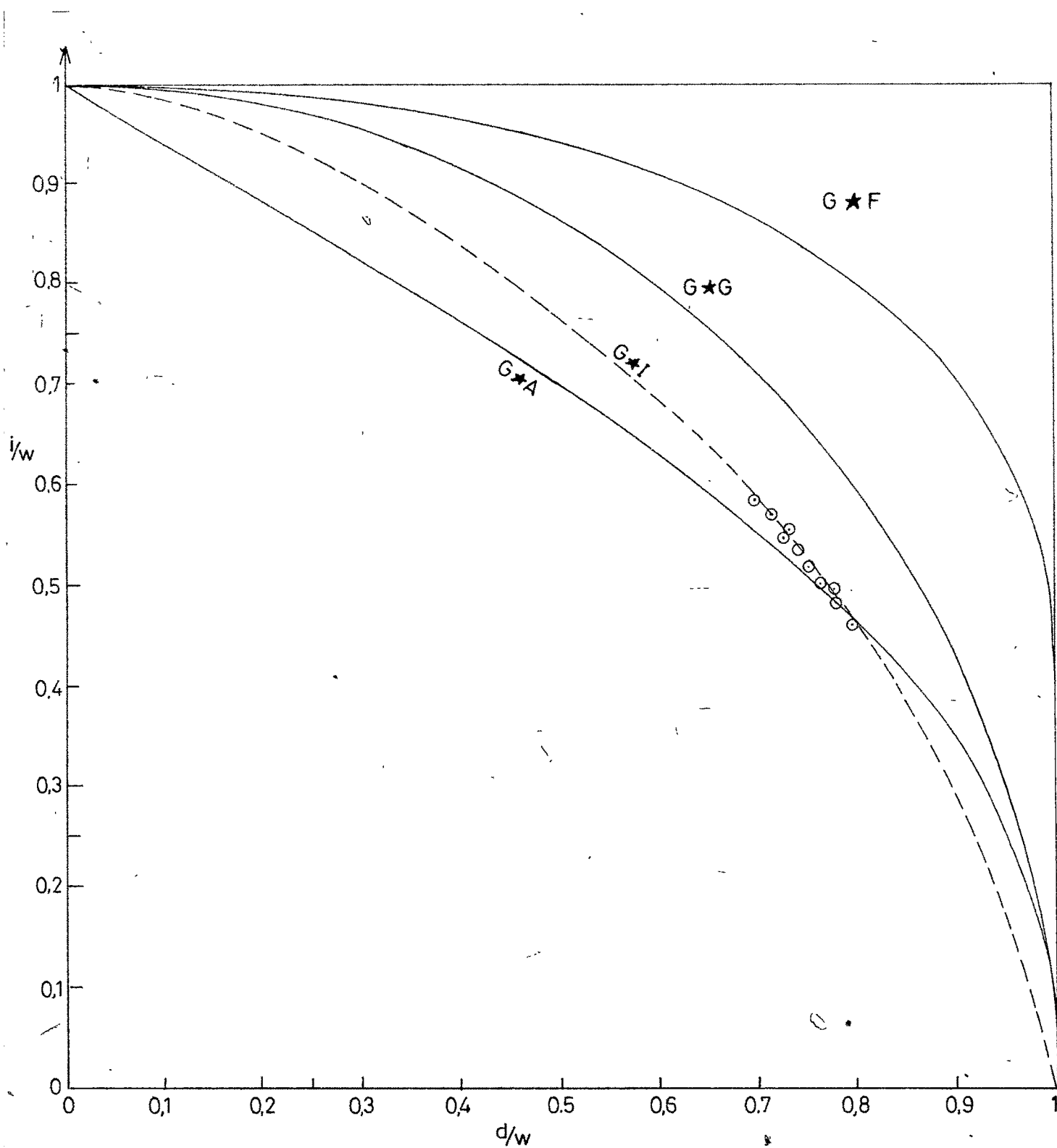


Fig. 17 Matching on $G \star I$ shows dispersion in calculated graph for instrument function observed on various days.

i = Width of instrument function ; I = Instrument function as observed
 d = Width of Doppler function for different temperatures w = Width of convoluted function $G \star Y$ when y is G, F, A or I

little dispersion. Departure of the convolution graph towards Airy side from gaussian side also indicates that misalignment has been the main factor governing the limitation of the instrument width. If plate curvature or size of the scanning aperture had been the limiting factor, then the instrument function would have been wider at the peak compared with Gaussian shape and the departure would have been towards $G * F$.

True Doppler width was calculated from the width of the observed profile as follows :

Suppose on a particular occasion width of the instrument function was 0.045 Å and the observed profile had a width of 0.06 Å widths refer here to full width at half maximum . Then

$$\frac{1}{1 * d} = \frac{0.045}{0.06} = 0.75$$

$$\therefore \frac{d}{1 * d} = 0.53 \text{ or } d = 0.0318 \text{ Å}$$

$$\therefore \text{Temperature } T = 795^{\circ}\text{K}$$

3.6 ERRORS IN TEMPERATURE MEASUREMENTS

The uncertainty of the temperature measurement consists broadly of two types, systematic error due to the instrument and the uncertainty due to data. All the factors contributing to the uncertainty of temperature estimates are discussed and error estimates are given. The problem of contamination of the line profile of $\lambda 6300 \text{ \AA}$ due to close emission lines in the airglow is also discussed. Reference can be made to BLAMONT AND LUTON (1972) for a ⁰through analysis of temperature accuracy estimates.

3.6.1 ERRORS DUE TO UNCERTAINTY IN FINESSE

Mean finesse observed for the spectrometer was 2.75 ie the mean instrument width was 0.048 \AA . For calibrations carried out on different days the value varied from 0.05 \AA to 0.044 \AA . However 70% of the values remained between 0.048 $\text{\AA} \pm 0.0018 \text{ \AA}$. Although in any particular calibration the probable error in the measurement of instrument width is fairly below 0.001 \AA , One can not rule out a possibility of change in the instrument width by that amount during the course of night. This would give an error in the measured temperature an amount $\simeq 70^\circ\text{K}$ in 1000°K .

3.6.2 ERROR DUE TO UNEVENNESS IN PRESSURE VARIATION

Pressure was varied stepwise in 217 steps over a total

pressure range of $\simeq 15$ cms of Hg. Although pressure was not monitored with a pressure transducer, there was no indication of any irregularity in pressure variation which should have become apparent in the scans over the laser light. Since the wavelength scan effected is $\simeq 0.32$ A in 217 steps, one step pressure change corresponds to a wavelength range of 0.0015 A. Error in halfwidth corresponding to half a step will cause a change in estimated temperature by 40°K .

3.6.3 ERROR DUE TO SCATTER IN THE EXPERIMENTAL DATA

Observation at each pressure step is a digital photon count, 'N' which follows Poisson statistics and has an inherent variation of \sqrt{N} . Typically $N \simeq 150$ at maximum of the fringe for airglow intensity of $\simeq 100$ Rayleighs. Raw data will therefore show large fluctuations which require to be smoothed. We have used running average over 10 samples as a smoothening procedure. The smoothed profiles showed uncertainty in halfwidth of about 0.0003 A for airglow intensity upto 50 Rayleighs, but could be much larger when the intensity was less. Hence the estimated random error in temperature measurements due to scatter in the data is estimated to be $\pm 40^{\circ}\text{K}$. This figure was arrived at by studying the statistics of the temperature

values obtained from different scans taken at approximately the same time. Since the random fluctuations in pressure due to basic step irregularity would also reflect in the scatter of the observed data, the two are really not independent but should be treated as a single factor.

3.6.4 ERROR DUE TO SMOOTHING PROCEDURE ADOPTED

The process of taking running average would also cause a systematic error. Essentially it causes, slight depression of the maximum, filling up at the minimum and practically no change near the half intensity point. Since the width is read at half the maximum, reduction in the height of maximum will mean reading the width at a slightly lower point of the profile and hence a slight increase in its value. Error due to this factor was evaluated by studying the effect of taking running average over the synthetic profiles. As one free spectral range is covered in about 100 samples the depression of the maximum was found to be only $\approx 1\%$. This causes overestimate of the temperature by 30°K . Temperature values given in the results do not take into account this overestimate.

3.6.5 DARK LEVEL FLUCTUATION

The photomultiplier tube is kept below -10°C always and the refrigeration system is continuously kept on.

Normally the noise level counts are below 10. The chances of getting an exorbitantly large value is hardly 1 %. Since our supply 230 V Ac is also derived from an inverter energised by 4 Nos of 12 V acid batteries the dark count level remained practically constant. An average dark count of 10 is subtracted from the signal before processing. A change in dark level of 2 to 3 counts will introduce a temperature uncertainty of $\pm 5^{\circ}\text{K}$.

3.6.6 STRAYLIGHT LEVEL FLUCTUATION

We have completely neglected the problem of stray light. The problem is not very severe in night airglow when compared to dayglow. Since we have used a narrow filter of 2.5 Å HBW it was assumed that the intensity is entirely due to $\lambda 6300 \text{ Å}$ only. We have not obtained any data on background emission.

3.7 CONTAMINATION PROBLEM

The presence of emission lines of the OH molecule very near to the 6300 Å emission line will contaminate the emission profile and may cause serious errors in temperature. Secondly the $\lambda 6300 \text{ Å}$ emission intensity can fluctuate drastically during the period of recording the profile and may lead to erroneous profiles. These are discussed below.

The presence of emission lines of the OH molecule $X^2 \Pi (9 - 3)$ band transition in the region of the OI ($3P_2 - ^1D_2$) transition at 6300.308 Å [CABANNES AND DUFAY (1956)] in the night sky have been recognised quite a while. The OH lines closest to the OI line and with significant emission rate are the $P_1(2)$, $P_2(3)$ and $P_1(3)$ lines located at 6287.5 Å, 6297.9 Å and 6307 Å respectively (KVIFTE, 1959 ; KRASSOVSKY ETAL, 1962, BASS AND GARVIN 1962 ; BLACKWELL 1960).

The contamination of the OI line by these OH lines in high resolution measurements made in order to obtain line profiles and thus a knowledge of the contamination in a given measurement must be known in order to allow or remove its effects. Although some authors (BIONDI AND FEIBELMAN 1968 ; ARMSTRONG 1969) have been aware of the contamination problem in high resolution measurements, they did not appreciate the extent and pervasiveness of this contamination. This problem is well discussed and solutions are given by HERNANDEZ (1974).

The problem of contamination is completely avoided in the present experiment by choosing postfilter to be of 2.5 Å HFW and centered at 6301 Å. By this $P_1(2)$ and $P_1(3)$ lines are totally suppressed and $P_2(3)$ line is thrown almost to the

tail of the pass band of the filter where the transmission for that wavelength becomes less than 7%. In some of the observations we have found that this $P_2(3)$ line slightly distorting the wing portion of the airglow profile. This particular effect is neglected when doing matching with synthetic profiles. HERNANDEZ (1974) had suggested to prefilter the skylight by a narrow filter to remove the offending lines altogether during the measurement. But to do prefiltering one has to have such a narrow band filter of the size of the Fabry-Perot used for the experiment which is very difficult. Hence we did post filtering wherein the size of the beam is reduced considerably and a smaller diameter filter will suffice.

3.8 EFFECT OF CHANGE IN 6300 Å INTENSITY

A change in 6300 Å emission rate during the time necessary to measure a line profile causes an error in the derived temperature [HAYS AND ROBLE (1971)]. This error is rendered negligible by eliminating measurements during which the emission rate changed by more than 20% during the measurement of a single profile HERNANDEZ (1975). From the airglow photometer which was running side by side the intensity values of $\lambda 6300 \text{ Å}$ were noted and before processing the data, it was checked whether the intensity changed by 20% during the scan. The data sets were rejected for which this change is more than 20%.

3.9 ERROR DUE TO LIGHT LEAKAGE

Finally there was a small amount of light leakage in the Fabry-Perot etalon chamber. This was due to the uncoated portion of the Fabry-Perot plates over which the etalon spacer was resting and was not properly baffled. This causes an error in the base level. Contribution from this factor was estimated by careful comparison of observed profiles with the synthetic profiles and was established to be 5%. Base values for all observed airglow profiles were corrected for this 5% light leakage of 6300 Å airglow. Due to uncertainty in the exact value of this factor ($\approx \pm 1\%$) all the temperature data reported in this work may have a systematic error of $\approx 50^\circ\text{K}$, sign correction being unknown. However the relative temperature variations would not have any error due to this factor because the leakage factor remained constant.

Considering all factors we conclude that,

- i) The final temperature values may have a random error of $\pm 70^\circ\text{K}$.
- ii) All temperatures are systematically overestimated by 30°K due to smoothing procedure adopted.
- iii) In addition there may be a systematic error by either + or $- 50^\circ\text{K}$.

CHAPTER - IVRESULTS

The night time F region neutral temperatures reported here were obtained during the period between 1976 - 78, over Mt Abu (24.6°N , 72.7°E geographic, 15.0° geomagnetic latitude), India. There were a few measurements made in the year 1974 also. About 32 nights of observation are presented here and the number of temperature values run into more than 125.

4.1 Temperature Plots and Analysis method

Figures 18 to 25 give the temperature plots for different hours of the night on various days. Temperatures are given in degree kelvin along the ordinate and time in hrs IST (LT + 40 min) along the abscissa. The Fabry-Perot Doppler temperatures are indicated by '+' sign, the vertical length of the '+' mark denotes the uncertainty in the measurement of temperature. Experimental temperatures are compared with model values. The continuous line with inbetween circles (o—o—o) indicate the temperature variation calculated using JACCHIA (1970) empirical model relating exospheric heating to values of the 10.7 cm solar flux $F_{10.7}$ and the planetary magnetic index K_p . The $\sum K_p$ values are indicated in figure.

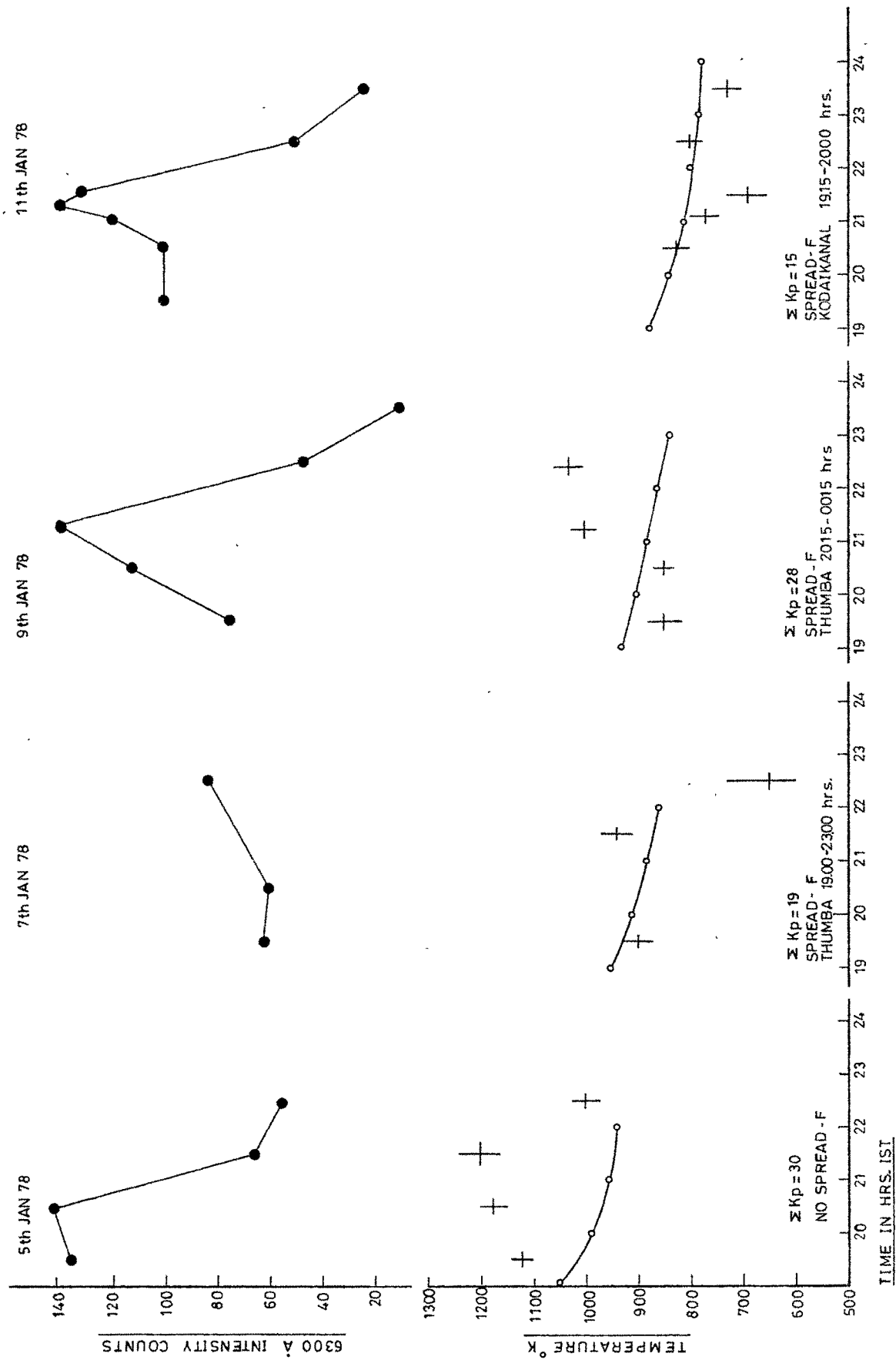


Fig. 18 Comparison of Fabry-Perot Doppler temperatures (+) with JACCHIA model (1971) exospheric temperatures (o---o) and 6300 Å airglow intensities.

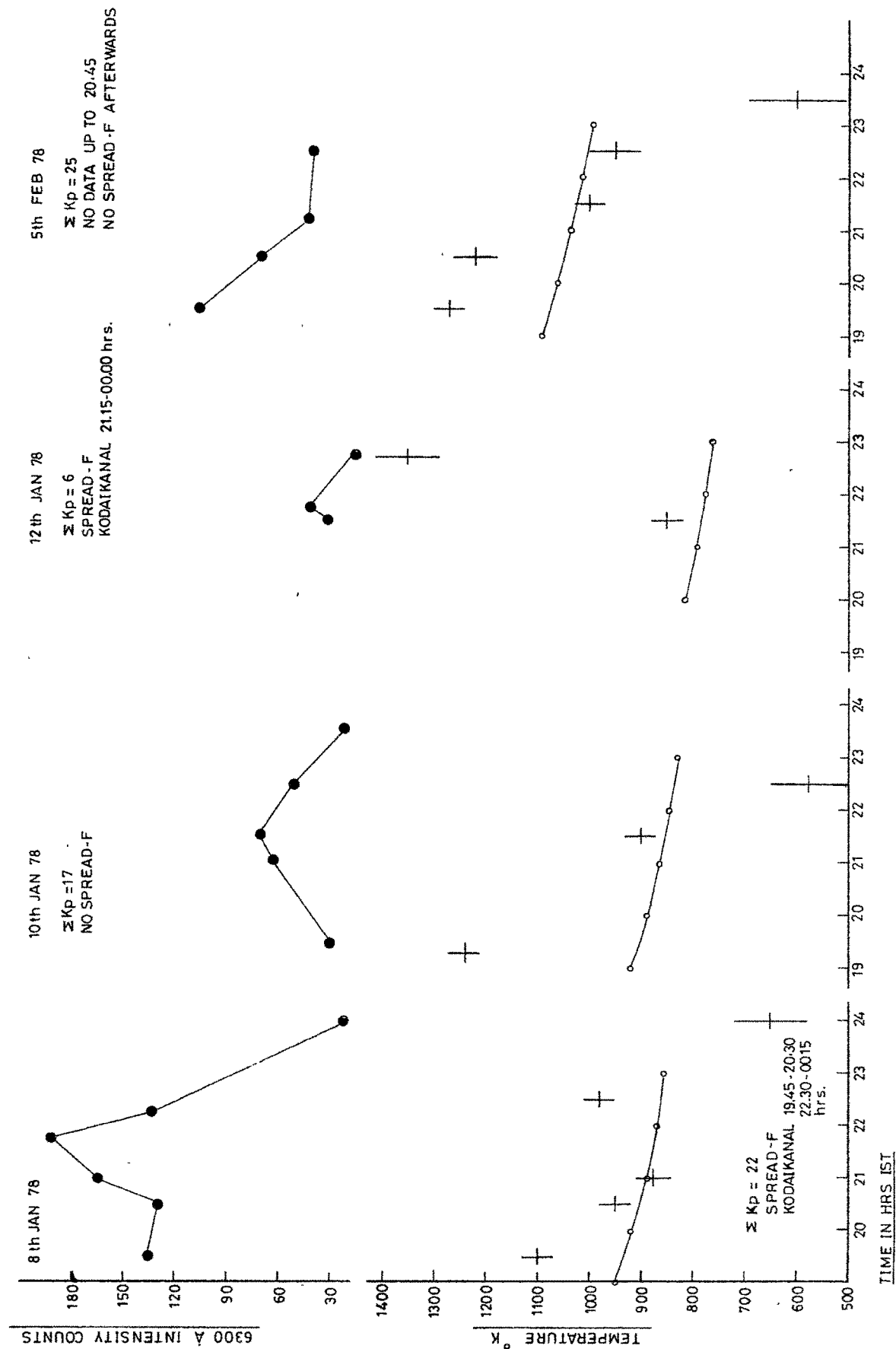


Fig 19 Comparison of Fabry-Perot Doppler temperatures (+) with JACCHIA model (1970) exospheric temperatures (o---o) and 6300 Å airglow intensities.

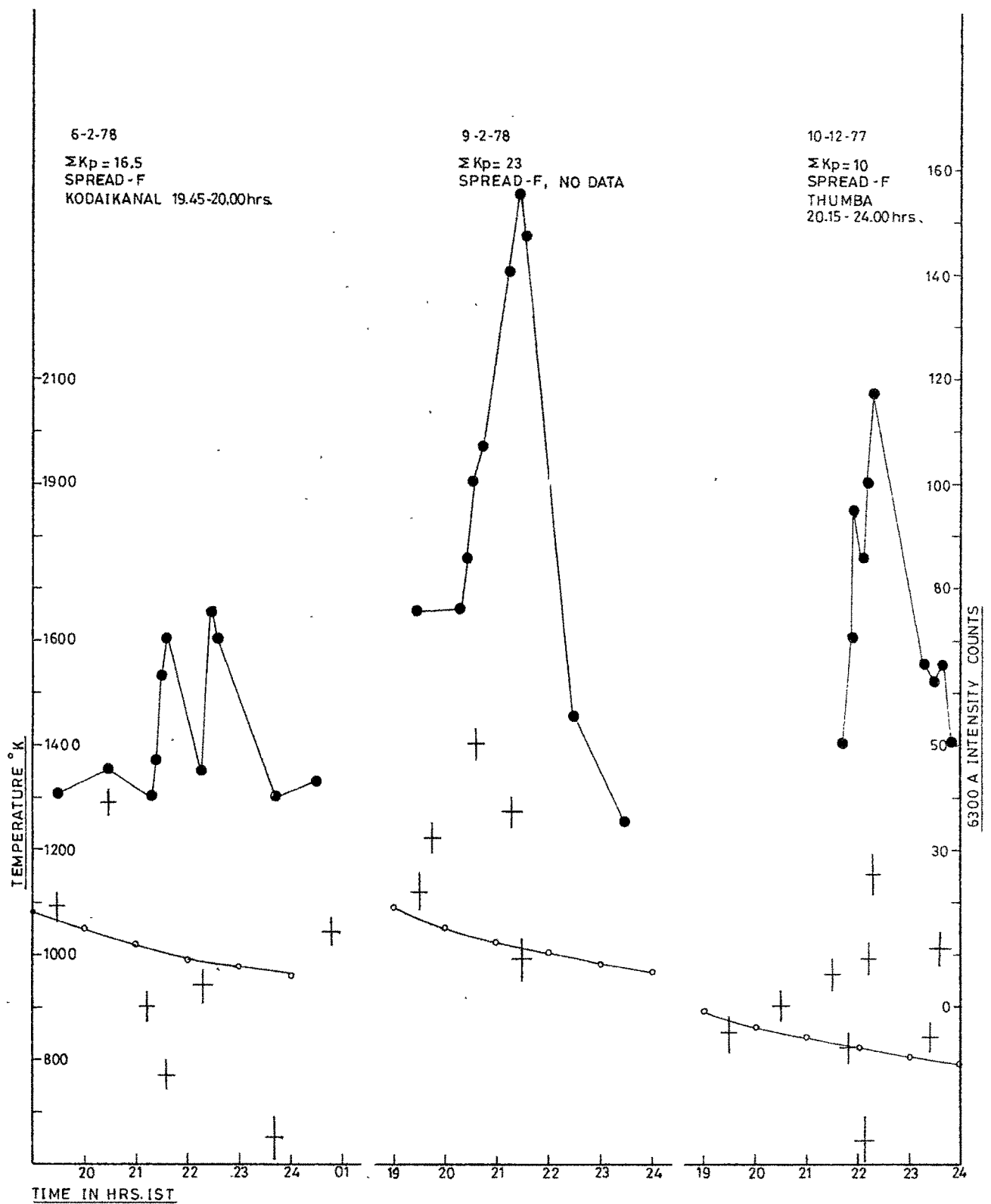


Fig. 20 Comparison of Fabry-Perot Doppler temperatures (+) with JACCHIA model (1970) exospheric temperatures (○—○) and 6300 Å airglow intensities. (●—●)

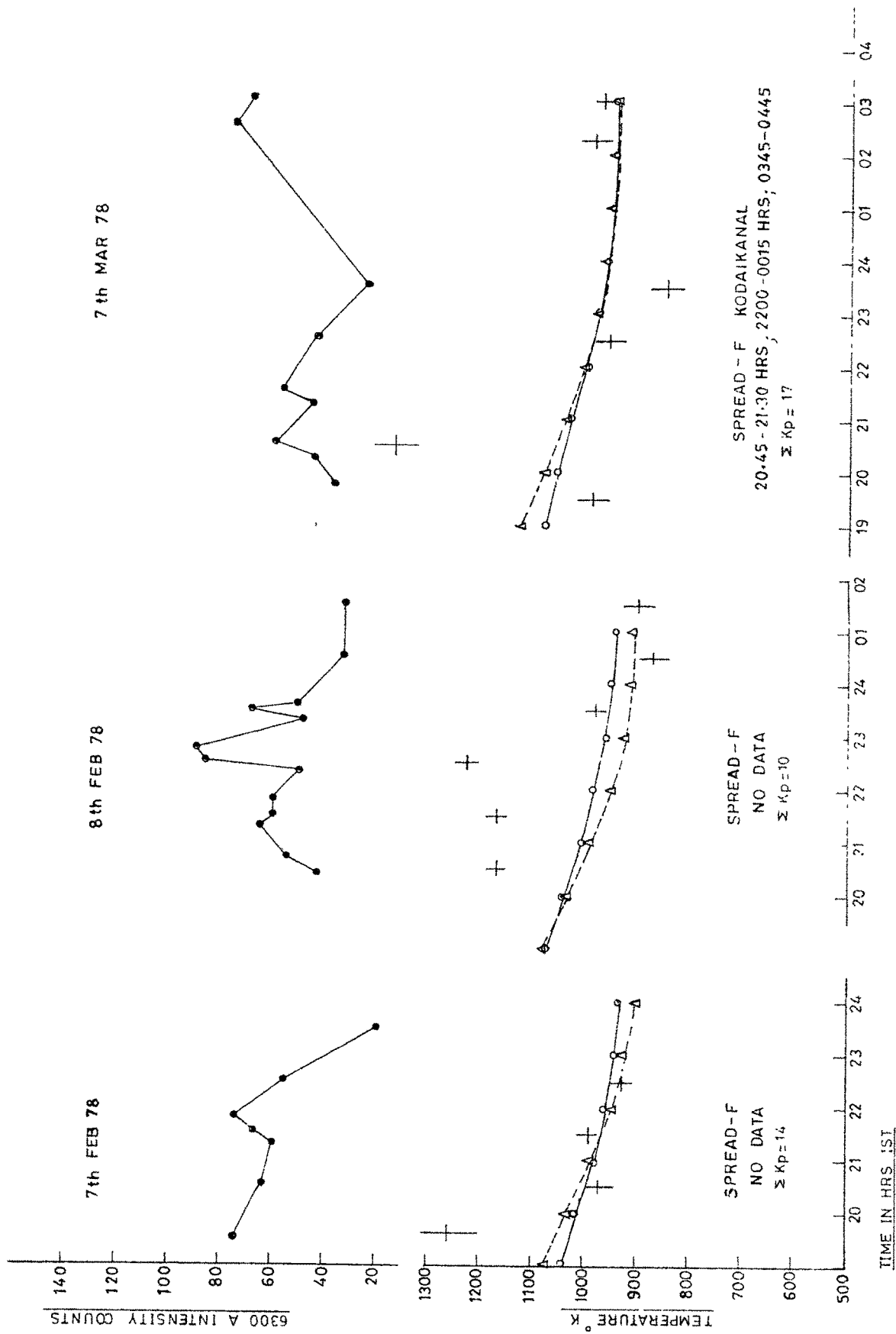


Fig 21 Comparison of Fabry-Perot Doppler temperatures (+) with JACCHIA, 1970 (o---o) and JACCHIA, 1977 (Δ-Δ-Δ) exospheric model temperatures and 6300 Å intensities

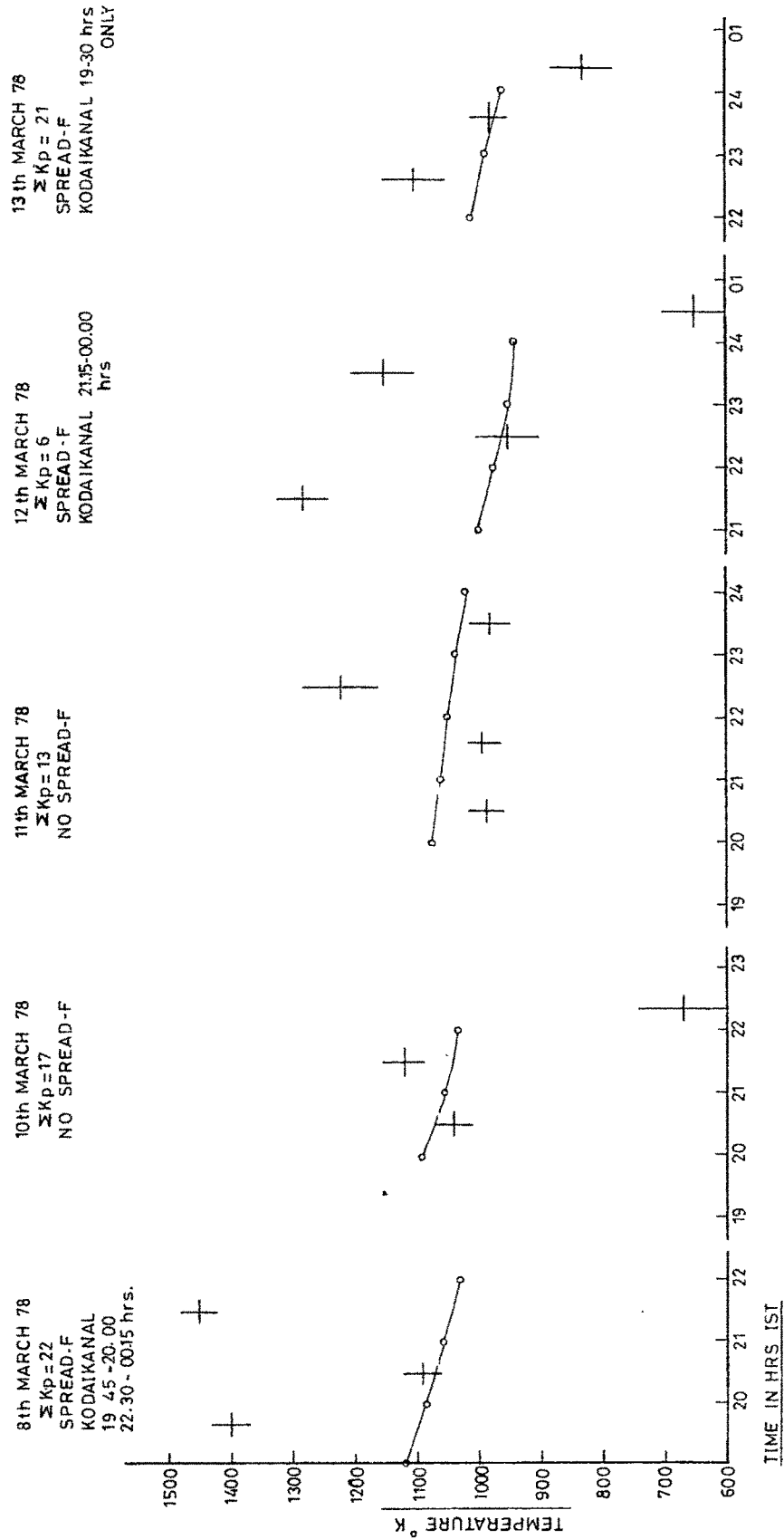


Fig. 22 Comparison of Fabry-Perot Doppler temperatures (+) with JACCHIA model (1970) exospheric temperatures (o---o).

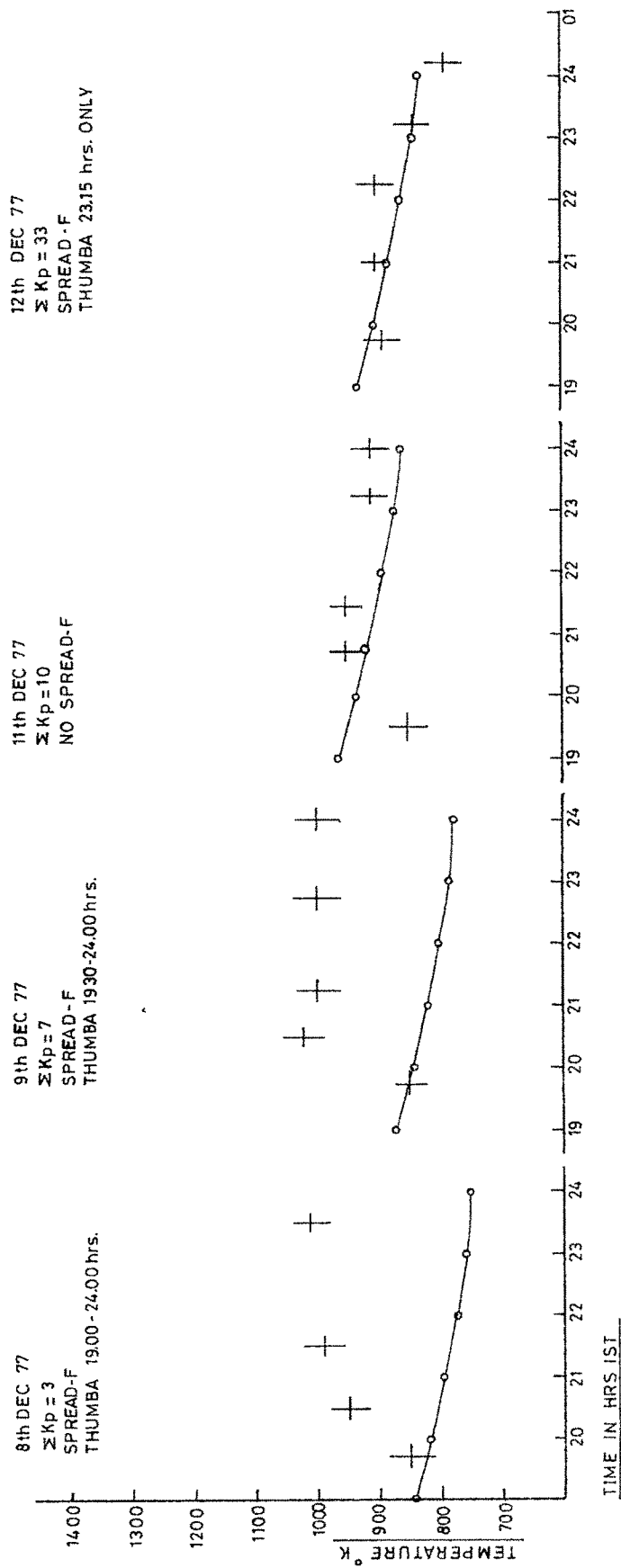


Fig. 23 Comparison of Fabry Perot Doppler temperatures (+) with JACCHIA model (1970) exospheric temperatures (o-o-o).

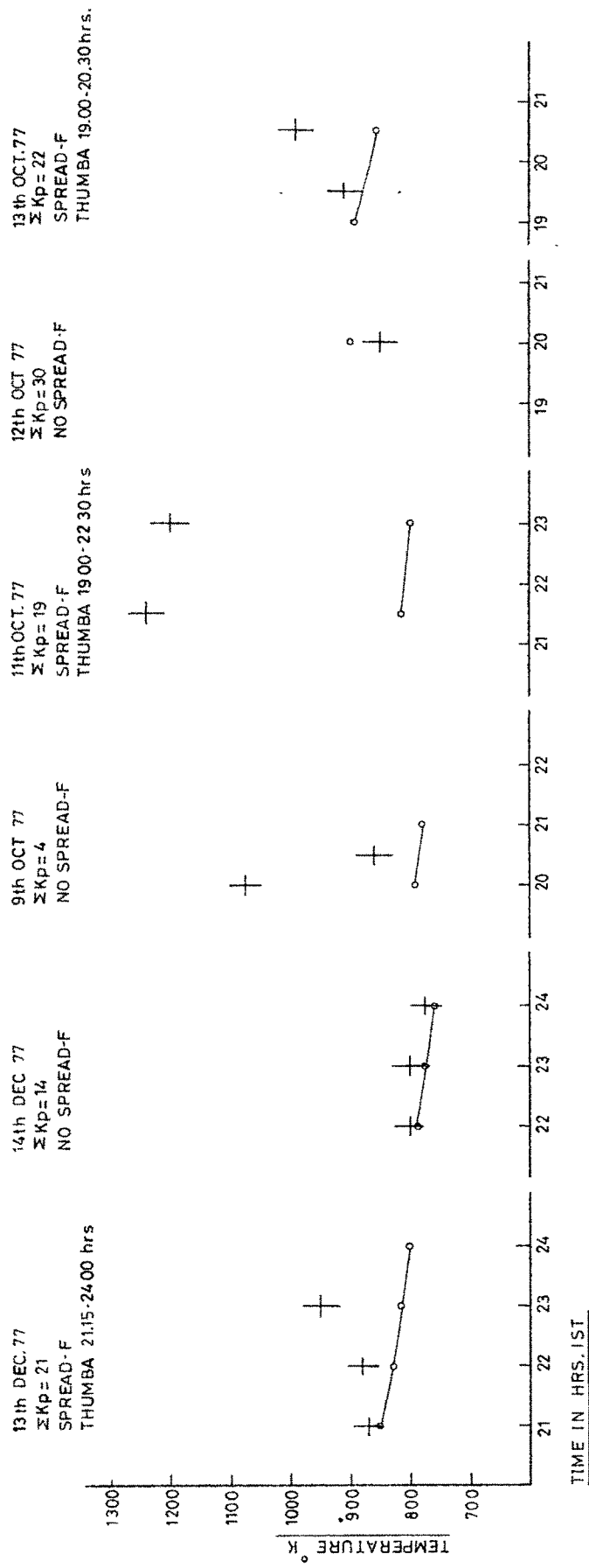


Fig. 24 Comparison of Fabry-Perot Doppler temperatures (+) with JACCHIA model (1970) exospheric temperatures (o—o).

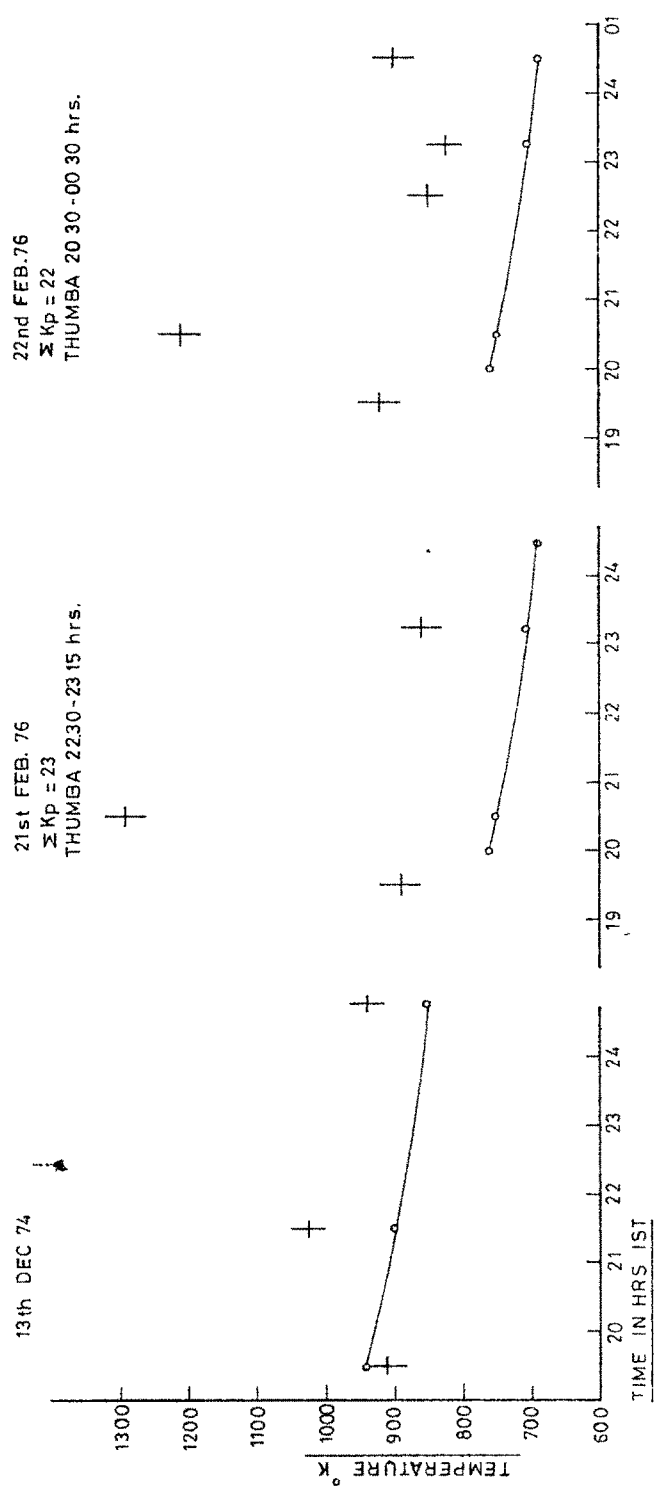


Fig. 25 Comparison of Fabry-Perot Doppler temperatures (+) with JACCIA model (1970) exospheric temperatures (o---o)

The temperatures observed and reported in figures 18 - 25 are analysed by grouping them in to three parts in the following way :

- a) Occasions on which the observed temperatures agree with JACCHIA (1970) model with in $\pm 50^{\circ}\text{K}$ (denoted as $J \pm 50^{\circ}\text{K}$).
- b) Occasions on which the temperatures are significantly higher than JACCHIA (1970) model viz. $(J + 50)$ to $(J + 300^{\circ}\text{K})$.
- c) Occasions on which the temperatures are significantly below the JACCHIA (1970) model viz. $(J - 50)$ to $(J - 400^{\circ}\text{K})$.

A histogram is plotted as per the above mentioned scheme for the temperature data given in figures 18 to 25 and is given in figure 26. The histogram shows that

- i) In 60% of the occasions the observed temperatures agree reasonably well with the JACCHIA (1970) model exospheric temperatures.
- ii) In 29% of the occasions the observed temperatures exceed JACCHIA (1970) model by $\simeq 50^{\circ}\text{K}$ to 300°K .
- iii) On $\simeq 6\%$ of occasions the observed temperatures are significantly below the model values.

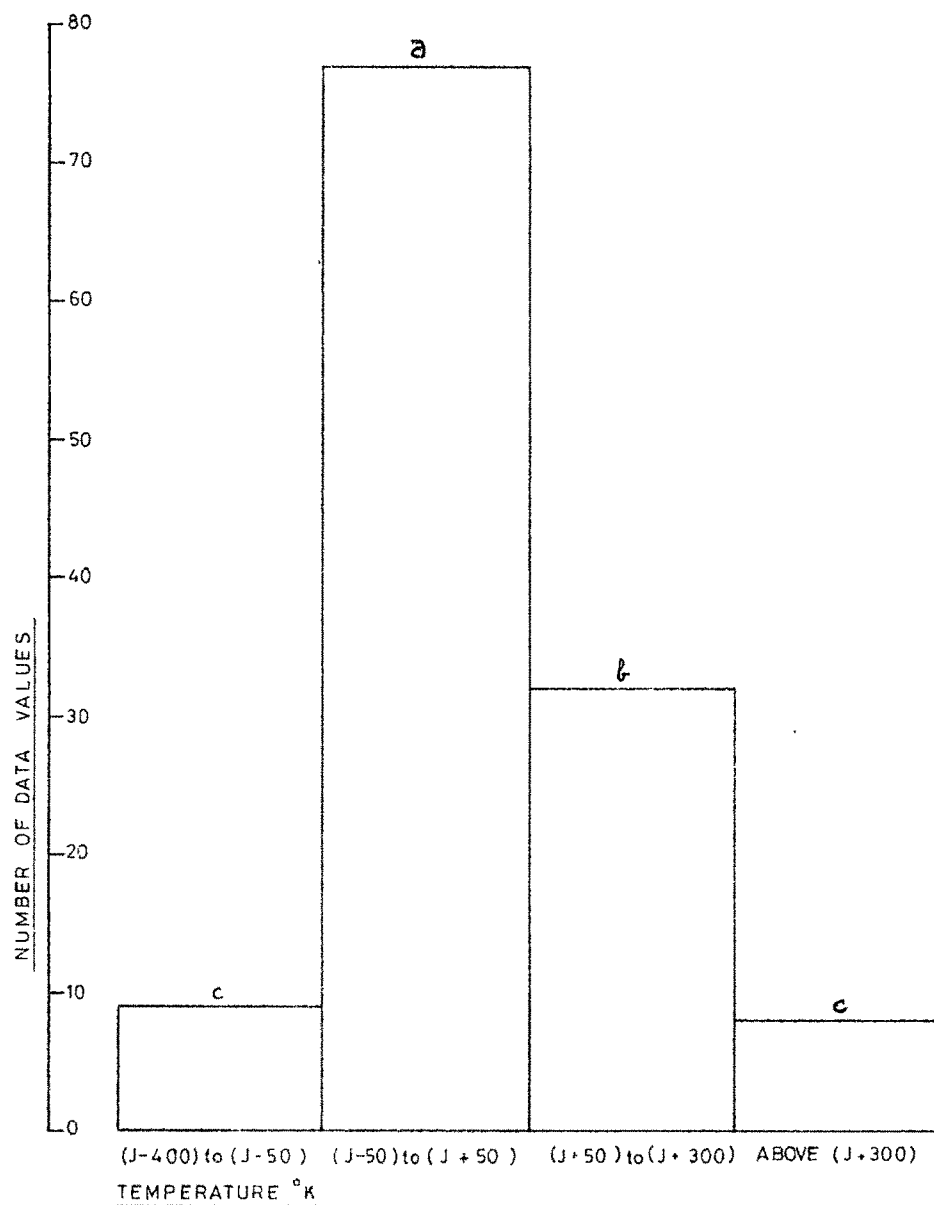


Fig 26 Histogram of temperature data from
 Fabry- Perot measurements ('J' refers
 JACCHIA model (1970) temperature)

- iv) In $\simeq 6\%$ of occasions the observed temperatures exceed JACCHIA model by a large value ($> 300^{\circ}\text{K}$).

4.2 Neutral Temperatures

From Group 'a' of the histogram in fig. 26 it is clear that very close agreement is seen (60% of the occasions) between the model predictions and experimental values of neutral temperature. The days of observation include magnetically quiet as well as disturbed days (high ΣK_p).

It is seen from figures 18 - 25 that the average Fregion neutral temperatures determined over Mt Abu, lie between 800°K - 1000°K . Comparing some earlier measurements by other workers, HAYS ET AL (1970) report an average temperature of 790°K from Michigan Airglow observatory (42.17°N , 83°W) and HERNANDEZ ET AL (1975) report an average temperature of 900°K from Fabry-Perot measurements from JICAMARCA (1° dip) observatory.

Although in general, we have used JACCHIA (1970) model for comparisons, for few nights the improved later model JACCHIA (1977) was also used. The temperature values calculated by JACCHIA (1977) model do not differ significantly from those calculated by JACCHIA (1970) model. However JACCHIA (1977) model predicts sharper decline of temperatures towards mid night hours. On three

nights viz. 7th & 8th Feb. 1978 and 7th March 1978 in fig. 21. When good agreement is observed with model temperatures ; the experimental temperatures show that the temperature decrease towards midnight hours is in better agreement with JACCHIA (1977) model than with JACCHIA (1970) model.

The neutral temperature values for 12th Dec. 1977 in fig. 23 show very close agreement with JACCHIA (1970) model. The planetary magnetic index $\sum K_p$ for the day was 33 which is quite high. The fact that the observed temperatures are in close agreement with the model values testify for the fact that the planetary magnetic index $\sum K_p$ does not have significant control on the low latitude thermosphere in conformity with JACCHIA (1970) model. The solar flux on that day was 114.5. On the other hand for 11th March 1978 in figure when $\sum K_p$ is only 13 the solar flux value was very large (177.5) giving high model atmospheric temperatures. Observed temperatures for this day also show close agreement with the model. Hence we conclude that 10.7 cm solar flux essentially determine the exospheric temperature for low latitude thermosphere.

4.3 Temperature enhancements and Spread F connection

On good number of occasions (29%) we observed significantly enhanced temperatures over JACCHIA (1970) model as evident from group 'b' of the histogram in fig. 26. It can be inferred from the temperature plots from figures 18 - 25, that enhancements of temperature from

100°K to 300°K are found to occur at specific hours of night. Another important feature observed is as seen for example on 8th Dec. 1977 in fig. 23 and 10th Dec. 1977 in fig. 20, that the initial temperatures were almost coinciding with model values and enhancement in temperature occurred thereafter.

For this group in which significantly increased temperatures are observed when compared to model values, we sought for the correlation with conditions over equatorial ionosphere. This was prompted through personal discussions with Prof. K. D. Cole • COLE (1974) has suggested that joule dissipation of strong turbulent electrifields associated with equatorial spread F can be a significant source of heat in the low latitude thermosphere and such time varying electric fields occur in a limited belt approximately $\pm 15^\circ$ about the magnetic equator. In the initial stage of this work, the first continuous data in October 1977 which showed such temperature enhancements were correlated with spread F activity over the equatorial station Thumba (8.5°N, 76.8°E geographic, 0.6°S geomagnetic) and a correlation of more than 60% was found to exist. The details are given in the earlier publication RAJARAMAN ET AL (1978). December 1977 temperature data when analysed showed more than 80% correlation with respect to the onset of spread F and the findings are discussed by RAJARAMAN ET AL (1979).

Here we present the total number of occasions in which temperature enhancements are seen against the presence or absence of spread F over the equator at Thumba or at Kodaikanal, a station very near to the equator. Spread-F information is given alongwith temperature plots in figures 18 to 25.

Table B gives the data and hour at which temperature enhancements are seen over the model values as per group 'b' of the histogram in fig. 26, against which the presence or absence of spread F either at Thumba or at Kodaikanal ($10^{\circ}14'N$, $77^{\circ}29'E$, $0.6N$ dip).

From table B it is evident that of the 32 cases in which such temperature enhancements are observed, on 21 occasions there was spread-F over equator. For 7 occasions we could not get ionospheric data over equator and only on 4 occasions there was no spread F over equator. The very striking part of this finding is that only 12% of the occasions alone the correlation fails and 22% of the occasions the spread F data is not available.

Table B indicates clearly that the increase in temperature is of the order of $100^{\circ}K$ to $300^{\circ}K$ and normally, an increase of 150° to $160^{\circ}K$ is usually observed. The following results are derived from the table and figures 18 to 25.

TABLE - B

Nö.	Date	hour	T ^{OK} Above Jacchia (1970)	Spread F present/Absent
1	9-10-77	20.00	250	No data
2	13-10-77	20.30	130	Present
3	8-12-77	20.30	130	Present
4		21.30	190	Present
5		23.30	230	Present
6	9-12-77	20.30	170	Present
7		21.15	180	Present
8		22.45	200	Present
9		24.00	200	Present
10	10-12-77	21.30	110	Present
11		22.15	150	Present
12		23.30	200	Present
13	13-12-77	23.00	140	Present
14	5-1-78	20.30	180	Absent
15		21.30	230	Absent
16	8-1-78	19.30	150	Present
17		22.30	120	Present
18	9-1-78	21.15	120	Present
19		22.25	160	Present
20	10-1-78	19.15	300	Absent
21	5-2-78	19.30	160	No data
22		20.30	150	No data
23	6-2-78	20.30	220	Present
24	7-2-78	19.30	180	No data
25	8-2-78	20.30	130	No data
26		21.30	160	No data
27		22.30	220	No data
28	7-3-78	20.30	280	Present
29	8-3-78	19.45	275	Present
30	11-3-78	22.30	130	Absent
31	12-3-78	21.30	250	Present
32		23.30	180	Present

- i) In the F region over Mt Abu the neutral temperature enhancements upto $100 - 300^{\circ}\text{K}$ are observed on about 65% of the nights when there is spread F activity over equator. On these occasions the temperatures measured before or after spread F agree very well with JACCHIA model temperatures.
- ii) There are only 4 occasions (12%) in which high temperatures are observed without spread F activity over equator.
- iii) There is good indication that the increase in F region temperature over Mt Abu is delayed with respect to the onset of spread F over equator by approximately 15 - 30 mts, as seen from the data on figures 18 to 25.

HERNANDEZ (1975) has studied the 6300 A Doppler temperatures over equatorial thermosphere (JICAMARCA, 11.9°S , 76.87°W , 1°N dip). He observes close agreement with model temperatures and no enhancements are reported. In the present work nearly 25% of the occasions increased temperatures are observed ; the observation being over 15° dip latitude. In this connection it should be noted that satellite observations by SPENCER ET AL (1979) show number of nights on which they find midnight to early midnight temperature increases of the order of $300 - 400^{\circ}\text{K}$ above the

model values centered around 17° dip latitude. However
their observations show no such increase over dip equator.
The authors have also reported that almost on 50% of the
total occasions such increased temperatures are observed.
We have observed temperature increase in 25% of the occasions.

There are two occasions which are shown in fig. 18
(viz. of 7th Jan 78 and 11th Jan 78) in which close
agreement of average temperatures with the model values are
observed but there is continuous spread F over equator.

Our data thus show a strong evidence that the night
time neutral atmosphere temperatures show enhancement of
the order of 100°K to 300°K over a dip latitude of 15° ,
when there is spread F over the magnetic equator. These
observations are consistent with the model of COLE (1974)
for formation of spread F on large scale field aligned
irregularities between conjugate dynamo regions of the
ionosphere and the estimates of heating in the spread
F regions.

Another important result derived from the figs. 18,
19, 20 & 21 where the 6300 Å intensity pattern is also
shown, is that the intensity variations do not show any
correlation with the temperature enhancements.

4.4 Low and very High Temperatures, Relation with Intensities

Figs. 18 to 21 give 6300 Å airglow intensity patterns along with temperature values. The intensities are given in terms of photon counts recorded for the peak of the fringe profile. A turret photometer monitoring the Zenith intensity of 6300 Å emission was also operated by the side of Fabry-Perot spectrometer. Since our direction of observation is 60° Zenith angle we have used the photon counts corresponding to the peak of the Fabry-Perot fringe profile as representative of the airglow intensities. A simple calculation of the solid angle, transmissivity and response of the detector system of the Fabry-Perot spectrometer revealed that 20 counts correspond to an emission intensity of 50 Rayleighs approximately. It is evident from figures that intensity variations do not correlate with temperature variations.

On large number of occasions the airglow intensities were sufficiently high to obtain profiles over individual scans with a high value of S/N ratio. On such occasions we have studied the variation of the linewidth of individual scans over a time interval of 30 - 40 minutes and frequently we find a very interesting behaviour. This is shown for the profiles of 6th Feb. 1978 (at 21.20 hrs) in fig. 27. When a maximum is observed on the airglow intensity variation,

Mt. Abu
6th Feb. 1978
21.20 - 21.40 hrs. IST

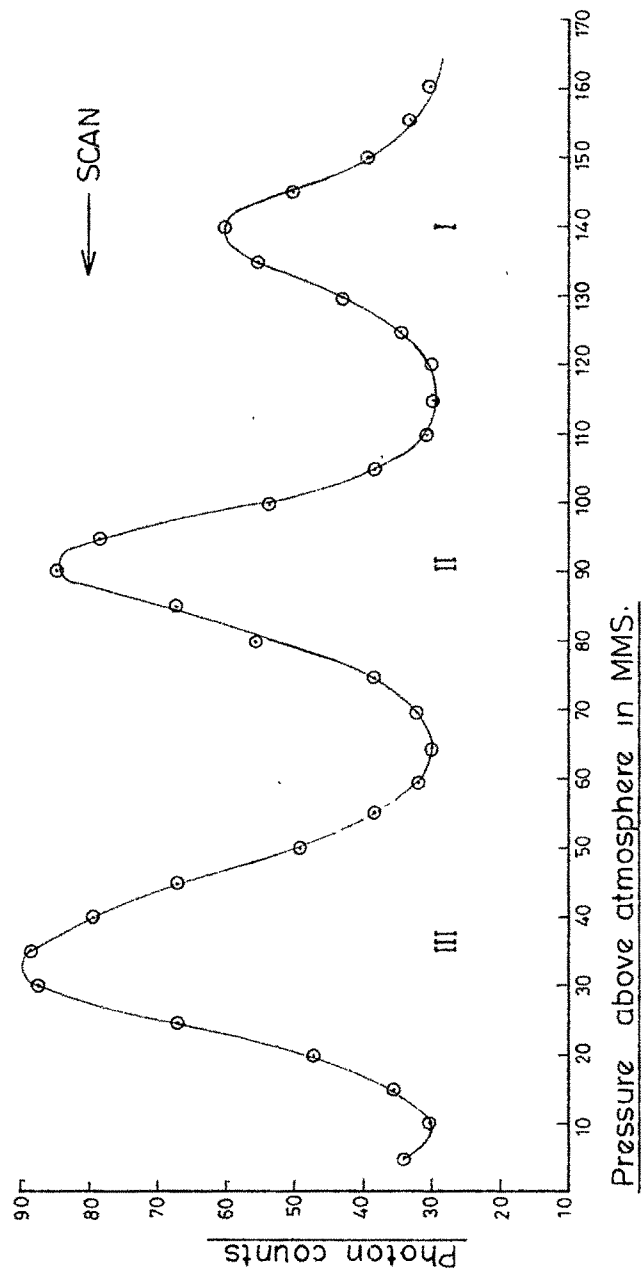


Fig. 27 Profile (II) showing narrowing as intensity goes to maximum

we observe that the particular profile acquired at the time the intensity reaches a sharp maximum is significantly narrower than the adjacent profiles. This is clearly shown for the profiles of 6th Feb. 78 (21.20 - 21.40 hrs) in fig. 27. The central profile is narrower than the I and III profiles. A low temperature is estimated because of this narrowing.

We have also observed that on occasions when the intensity rises steeply then the fringe becomes broader giving a much higher temperature.

The two effects are clearly shown in the observations for 9th Feb. 78 and 10th Dec. 77 in fig. 20. On 9th Feb. the intensity was rising rapidly from 20.15 hrs to 21.15 hrs and temperatures determined at 20.30 hrs and 21.15 hrs are very high and the temperature at 21.30 hrs had fallen by 300°K (in a matter of 15 minutes) and the intensity also started dropping fast. Similar observation is seen on 10th Dec. 77, two temperatures determined from individual profiles around 22.15 hrs one shows a high value and another low value and the 6300 Å intensity at that time showing a sharp reversal. Reason for this type of behaviour is not very clear at present. These two types form about 10% of the total number of cases represented under group 'c' of the histogram in fig. 26.

HERNANDEZ (1975) in his data reduction method adopts the procedure of systematically rejecting the observations for temperature estimation, in which the airglow intensity changes by more than 20% or more during the time interval of scanning a single profile. This we have also adopted upto some extent. Although such sharp intensity change will obviously distort the fringe profile we have chosen not to reject the data totally. Instead we have taken the average of the rising part of the fringe and falling part of the fringe in calculating its width. Essentially this amounts to assuming that intensity is changing linearly with time during the acquisition of the fringe. The width so obtained as above should then be the correct width. We have chosen to analyse such profiles particularly because the sharp change in the airglow intensity is a measure of strong dynamical change in ionospheric conditions and one would expect it to be reflected in the linewidths.

CHAPTER - V

NEUTRAL WIND ACCELERATIONS AND CORRELATION STUDIES

Observational evidence of neutral particle winds in the thermosphere near F2 maximum has been obtained by the study of variations of inclinations of satellite orbits (KING-HELE & SCOTT, 1967). These authors deduced that the average angular velocity of the upper atmosphere exceeds that of the earth giving rise to east-west winds with a speed of 30 mts/sec at a height of 210 km and 130 mts/sec at 260 km within a latitude range of $0 - 30^{\circ}$. Most of the present knowledge of the neutral winds in the thermosphere at F layer heights is based on calculations made by using semi empirical dynamical models of the neutral thermosphere (GEISLER 1966 ; KOHL & KING 1967). In general they utilise the global distribution of pressure as specified by a global empirical model of neutral temperature and composition, such as those given by JACCHIA (1965, 1971). The pressure gradients inherent in these global empirical models provide the pressure forces that drive the thermospheric circulation. By specifying the global distribution of electron density as given in models such as those of NISBET (1971) or CHING AND CHIU (1973) to determine the ion drag, the global thermospheric wind system can be directly calculated by integrating the

NAVIER - STOKES equation adapted for thermospheric heights. While there is agreement in a general way between the models, each model nevertheless showed some characteristics not shared by others. The night time winds are of particular interest here. Hence any additional observational material on neutral winds could be of considerable value. Good number of ground based measurements of neutral winds have been made with a Fabry-Perot spectrometer by Doppler shift method by several authors [ARMSTRONG 1969 ; HAYS AND ROBLE 1971 ; HERNANDEZ 1976].

5.1 TECHNIQUE FOR MEASURING WINDS

Fabry-Perot interferometer has been used for many years to measure Doppler temperature in the earth's upper atmosphere from the emission lines in the airglow and aurora [WARK (1960) ; TURGEON AND SHEPHERD (1962), JARRETT AND HOEY (1966) ; BIONDI AND FEIBELMAN (1968) ; HAYS ET AL (1969) ; ARMSTRONG AND BELL (1970)]. These emission lines are Doppler broadened and the half width of the line is indicative of the temperature of the emitting region.

If a steady horizontal neutral particle wind exists at an altitude near the F2 maximum the O_2^+ ions initially responsible for the $\lambda 6300 \text{ \AA}$ emission will not be moving with the neutral particle stream, being constrained by the earth's magnetic field. Once dissociative recombination

occurs, however, the resulting neutral oxygen atoms will take up the wind velocity. A percentage of these atoms will be in the 'D state and at altitudes given above they will emit after they are already moving with the wind since the life time in the 'D state is 110 sec. They will also ofcourse be thermalized. A Doppler shift should thus be detectable in the wavelength of the emission when observing at large zenith distances. Normally the method of observation will be to record the emission from two regions of the sky alternately while scanning is in progress with a Fabry-Perot photoelectric spectrometer and the two sets of fringes so obtained will be examined for any order of shift between them. If the two regions of the sky chosen for observation are 180° apart in azimuth and aligned along the direction of wind belowing over an extended distance, the fringe recorded from one region should indicate a velocity of approach and other a velocity of recession. The magnitude of the shifts will depend upon the magnitudes of the projections of the wind vector along the lines of sight. By choosing in such a manner the shift between the two fringes of a pair will be twice that would be obtained from, comparing the fringe from one region only with that from a laboratory source. Typically for a wind speed of 100 mts/sec the two sets of fringes observed at a zenith angle of 60° would show a split of $\Delta\lambda = 0.0036 \text{ \AA}$.

5.2 Present Method

The primary aim of the present work was to obtain only the Doppler width temperatures and no special attempt was made to observe shifts due to winds. The Fabry-Perot pressure scanning range was $2\frac{1}{2}$ orders and hence in each scan more than two fringes were recorded. The pressure interval between two fringe peaks was expected to have a constant value of 5.5 cm of Hg, corresponding to a wavelength scan of 0.129 Å. The S/N ratio with which the fringes were observed permitted the determination of pressure interval between two successive fringes with an accuracy better than ± 0.05 on most occasions. However on large number of occasions it was observed values significantly different from 5.5 cm. This departure from the expected value of 5.5 cm of Hg could arise due to one of the following reasons.

- i) Unexpected irregularities in pressure variation during scanning i.e. pressure not varying smoothly at each step. Since pressure values were not monitored this possibility could not be ruled out. However, later, a digital pressure transducer was coupled to the system which showed no such irregularity in pressure steps.
- ii) Other possibility is that the observed departures are genuine Doppler shifts due to thermospheric winds ;

i.e. during the time interval of recording the fringes winds change significantly. Essentially it means that the observed departure on the pressure interval between two fringes in the same scan represent " Acceleration " of neutral particles. Since the equipment was looking in only one direction a constant wind could not be detected, only a change in the wind velocity could be detected.

Histogram in fig. 28 compared the pressure intervals between two successive fringes observed in the same scan 'a' is plotted for the laser calibration fringes and 'b' is plotted for the airglow profiles. Since any irregularity in pressure variation should have occurred with the same probability for laser instrument profiles as well as for airglow profiles, the comparison of histograms very clearly show that the observed fluctuation in the pressure interval represent genuine change in the neutral wind vector. Small number of cases wherein laser calibration also showed departures from the expected value of 5.5 cm could be associated with insufficient time allowed for the stabilisation of the laser.

A change of 1 mm of Hg (ΔP) in the pressure interval correspond to a change in wind speed of 230 mts/sec. ($\Delta \lambda = 0.0024 \text{ \AA}$).

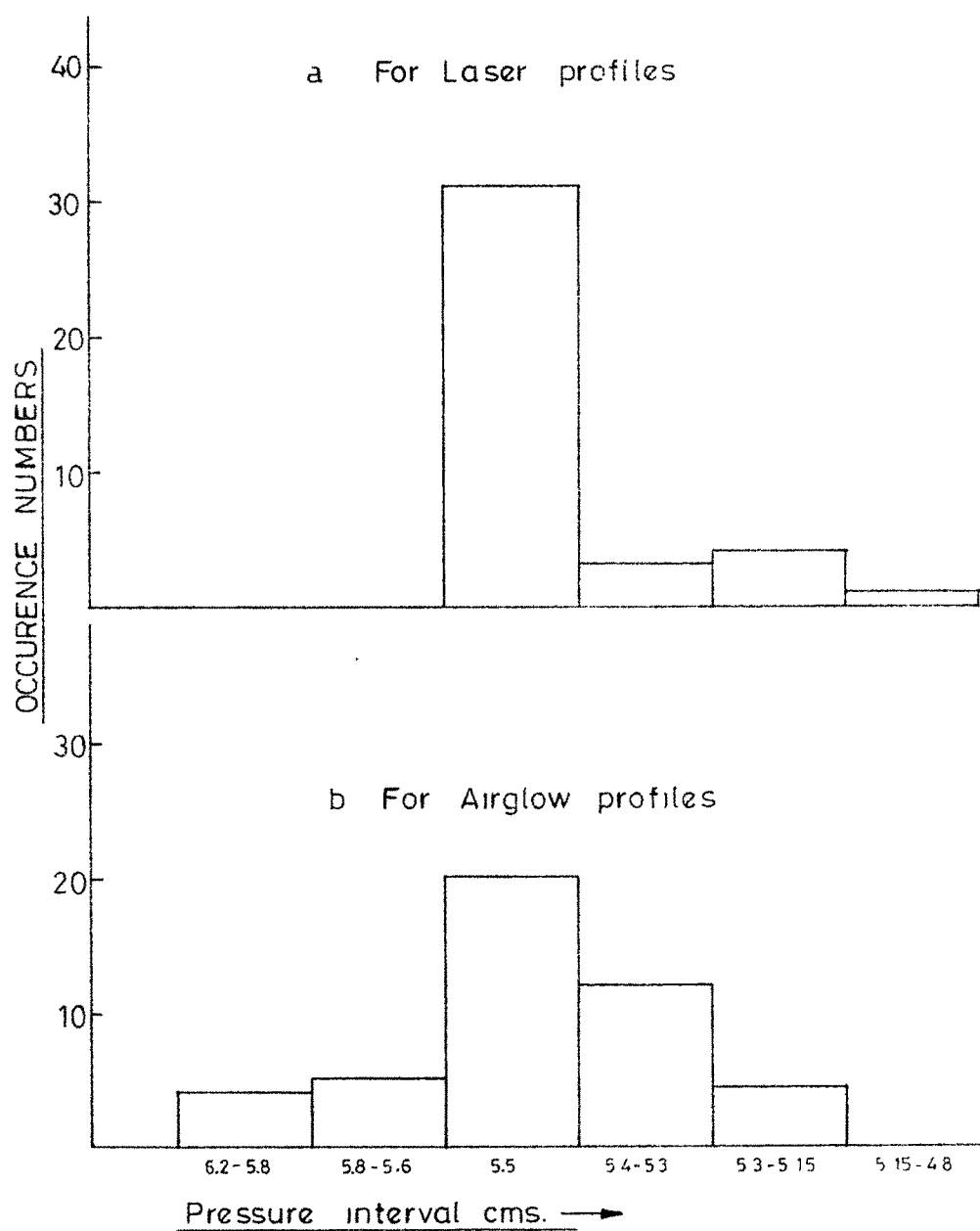


Fig 28 Histogram of pressure intervals between two fringes in the same scan.

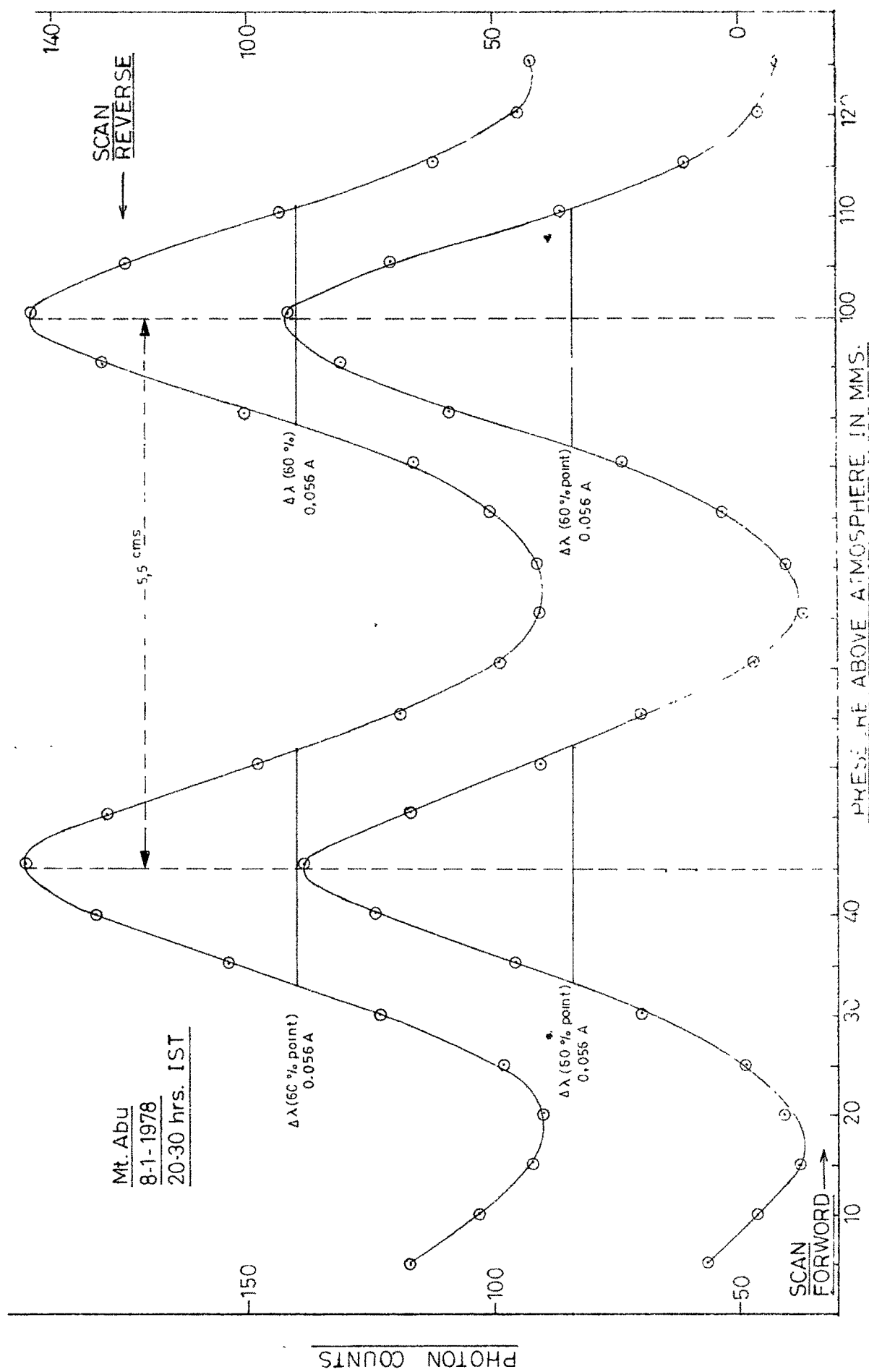


Fig.29 Airglow profiles (upper) and (lower) at Mt. Abu.

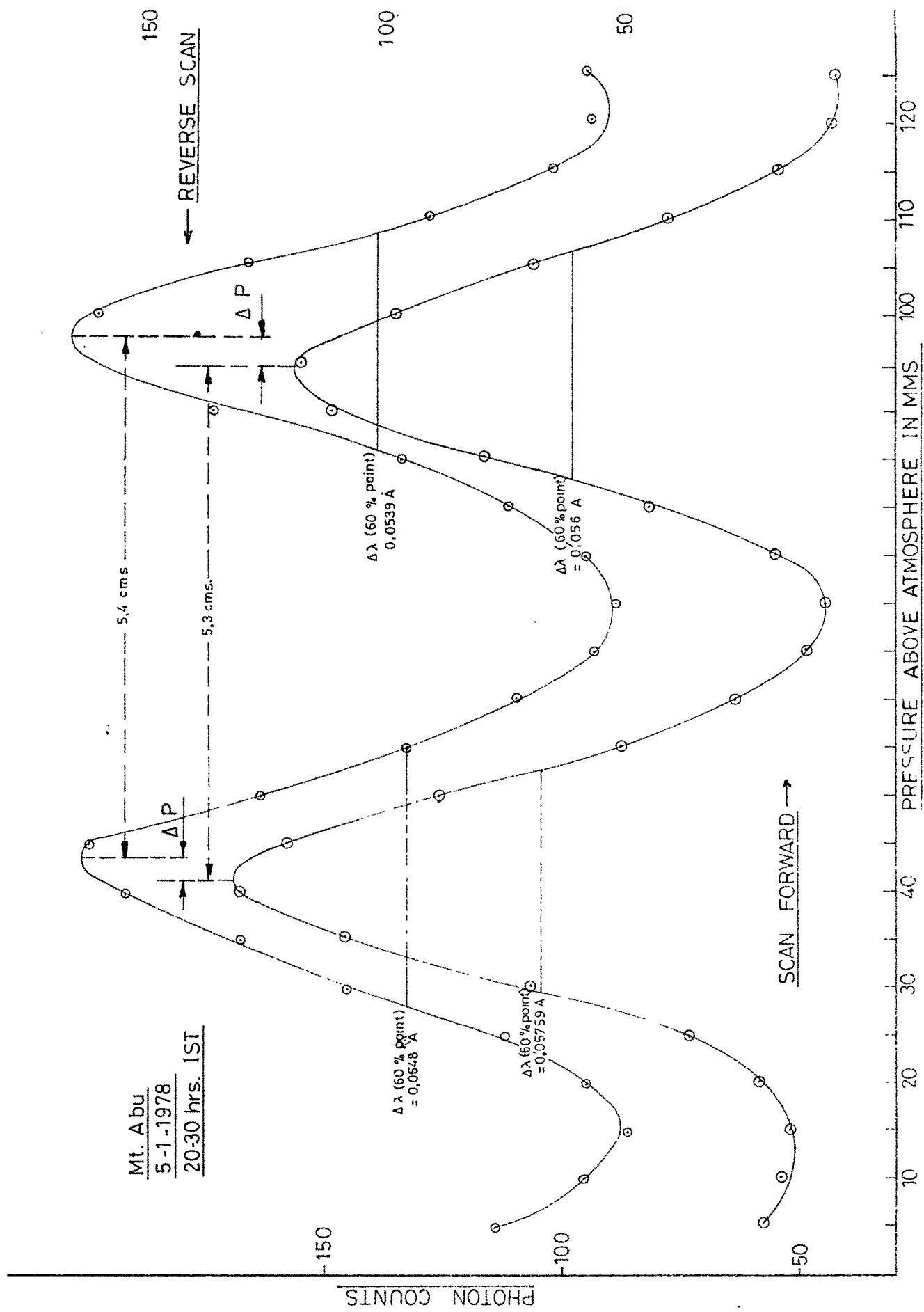


Fig 30 Profiles showing Doppler shift of fringe center

Fig. 29 gives the profiles on the same scan where the pressure interval remains the same and in fig. 30 a change is observed indicating a change in wind vector. The following procedure was used to quantify the neutral air acceleration. Only those scans were studied when the fringes were scanned more than once (as in figs. 29 and 30 a forward scan and a reverse scan). Shift along the pressure axis of the fringes on the second scan (scan reverse) relative to that on the first scan (scan forward) was attributed to neutral air acceleration. ΔP values are reckoned to be positive if the shift of the fringes in the reverse scan is towards longer wave lengths or larger pressure values as in fig. 30, otherwise ΔP is negative. Positive values of ΔP means the acceleration is westward in the present observation geometry. (Since observation being due east).

5.3 RESULTS & CORRELATION STUDIES

The Fabry-Perot spectrometer was looking at 60° zenith angle due east and all the measurements of wind accelerations reported here correspond to east west direction only. About 12 days of observational results are given in figures 31, 32, 33 and 34. Changes in the wind vector of the order of 50 mts/sec ($\Delta P = 0.25$) to 400 mts/sec ($\Delta P = 2$) have been observed over a single scan which is of the order of ≈ 10 minutes duration, successive peaks observed at

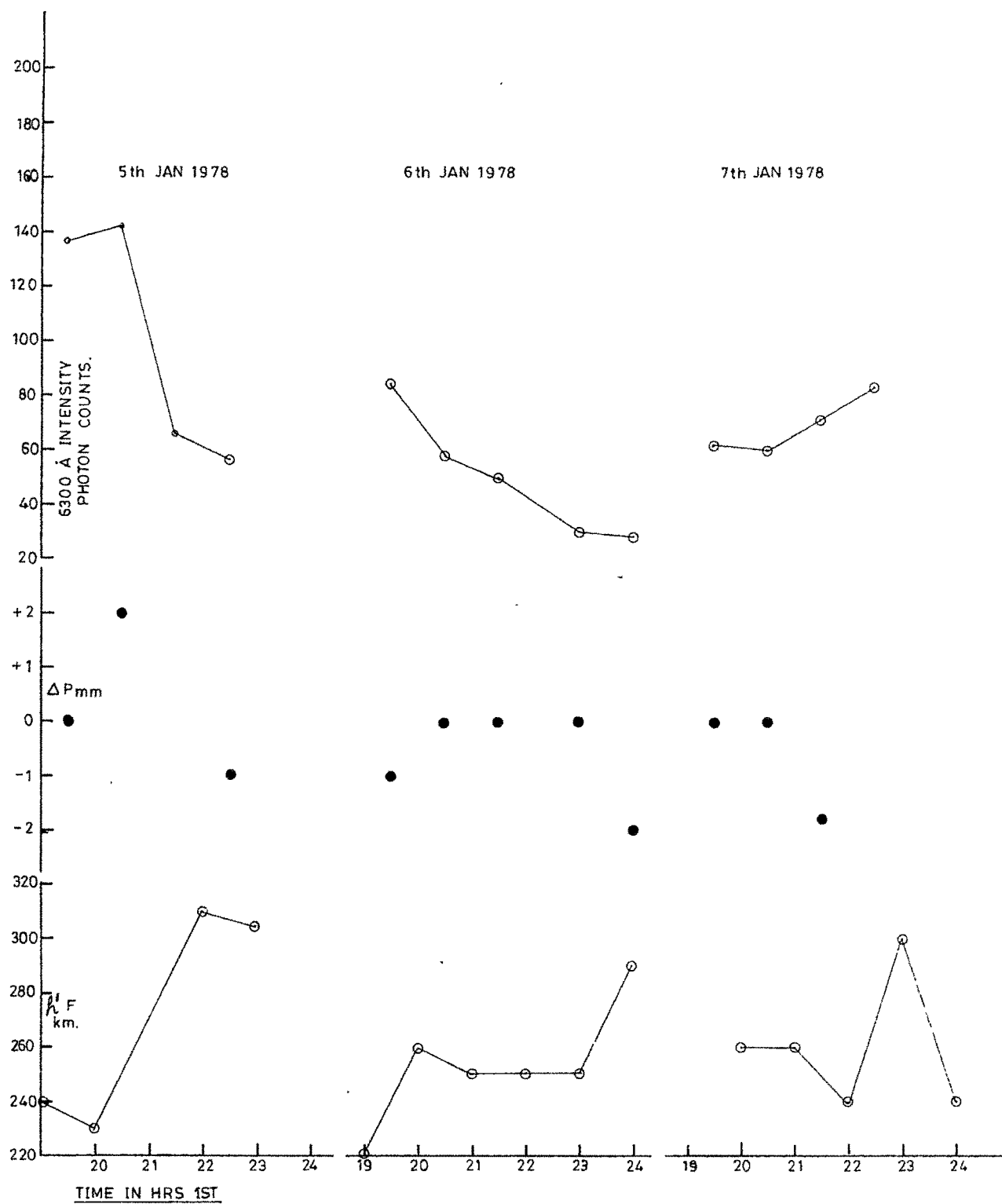
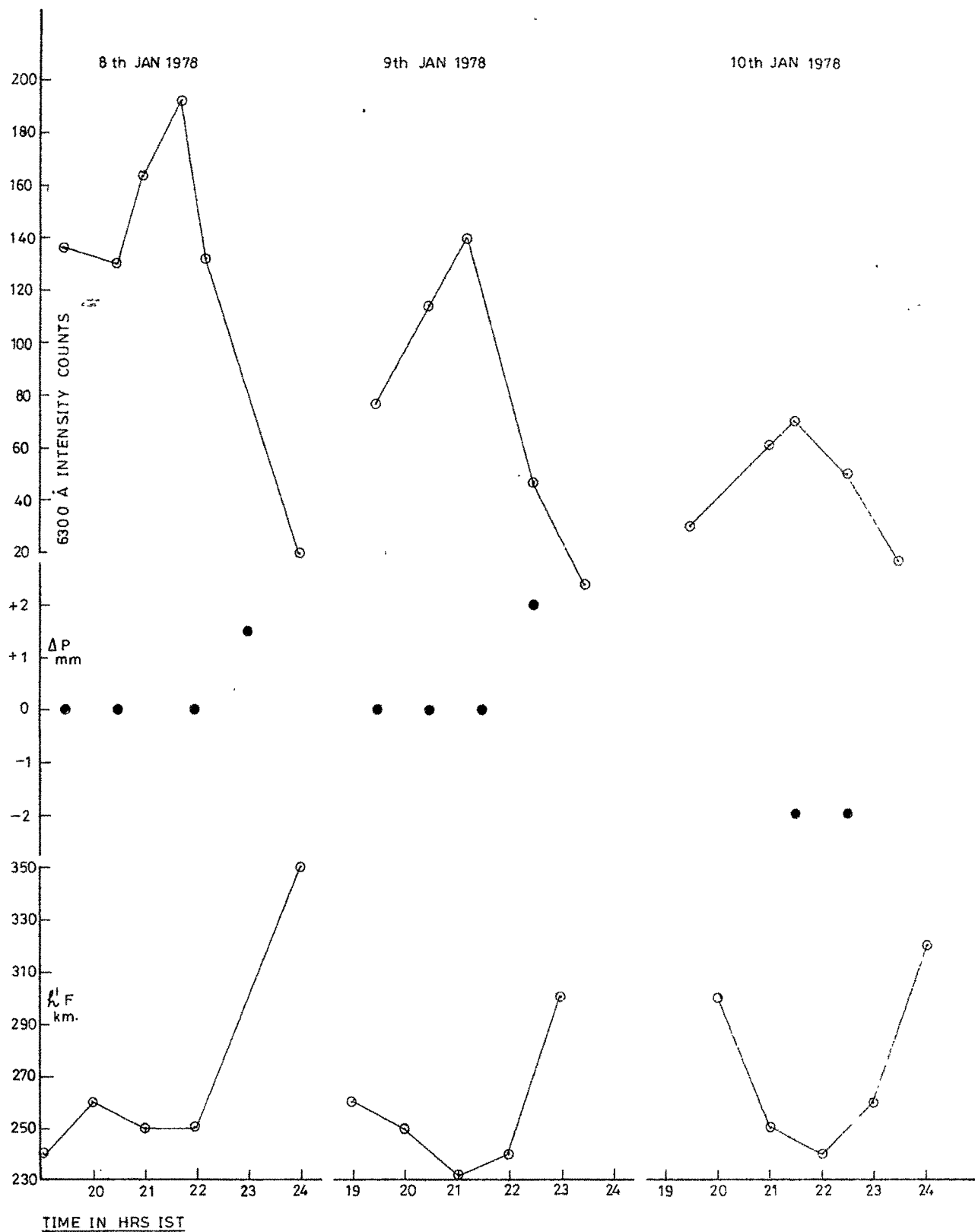


Fig. 31 Wind accelerations (ΔP units) with corresponding changes in $h'F$ values and 6300 Å intensities for different hours on various days.



TIME IN HRS IST

Fig.32 Wind accelerations (ΔP units) with corresponding changes in $h'F$ values and 6300 Å intensities for different hours on

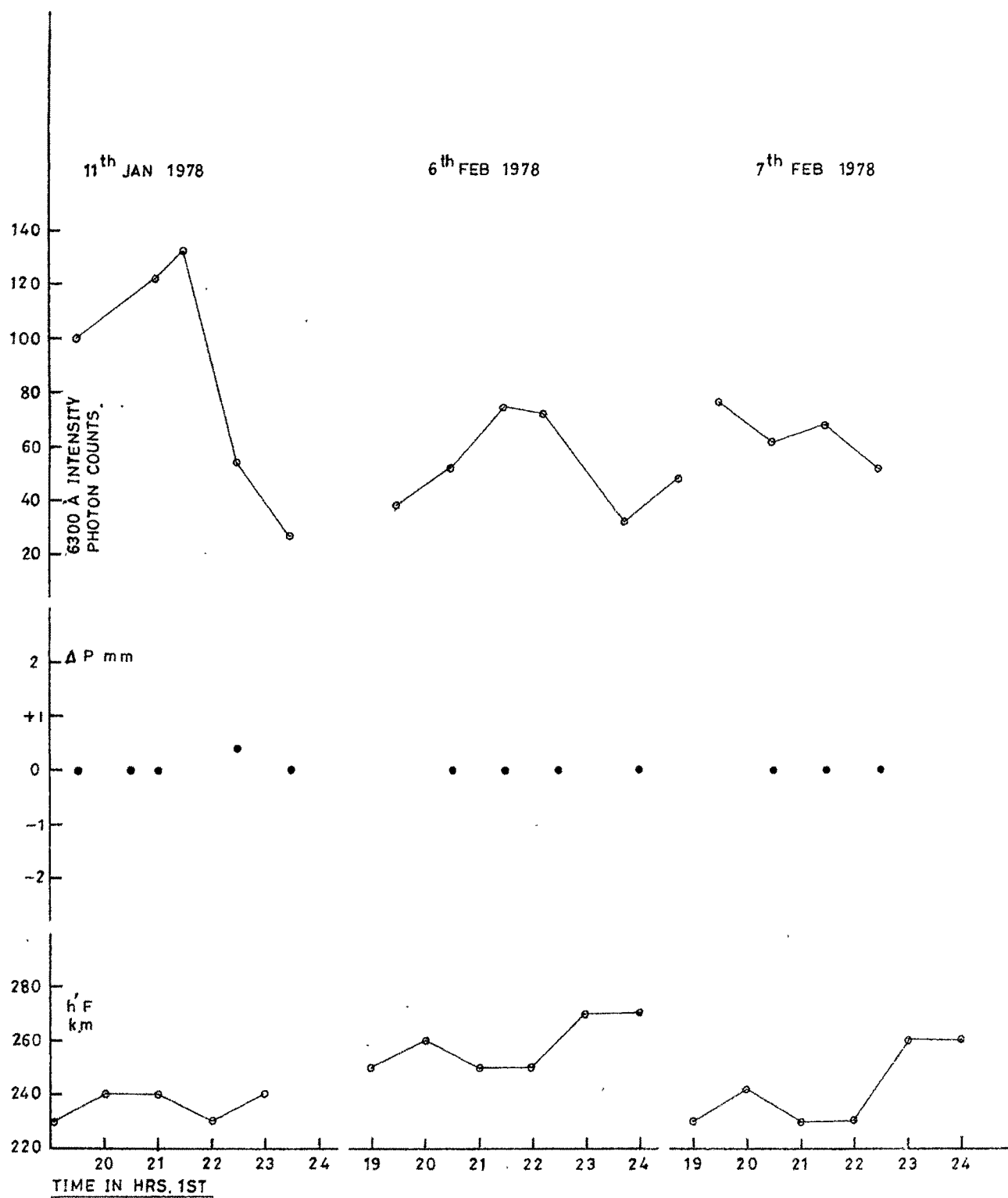


Fig. 33 Wind accelerations (ΔP units) with corresponding changes in $h'F$ value and 6300 Å intensities for different hours on various days.

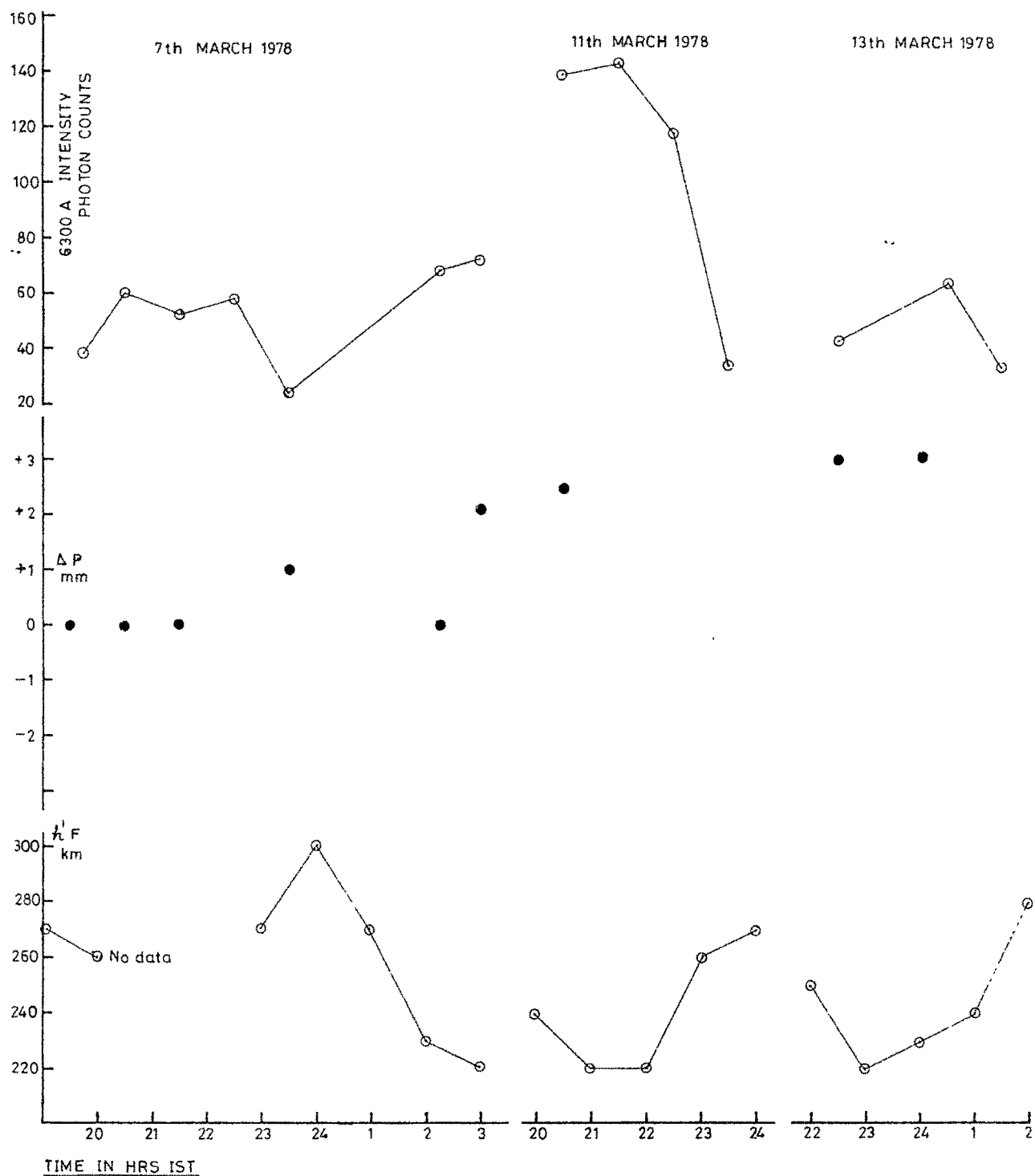


Fig. 34 Wind accelerations (ΔP units) with corresponding change in $h'F$ values and 6300 Å airglow intensities for different hours on different days.

an interval of 5 minutes. ARMSTRONG (1969) and BIONDI AND FEIBELMAN (1968) have reported winds of this order. Another important feature observed is that many times the accelerations are short lived. The results of 6th Jan. 78 in fig. 31, 8th Jan. 78 in fig. 32 and 11th Jan. 78 in fig. 33 clearly show that the accelerations persist for sometime, disappears and then reappear. ARMSTRONG (1969) has reported such short lived winds. Though there is general agreement between the findings in this experiment with similar observations by other workers in this field, a direct comparison is difficult as the results presented here refer to change in wind vector and not the actual winds.

As it was mentioned earlier wind speeds of the order of 400 mts/sec is not uncommon in evening hours (BIONDI AND FEIBELMAN, 1968). The satellite drag method gives large scale winds of the order of 100 - 150 mts/sec, the wind fields of larger magnitude reported above (> 200 mts/sec) could be generated by local ionospheric conditions and could be of shorter spatial scales. Associating such winds with gravity waves the change in the wind vector of ≈ 200 mts/sec on 5 minutes time interval is not inconsistent with a periodicity of ≈ 20 minutes or somewhat longer.

A correlation study was made of the neutral air accelerations with the movement in the height of " F_2 ",

the virtual height of the F2 layer, on the basis of the expectation that such large neutral air accelerations should be of local ionospheric origin. Figs. 31, 32, 33 and 34 show the comparative plots of

- i) Airglow intensities
- ii) Observed neutral air accelerations (ΔP units)
- iii) $h'F$, the virtual height of F2 layer.

These figures clearly bring out the following features :-

- (1) Doppler shifts or change in winds have been observed when there was a movement of $h'F$ level by more than 30 km. Results of 5th & 6th Jan. 78 in fig. 31 and 8th Jan. 78 in fig. 32 clearly manifest this point.
- (2) In many occasions when observation showed no change in wind vector ($\Delta P = 0$), $h'F$ values also remained practically at the same level as seen from fig. 32 (11th Jan.) and fig. 33 (6th & 7th Feb.).
- (3) A rise in airglow intensity accompanying a fall of $h'F$ or vice versa are seen in 70% of the cases.
- (4) Airglow intensity variations have not shown any correlation with the occurrence or non occurrence of wind accelerations.

Thus, the plots in figs. 31 - 34 have clearly shown that there is good correlation between the onset of wind

acceleration and movement of $h'F$. It also shows that mostly the westward acceleration (+ve ΔP) coincides with the upward movement of $h'F$. There are about 20% of cases where the reverse phenomenon is also observed. We have not attempted any explanation for the observed behaviour of $h'F$ level with the onset of wind acceleration.

Correlation between 6300 A intensity values and $h'F$ is very obvious. Intensity increases as $h'F$ level comes down due to increased rate of recombinations and intensity going low as $h'F$ goes up indicating slowing of recombination rate. It can be said that $h'F$ level can be taken as indicative of airglow source height (which is well justified by its correlation with 6300 A intensity behaviour) and the airglow source descends or ascends through a stratum to which the wind is confined. It is important at this point to say that no correlation exists between the occurrence of wind accelerations and 6300 A intensity.

5.4 STUDY OF LINEWIDTH FLUCTUATIONS

For airglow intensities exceeding $\simeq 75$ Rayleighs the individual profiles acquired during the scans were of sufficient S/N ratio, to be analysed individually. These profiles were studied individually with respect to their linewidths and found to exhibit a very interesting behaviour in relation to the earlier mentioned neutral air

accelerations. We find that on occasions when large neutral air accelerations were observed, the line widths of the individual profiles also exhibited variations.

The linewidth fluctuations observed in a single series of scans can only be indicative of real linewidth fluctuations since the fringes are observed with a constant instrument profile. As an example we compare the fringe profiles observed at 2030 hrs on 5th Jan. in fig. 29 and on 8th Jan. in fig. 30. The apparent widths (measured at 60% of the peak, 60% being chosen being the steepest point of descent) clearly show fluctuations on 5th Jan. while fringes on 8th Jan. do not show fluctuations where the neutral air acceleration also is absent. Fig. 35 gives the plot of measured linewidths at two different hours on 12th Dec. 77. It is a clear evidence of fluctuating linewidths for observations between 2300 - 2340 hrs. The chamber pressure for the fringe centre also showed fluctuations given by the values of ΔP . Converting the ΔP values to neutral air accelerations, Values from 50 mts. to 400 mts/sec. are obtained as shown in fig. 35.

Since the observation of neutral air accelerations correlate well with the movements of F2 layer the observed linewidth fluctuations are almost certainly connected with the dynamics of the ionosphere - presumably associated with the occurrence of strong gravity waves. Whether the

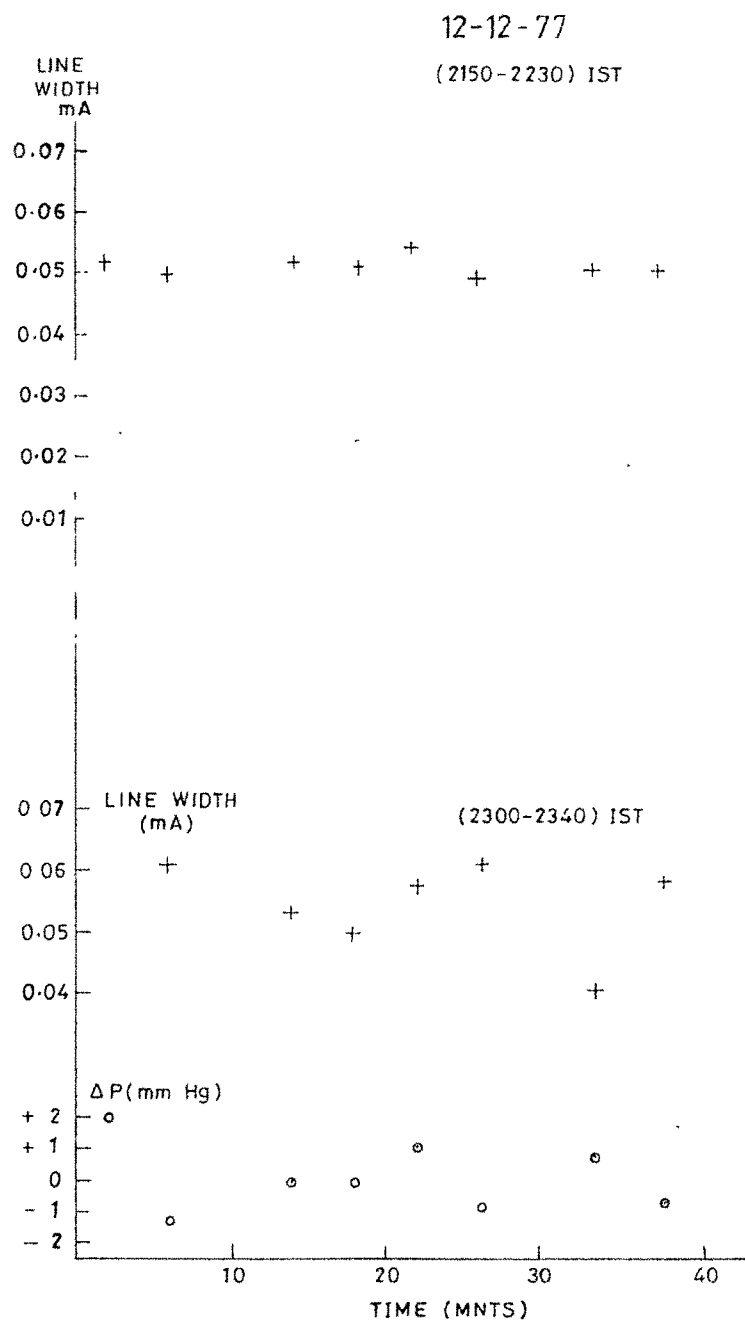


Fig.35 TOP Observations showing no fluctuation in linewidth

BOTTOM Observations showing fluctuations in linewidth and corresponding wind accelerations (ΔP Values) from fringe centre shifts.

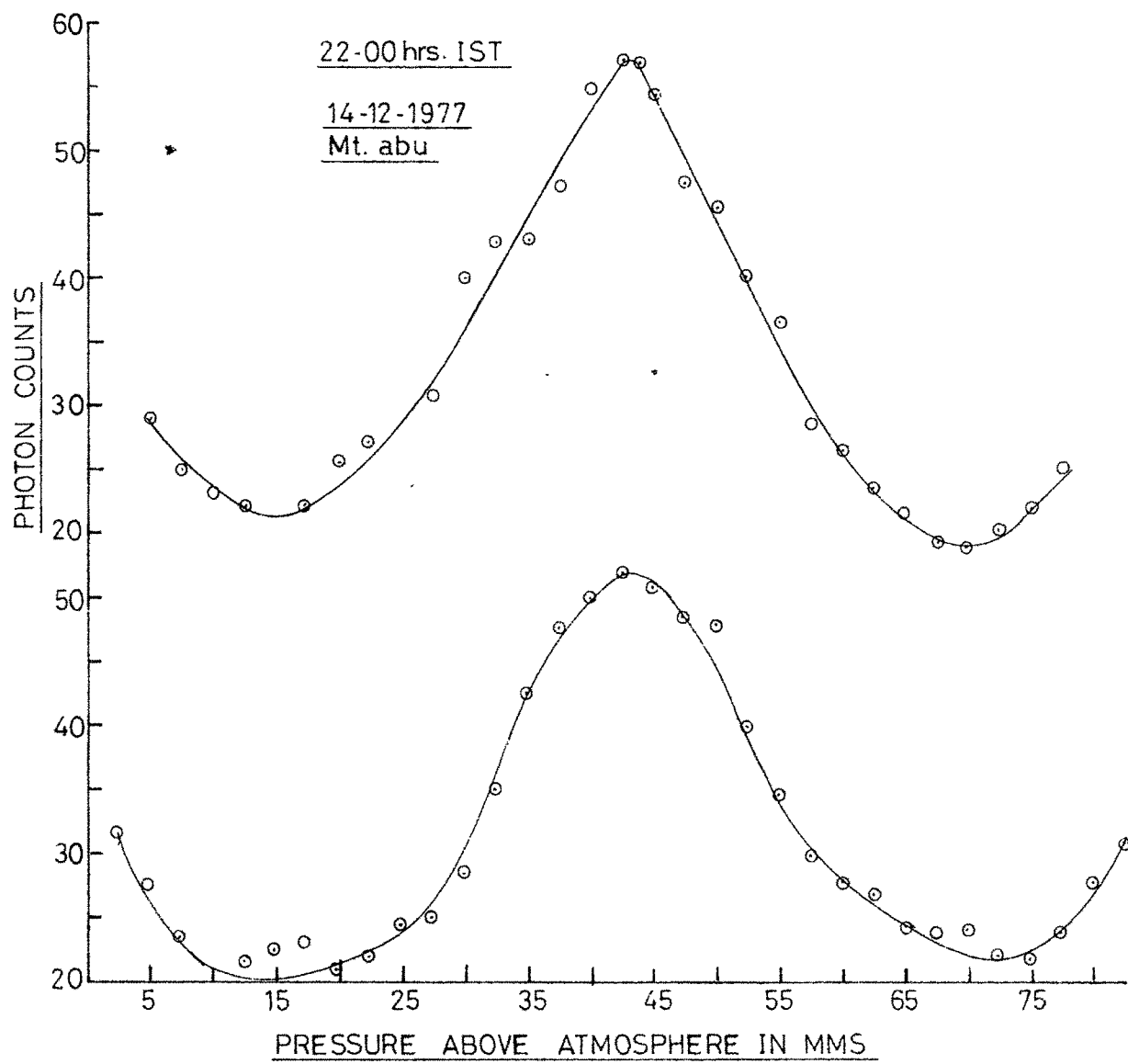


Fig. 36 Top : Sharp profile with narrow peak
Bottom : Profile with relatively extended wings

observed fluctuation in linewidths mean a real fluctuation in temperature or not is a different problem. The recombination of O_2^+ ion create excited 'O' atoms with a velocity field and distribution corresponding to O_2^+ which may be different from the neutrals. If the collision frequency is not sufficient one may observe linewidth temperature much different from that of the ambient neutral atmosphere.

Comparing the shapes of the individual line profiles it was observed on most occasions, line profiles which are nearly gaussian. However on sufficient number of occasions we have observed peculiar line profiles of the types shown in figure 36. The basic peculiarities are

- i) Very sharp and narrow peak.
- ii) Relatively extended wings.

One way to synthesise such a profile is to associate the emitting regions with a large difference of temperature. The sharp peak of the lower temperature region will then show up as superposition on the broader fringe of the higher temperature region.

Inhomogenities in the form of " Pockets " or " Cells " with different temperatures could cause such abnormal profiles as well as large fluctuation in widths over time scales of the order of minutes.

CHAPTER - VI

DISCUSSION OF RESULTS AND SCOPE FOR FURTHER WORK

The results obtained in the present study (given in Chapters IV and V) can be grouped into three major parts as :

- (1) Neutral Temperatures
- (2) Temperature enhancements and spread F connection
- (3) Neutral wind acceleration and linewidth fluctuations.

The following gives a discussion on the results, important findings and conclusions drawn from the studies and suggestions for further work.

6.1 NEUTRAL TEMPERATURES

The measurement of Doppler broadening of the 6300 Å oxygen emission line provides an excellent source of direct information on upper atmospheric temperatures. The average temperatures determined in the present study, in general, agree very well with JACCHIA model atmospheric temperatures to an accuracy of $\pm 50^{\circ}\text{K}$. This group forms 61% of the total number of temperature measurements. This brings out the fact that Fabry-Perot Doppler temperatures can be conveniently used to monitor exospheric temperatures. The observations reported here thus generally confirm the previous optical interferometer and backscatter measurements in finding that the JACCHIA model provides a good prediction of exospheric temperature.

Mc Clure (1969, 1971) has argued that in the night time equatorial F2 region $T_e = T_i = T_n$ where T_e is electron temperature and T_i and T_n are ion and neutral temperatures respectively. Briefly at JICAMARCA (1°N dip) T_e is observed to be independent of height in the night time F2 region near the dip equator. Then, since T_n is known to be nearly independent of height in the night time F2 region, either T_e must be equal to T_n or it must differ from T_n by an amount that is very nearly independent of height. A constant difference could be caused by a height independent relative motion between the plasma and the neutral atmosphere [STUBBE AND CHANDRA (1971)].

HERNANDEZ (1975) has shown that the difference between the optical and incoherent scatter measurements over equator is hardly 26°K and the difference is consistent with JACCHIA (1971) model.

HAYS ET AL, (1970) have shown, by simultaneous measurements over Millstone Hill ($42^\circ 30'\text{N}$, $71^\circ 36'\text{W}$) with incoherent scatter facility and Fabry-Perot interferometer, the close agreement between Doppler temperatures and ion temperatures. The average Doppler temperature obtained is 790°K , whereas the backscatter mean temperature is 745°K . This corresponds to a systematic difference of about 5.7% which is well within the claimed accuracy limits. The results presented by HAYS ET AL, (1970) in fig. 3 provide added confidence in the ion temperature values obtained

with the radar back scatter technique and show that the 6300 Å Doppler temperatures can be used as a monitor of exospheric temperature.

In the present study which pertains to dip 15° , of the total temperature measurements, 61% measurements agree well with JACCHIA model exospheric temperatures. For the situations in which good agreement is observed with model atmospheric values, it should be very useful to have continuous and extended observations so that the daily variation and also the rate of fall during night time can be studied more accurately. Simultaneous measurements of ion temperature (T_i) with a back scatter radar facility and neutral temperature (T_n) with a Fabry-Perot spectrometer would be of great value to understand more about the dynamics of the ionosphere in these low latitudes where measurements of this type are very few.

6.2 Temperature Enhancements and Spread-F

It is found that of those occasions in which temperature enhancements are seen, 65% of them correlate well with the onset of spread-F over equator and only 12% of them show negative correlation ; for the rest there being no ionospheric data. Hence it is clear that the neutral atmospheric temperature at Mt Abu (dip latitude 15°) during occurrence of equatorial spread-F as seen over Thumba

(dip 0.6°S) or a nearby station Kodaikanal (dip 0.6°N) is $200^{\circ}\text{K} - 300^{\circ}\text{K}$ higher than when there is no equatorial spread F. These temperature enhancements imply a temperature gradient between the F and E regions of the order of 1°K per km, the same as predicted by COLE (1974).

Temperature enhancements well correlated with equatorial spread F observed in the present work are consistent with the model of COLE for formation of field aligned irregularities between conjugate dynamo regions of the ionosphere and the estimates of heating in the spread F events (COLE, 1974). Thus, these results provide fairly unambiguous evidence that there is significant heating of the atmosphere above 300 km due to Joule dissipation of currents generated in the F region by turbulent electric fields during spread F events over and near the magnetic equator. KELLEY (1972) has determined from OVI 17, satellite measurements that the electric fields associated with spread F are electrostatic. The energy density of the broad band electric field detected by the OVI 17 experiment in the characteristic regions was 400 times the energy density due to thermal fluctuations of a 1000°K plasma (ROSTOCKER 1961). The energy density of the observed electric field was more than 10^4 times the thermal background on several occasions. Thus the observed electrostatic fluctuations can be described as turbulent.

Hence the insitu measurements have shown the existence of turbulent large scale electric fields during spread F events.

Whereas the basic mechanism of heat input can be attributed to the Joule dissipation of electric currents associated with turbulent electric fields at the time of equatorial spread F, the exact process through which the increase in temperature takes place at the altitude of emission is not clear. It seems possible, however that the heating in F region over Mt Abu takes place through heat conveyed by charged particles from spread F region downwards along the magnetic field line. 250 to 300 km altitude field lines over Mt Abu connect with 700 km region over the magnetic equator, hence the spread F activity in the topside ionosphere over the magnetic equator is expected to contribute to the increase in the F region temperature over Mt Abu. Topside ionospheric soundings have shown (KRISHNAMURTHY, 1966) that the occurrence of spread F in the topside is very well correlated with the spread F in the bottomside. To summarize, there is a heating source at F region altitudes for low latitude stations whose spatial extent and time variations are required to be investigated further. Since the observed excess temperatures are fairly large its implications on the dynamics of the neutral atmosphere are important.

Recent satellite observations of SPENCER ET AL (1979) have given additional confirmation on the night time temperature enhancements. Using the neutral atmosphere temperature instrument on Atmospheric Explorer-E satellite operating in a circular orbit at 275 km and orbit inclination 19° , they have measured the kinetic temperature of N_2 throughout many orbits, providing for the first time direct in situ measurement of the diurnal temperature variation. They have observed that near midnight the temperature increases substantially up to $300 - 400^\circ K$ which normally happens to be near $15 - 19^\circ$ dip latitude. Increases near mid night are observed about one half the time measurements are made, showing the feature to be a persistent one. They have not observed any such increase over equator. The authors could not explain the cause for such temperature enhancements but they do suggest that it could be either due to

- a) momentum coupling associated with ion drag
- b) tidal waves from the lower atmosphere and
- c) high latitude heating followed by energy transfer to low latitudes.

They guess that ion drag and tidal waves are the likely candidates for generating the temperature increase.

If we take our results, results of SPENCER ET AL (1979) which show temperature increase around 17° dip latitude and no increase over dip equator and the results of HERNANDEZ (1975) who find close agreement with model temperatures over equator, it is clear that simultaneous latitudinal coverage of temperature measurements from dip 0° to dip 17° is very essential. It is also very likely that the heating observed would be strongly associated with dynamical effects like winds and currents. In order to get a comprehensive understanding it seems very important to have simultaneously the wind measurements and monitoring of ionospheric parameters. This, of course, needs large cooperative efforts and was certainly beyond the scope of present study which was of the nature of exploratory work.

Simultaneously if mesospheric temperatures are observed together with exospheric temperatures, the study, perhaps provide more clues. We suggest linewidth measurements on 5577 Å O(I) and rotation vibration spectra of OH for this purpose.

6.3 NEUTRAL WIND ACCELERATIONS AND LINEWIDTH FLUCTUATIONS

Changes in the wind vector of the order of 50 mts/sec to 400 mts/sec have been measured. Also many times the winds are of short lived type. It is worthwhile to mention

here that wind speeds of the order of 400 mts/sec are not uncommon and such magnitudes have been reported by BIONDI AND FEIBELMAN (1968). The satellite drag method gives large scale winds maximum up to 150 mts/sec. We strongly feel that wind fields of larger magnitude (> 200 mts/sec) reported here could be of local ionospheric origin. Associating such winds with gravity waves the change in the wind vector of ≈ 200 mts/sec on five minutes time interval is not inconsistent with a periodicity of 20 minutes or longer.

The good correlation that is established between the movement of $h'F$ (virtual height of F2 layer) and the onset of wind acceleration gives justification to our prediction that such large wind fields are generated by local ionospheric conditions. The correlation between 6300 Å intensity behaviour and movement of $h'F$ is very obvious. Intensity increases as $h'F$ comes down due to increased rate of recombinations and vice versa. This indicates that the level of $h'F$ can be taken to represent the airglow source height.

The linewidth fluctuations observed in individual scans also give wind accelerations of 50 - 400 mts/sec. Whether the observed fluctuations in linewidth mean a real fluctuation in temperature or not ~~is~~ is difficult

to explain. Since neutral air accelerations correlate well with the movements of F2 layer the observed linewidth fluctuations are almost certainly connected with the dynamics of the ionosphere - presumably associated with the occurrence of strong gravity waves.

The usual technique of observing winds in the height region involves obtaining 6300 Å night airglow fringe in two directions, 180° apart in azimuth and at equal zenith angle of $50 - 60^\circ$. The shift in the line centre due to Doppler shift is then interpreted in terms of winds. However, this technique measures winds assuming that the wind field is constant over a spatial scale of ≈ 1000 kms. In light of the short period fluctuations in fringe centre indicated in our study (page 80), we feel that it would be much more valuable to measure winds over a single spatial region. This could be done by comparing the fringe centre of 6300 Å night airglow line with the fringe centre of a frequency stabilised He-Ne laser (λ 6328 Å).

Finally the nature and cause of fringe narrowing observed by us on a few occasions (page 72) remain unexplainable by us at present and call for a further study.

REFERENCES

- ARMSTRONG E. B. (1953) : J. ATMOS. TERR. PHYS., 3, 274
- ARMSTRONG E. B. (1956) : IN " AURORA AND AIRGLOW " Edited
by DALGARNO & ARMSTRONG
- ARMSTRONG E. B. (1968) : PLANET. SPACE. SCI. 16, 211
- ARMSTRONG E. B. (1969) : PLANET. SPACE. SCI. 17, 957
- ARMSTRONG E. B. AND BELL J. A. (1970) : PLANET. SPACE.
SCI. 18, 784
- BABCOCK H. D. (1923) : ASTROPHYSICS JOURNAL, 57, 209
- BASS A. M. AND GARVIN D. (1962) : J. MOLECULAR SPECTROSCOPY.
19, 114
- BIONDI M. A. AND FEIBELMAN W. A. (1968) : PLANET. SPACE.
SCI., 16, 431
- BLACKWELL D. E., INGHAM M. F. AND RUNDLE H. N. (1960) :
ASTROPHYSICS JOURNAL 131, 15
- BLAMONT J.E. AND BARAT J. (1967) : ANNALS DE GEOPHYSIQUE,
23, 173
- BLAMONT J. E. AND LUTON J. M. (1972) : J. GEOPHYS. RES.,
19, 3534
- BLUM P. W. AND HARRIS I. (1973) : PLANET. SPACE. SCI.,
21, 377
- BORN M. AND WOLF E. (1959) : " PRINCIPLES OF OPTICS "
PERGAMON PRESS
- BOWLES K. L. (1961) : J. RES. NAT. BUR. STD. 65, D
- BUISSON H. AND FABRY C. H. (1912) : J. PHYS. 11, 442

- CANDLER C. (1951) : " MODERN INTERFEROMETERS " HILGER
WATTS, LONDON
- CARRU H., PETIT M. AND WALDTEUFEL P. (1967) : PLANET.
SPAC. SCI., 15, 944
- CHABBAL R. (1953) : J. RECH. CNRS, 24, 318
- CHABBAL R. (1958) : REVUE D' OPTIQUE, 37, 49
- CHAMPION K.S.W. (1970) : SPACE RESEARCH 10, 347
- CHAMPION K.S.W. AND SCHWEINFURTH R. A. (1971) : PRESENTED
AT THE 14TH COSPAR MEETING SEATTLE, WASHINGTON
- CHANDRA S. AND STUBBE P. (1970) : PLANET. SPAC. SCI.,
15, 949
- CHANTREL H. (1958) : J. PHYS. RAD. 19, 355
- CHING B. K. AND CHIU Y. T. (1973) : J. ATMOS. TERR.
PHYS, 35, 1616
- CIRA (1965) : COSPAR INTERNATIONAL REFERENCE ATMOSPHERE,
NORTH HOLLAND, AMSTERDAM
- COLE K. D. (1974) : J. ATMOS. TERR. PHYS. 36, 1099
- CONNES P. (1958) : J. PHYS. RAD. 19, 262
- CONNES P. AND GUSH H.P. (1960) : J. PHYS. RAD. 21, 645
- DESAI J. N. AND NARAYANAN M.S. (1969) : J. ATMOS. TERR.
PHYSICS. 32, 1235
- DESAI J. N., BHAVSAR P. D., RAGAVARAO R. AND NARAYANAN
M. S. (1975) : SPACE RESEARCH XV ACADEMIC VERLAG, BERLIN
- DESAI J. N. AND RAJARAMAN T. N. (1976) : INDIAN J. RADIO
AND SPACE PHYS. 5, 58

: R-iii :

- DUFOUR C. H. AND PICA (1945) : REVUE D'OPTIQUE 24, 13
- FEIBELMAN W. A., HAKE R. D., SIPLER D. P. AND BIONDI
M. A. (1972) : J. GEO. PHYS. RES. 77, 1669
- GEISLER J. E. (1966) : J. ATMOS. TERR. PHYSICS 28, 703
- GIRARD A. AND PETIT M. (1978) : IN " IONOSPHERIC
TECHNIQUES AND PHENOMENA " PAGE 13-110 D. REIDEL
PUBLICATIONS
- GOLOMB D. AND MACLEOD M. A. (1966) : J. GEO. PHYS. RES.
71, 2299
- GORDON W. E. (1958) : PROC. IRE. 46, 1824
- GROVES (1971) : AFCRL REPORT NO 71-0410
- HARRIS I. AND PRIESTER W. (1962A) : J. ATMOS. SCI 19, 286
- HARRIS I. AND PRIESTER W. (1962B) : J. GEO. PHYS. RES.
67, 4585
- HAYS P. B., NAGY A. F., AND ROBLE R. G. (1969) :
J. GEO. PHYS. RES. 74, 4162
- HAYS P. B., NAGY A. F., AND MC WATTERS K. D. (1970) :
J. GEO. PHYS. RES. 75, 4881
- HAYS P. B. AND ROBLE R. G. (1971) : J. GEO. PHYS. RES.
76, 5316
- HERNANDEZ G. (1966) : APP. OPTICS 5, 1745
- HERNANDEZ G. (1970) : APP. OPTICS 9, 1225
- HERNANDEZ G. (1974) : J. GEO. PHYS. RES. 79, 1119
- HERNANDEZ G. (1975) : J. GEO. PHYS. RES. 80, 3271

- HERNANDEZ G. AND MILLS O. A. (1973) : APP. OPTICS.
12, 126
- HERNANDEZ G. AND ROBLE R. G. (1974) : J. GEO. PHYS. RES.
81, 2065
- HERNANDEZ G. AND ROBLE R. G. (1976) : J. GEO. PHYS. RES.
81, 5173
- HERNANDEZ G. AND TURTLE J. P. (1965) : PLANET. SPAC. SCI,
13, 901
- HERNANDEZ G., VANZANDT T. E., PETERSON V. L. AND TURTLE
J. P. (1975) : J. GEO. PHYS. RES. 80, 327
- HILL R. M. (1963) : OPTICA ACTA, 10, 141
- HILLIARD R. L. AND SHEPHERD G. G. (1966) : PLAN. SPAC.
SCI, 14, 383
- HINES C. O. (1965) : J. GEO. PHYS. RES. 70, 177
- HUNTEN D. M., RAWSON E. G. AND WALKER J. K. (1963) :
CANADIAN J. PHYS. 41, 258
- HUNTEN D. M., ROACH F. E. AND CHAMBERLAIN J. W. (1956) :
J. ATMOS. TERR. PHYS. 8, 345
- JACCHIA L. G. (1963) : REV. MOD. PHYS. 35, 973
- JACCHIA L. G. (1965) : SMITHSON CONTRIB. ASTROPHYSICS 8, 215
- JACCHIA L. G. (1970A): J. GEO. PHYS. RES. 75, 4347
- JACCHIA L. G. (1970B): S.A.O. SPECIAL REPORT 313 CAMBRIDGE,
MASS
- JACCHIA L. G. (1977): S.A.O. SPECIAL REPORT 375

: R-v :

- JACQUINOT P. (1948) : J. RECH. CNRS. 6, 91
- JACQUINOT P. (1954) : J. OPT. SOC. Ame 44, 761
- JACQUINOT P. (1960) : REV. PROG. PHYS 23, 267
- JARRETT A. H. AND HOEY M. J. (1966) : J. ATMOS. TERR.
PHYSICS. 28, 175
- KARANDIKAR R. V. (1968) : PLANET. SPAC. SCI 16, 539
- KELLEY M. C. (1972) : J. GEO. PHYS. RES. 77, 1327
- KING-HELE D. G. (1966) : ANN. GEO. PHYS. 22, 40
- KING-HELE D. G. AND SCOTT D. W. (1967) : PLANET SPAC.
SCI, 15, 913
- KOHL H. AND KING J. W. (1967) J. ATMOS. TERR. PHYS.
29, 1045
- KRASOVSKY V. L., SHEFOV N. N. AND YARIN V. I. (1962) :
PLANET. SPAC. SCI, 9, 883
- KRISHNAMURTHY B. V. (1966) : J. GEO. PHYS. RES. 71, 4527
- KHUN H. G., LEWIS E. L., STACEY D. N. AND VAUGHAN J. M.
(1968) : REV. SCI. INSTRU 39, 86
- KVIFTE G. (1959a) : J. ATMOS. TERR. PHYS 16, 252
- KVIFTE G. (1959b) : GEO. PHYS. PUBLI 20, 12
- KVIFTE G. J. (1967) : PLANET. SPAC. SCI 15, 1515
- LLOYD K. H. AND SHEPHERD L. M. (1966) : AUST. J. PHYS.
19, 323
- MAYR H. G. AND MAHAJAN K. K. (1971) : J. GEOPHYS. RES.
76, 1017

: R-vi :

- Mc CLURE J. P. (1969) : J. GEO. PHYS. RES. 74, 279
- Mc CLURE J. P. (1971) : J. GEO. PHYS. RES. 76, 3106
- MEABURN J. (1976) : IN " DETECTION AND SPECTROMETRY OF
OF FAINT LIGHT ", J. REIDEL PUBLICATION
- MILLER S. A. (1968) : REV. SCI. INSTRU. 39, 1923
- MILLER J. R. (SHEPHERD G. G. (1968) : ANN. GEO. PHYS.
24, 305
- MULYARCHIK T. M. (1959) : USSR. SECTION IV OF IGY
PROGRAM 1, 30
- NICOLET M. (1961) : PLANET. SPAC. SCI. 5, 1
- NILSON J. A. AND SHEPHERD G. G. (1961) : PLANET. SPAC.
SCI. 5, 299
- NISBET J. S. (1967) : J. ATMOS. SCI. 24, 586
- NISBET J. S. (1971) : RADIO SCI. 6, 437
- NOXON J. F. (1964) : J. GEO. PHYS. RES. 69, 4087
- O'NEIL R. R. (1972): PRESENTED AT THE 15TH COSPARMEETING,
MADRID, SPAIN
- PRIESTER W., ROEMER M. AND VOLLAND H. (1967) : SPAC.
SCI. REV. 6, 707
- RAJARAMAN T. N., DESAI J. N., DE GAONKER S. S. AND
COLE K. D. (1978) : NATURE, 272, PAGE 516
- RAJARAMAN T. N., DESAI J. N. AND DEGAONKER S. S. (1979) :
PROC. IND. ACA. SCI. 88A, 69
- RAMSAY J. V. (1962) : APP. OPTICS 1, 411

: R-vii :

- RAMSAY J. V. (1966) : APP. OPTICS 5, 1297
- RAUTION S. G. (1958) : SOVIET PHYSICS USP 1, 245
- REES D. (1971) : J. BRIT. INTERPL. SOC. 24, 643
- REES D. (1971A) : PLANET. SPAC. SCI. 19, 233
- ROBLE R. G., HAYS P. B. AND NAGY A. (1968) :
PLANET. SPAC. SCI 16, 1109
- ROEMER M. (1971) : IN " PHYSICS OF THE UPPER ATMOSPHERE "
Ed. By VERNIANI P. 229. EDITRICE, COMPOSITORI, BOLOGNA
- ROSTOCKER N. (1961) : NUCLEAR FUSION 1, 101
- RUSTER R. AND KING J. W. (1973) : J. ATMOS. TERR. PHYS.
33, 1317
- SHEPHERD G. G. (1971) : " SPECTROSCOPIC MEASUREMENT OF
UPPER ATMOSPHERIC TEMPERATURES " PRESENTED AT THE FIFTH
SYMPOSIUM ON TEMPERATURE, WASHINGTON D.C.
- SIEGFRIED J. BAVER (1973) : " PHYSICS OF PLANETARY
IONOSPHERES " SPRINGER VERLAG PUBLI, NEWYORK
- SPENCER N. W., NEWTON G. P., CARIGNAN G. R. AND TAEUSCH
D. B. (1970) : SPAC. RES. 10, 389
- SPENCER N. W. AND CARIGNAN G. R. (1972) : PRESENTED AT
THE 15TH COSPAR MEETING MADRID, SPAIN
- SPENCER N. W., CARIGNAN G. R., MAYR H. G., NIEMANN H. B.,
THEIS R. F. AND WHARTON L. E. (1979) : GEO. PHY. RES.
LETTERS 6, 444
- STUBBE P. AND CHANDRA S. (1971) : PLANET.SPAC. SCI. 19, 731
- STUBBE P. (1972) : PLAN. SPAC. SCI. 20, 209